Accepted Manuscript

Reconstruction of northeast Asian deformation integrated with western Pacific plate subduction since 200Ma

Shaofeng Liu, Michael Gurnis, Pengfei Ma, Bo Zhang

PII: S0012-8252(17)30359-8
DOI: doi:10.1016/j.earscirev.2017.10.012
Reference: EARTH 2512

To appear in: *Earth-Science Reviews*

Received date: 10 July 2017
Revised date: 9 October 2017
Accepted date: 21 October 2017

Please cite this article as: Shaofeng Liu, Michael Gurnis, Pengfei Ma, Bo Zhang , Reconstruction of northeast Asian deformation integrated with western Pacific plate subduction since 200Ma. The address for the corresponding author was captured as affiliation for all authors. Please check if appropriate. Earth(2017), doi:10.1016/j.earscirev.2017.10.012

Reconstruction of northeast Asian deformation integrated with western Pacific plate subduction since 200 Ma

Shaofeng Liu[a, *], Michael Gurnis[b], Pengfei Ma[a], Bo Zhang[a]

[a] State Key Laboratory of Geological Processes and Mineral Resources and School of Geosciences and Resources, China University of Geosciences (Beijing), Beijing 100083, China

[b] Seismological Laboratory and Division of Geological and Planetary Sciences, California Institute of Technology, Pasadena, CA 91125, United States

Abstract

The configuration and kinematics of continental deformation and its marginal plate tectonics on the Earth's surface are intrinsic manifestations of plate-mantle coupling. The complex interactions of plate boundary forces result in plate motions that are dominated by slab pull and ridge push forces and the effects of mantle drag; these interactions also result in continental deformation with a complex basin-mountain architecture and evolution. The kinematics and evolution of the western Pacific subduction and northeast Asian continental-margin deformation represent a first-order tectonic process whose nature and chronology remains controversial. This paper implements a "deep-time" reconstruction of the western Pacific subduction, continental accretion or collision and basin-mountain deformation in northeast Asia since 200 Ma based on a newly revised global plate model. We use GPlates software to examine strain recovery, geological and seismic tomography constraints for the western Pacific plate subduction, and sequentially backward rotations of deforming features. The results indicate a NW-SE-oriented shortening from 200-137 Ma, a NWW-SEE-oriented extension from 136-101 Ma, a nearly

* Correspondingauthor. Tel.: +86 10 82321159; fax: +86 10 82321159.
E-mail address: shaofeng@cugb.edu.cn (S.F. Liu).

N-S-oriented extension and uplift with a short-term NWW-SEE-oriented compressional inversion in northeast China from 100-67 Ma, and a NW-SE- and nearly N-S-oriented extension from 66 Ma to the present day. The western Pacific oceanic plate subducted forward under East Asia along Mudanjiang-Honshu Island during the Jurassic, and the trenches retreated to the Sikhote-Alin, North Shimanto, and South Shimanto zones from ca. 137-128 Ma, ca. 130-90 Ma, and in ca. 60 Ma, respectively. Our time-dependent analysis of plate motion and continental deformation coupling suggests that the multi-plate convergent motion and ocean-continent convergent orogeny were induced by advance subduction during the Jurassic and earliest Cretaceous. Our analysis also indicates that intra-continent rifting and back-arc extension were triggered by trench retreat during the Cretaceous and that the subduction of the oceanic ridge and arc were triggered by trench retreat during the Cenozoic. Therefore, reconstructing the history of plate motion and subduction and tracing the geological and deformation records in continents play a significant role in revealing the effects of complex plate motions and the interactions of plate boundary forces on plate-mantle coupling and plate motion-intracontinental deformation coupling.

Keywords: northeast Asia; reconstruction of deformation and subduction; strain; relative plate motion; advanced slab subduction; trench retreat

1. Introduction

The configuration and kinematics of continental deformation and its marginal plate tectonics on the Earth's surface are intrinsic manifestations of plate-mantle coupling. Global plate tectonic reconstructions provide a spatial and temporal framework for geological data and have proven to be effective tools for exploring regional processes. Newly published topological plate motion models (Seton et al., 2012; Müller et al., 2016) have played a key role in reconstructing time-dependent deformation. These models enable the computation of plate velocities and directions for the entire surface of the globe through time (Zahirovic et al. 2015) and allow evaluation of the evolving plate ages of subducting oceanic crust (Müller et al., 2016).

However, a key component of a model's utility rests in its ability to reveal the coupling between plate motions and intracontinental deformation and in linking the kinematics of continental deformation and the marginal plate tectonics on the Earth's surface.

Northeast Asia consists of a complex mosaic of tectonic units, including accretionary continental fragments, exotic terranes, and intra-oceanic island arcs. This region is presently delineated by suture zones and remnants of ancient proto-Pacific and Tethyan ocean basins that once separated them and collided with the North China and South China plates (Fig. 1) (e.g., Taira 2001; Barnes, 2003; Metcalfe, 2006; Seton et al., 2012; Zahirovic et al., 2014; Li et al., 2017; in press). The tectonic framework of northeast Asia was inherited from the long-term convergence between the (proto-) Pacific and Eurasian plates and cyclical Gondwana-derived terrane detachment (Metcalfe, 2006; Seton et al., 2012; Zahirovic et al., 2014). The kinematics and evolution of the western Pacific subduction and the northeast Asian continental-margin deformation is a first-order tectonic process whose nature and chronology remain controversial. Although many geological investigations have proposed that the structural deformation, rifting, thrusting, and destruction of the North China Craton were related to the western Pacific plate's subduction, plate motion models around Eurasia have been ambiguous, and the deformation mechanism of northeast Asia has remained subject to debate, resulting in poorly constrained dynamics for plate tectonics in east Asia and the western Pacific (e.g., Engebretson et al., 1985; Sager, 2006; Beaman et al., 2007; Zhu et al., 2011; Seton et al., 2012). Newly developed global plate motion models (Seton et al., 2012; Müller et al., 2016) can provide initial or time-dependent tectonic boundary conditions through time for models of basins and orogenic belts, as well as initial or time-dependent surface boundary conditions for plate-driving forces and the coupling of plates to the deep mantle (Müller et al., 2016). Here, we use the GPlates software and onshore and offshore geological evidence to constrain the nature and chronology of the deformation of northeast Asia and the surrounding plate motions. Accordingly, we implement a reconstruction of the plate subduction, continental accretion or collision

and basin-mountain deformation in northeast Asia since 200 Ma. The kinematic scenario that best reproduces the large range of deformation velocities and directions and plate subduction and collision as interpreted from geological observations should closely represent the tectonic evolution of northeast Asia; this scenario should also facilitate an exploration regarding how the interactions between the convecting mantle and the plates cause major perturbations in plate-driving forces and global or regional tectonic events (Müller et al., 2016).

Fig. 1. Structural map of northeast Asia. The inset map shows the present-day plate tectonics in Eurasia and eastern Tethys. 1. Jurassic-early Early Cretaceous basin (or accreted terrane); 2. Cretaceous basin; 3. Tertiary basin; 4. Late Paleogene-Neogene basin; 5. Neogene basin; 6. Oceanic crust; 7. Block or uplift in a marine basin; 8. Pre-Jurassic suture; 9. Jurassic suture or subduction zone; 10. Cretaceous suture or subduction zone; 11. Tertiary suture or subduction zone; 12. Present-day subduction zone; 13. Normal fault; 14. Thrust fault; 15. Strike-slip fault; 16. Ridge and transform fault. WHB = West Hills of Beijing; CDT = Chengde thrust; XLT = Xinglong thrust; KCTL = Kashiwazaki-Choshi Tectonic Line; FMB = Fossa Magna basin; JT = Jiamusi terrane; NBT = Nadanhada-Bikin terrane; ST = Samarka terrane; Z-A-TT = Zhuravlevka-Amur-Taukha terranes; MT = Mino-Tanba terrane; RK = Ryoke terrane; CB = Chichibu terrane; SB = (older and younger) Sanbagawa terranes; SM = Shimanto terrane. Modified from the China Geological Survey (2004) and Ren et al. (2013).

2. Methods

Global plate motion models provide reconstructions with four components: an absolute reference frame, the relative motions between tectonic plates that are linked through a plate circuit, the geomagnetic polarity timescale, and a collection of plate boundaries that combine to form a network of continuously closed plate polygons (Gurnis et al., 2012; Seton et al., 2012). However, not all surface regions are governed by the rules of rigid plate motion. Most regions undergo permanent deformation, which usually occurs slowly over long timescales. Thus, our GPlates-based northeast Asian deformation reconstruction since 200 Ma involves the following procedures

(Gurnis et al., 2012): (1) strain recovery at five deformation stages defined based on balanced-section analyses; (2) geological and seismic tomography constraints for subduction and the accretion history of the western Pacific; and (3) kinematic reconstruction implemented by creating deformation regions with features inserted within the interior of the network, integrating sequentially backward rotations of deforming features, interpolating dilatational strain rate with Delaunay triangulation, and forward computing the accumulated finite strain for strain markers. Moreover, we largely use the reconstruction methods for relative and absolute plate motion of Zahirovic et al. (2015) and Müller et al. (2016) to calculate plate motion fields.

2.1. Deformation stages and strain recovery

Northeast Asia underwent multiple deformation episodes with different mechanisms, including both extension and compression, since 200 Ma. These deformation events overlapped and transformed one another in both time and space, and their kinematic reconstruction within topological networks (deforming plates) was implemented by reconstructing individual features (faults, basin boundaries, outcrop points, etc.) backward in time. Therefore, geological observations from the field, well and seismic data from basins, and age testing and balanced cross sections serve as our primary evidence for this reconstruction, including the periods of deformation (stages) and deformation (strains) of features. Since the Jurassic, northeast Asia has mostly undergone intracontinental deformation, which developed into a fold-thrust belt-flexural basin system and a high-standing block (horst)-rift-basin system. The geochronology, well-exposed unconformities, deformation sequence and basin fill characterize the Jurassic-Tertiary deformation into five deformation stages (from oldest to youngest), namely, the Early-Middle Jurassic, Late Jurassic-earliest Cretaceous, Early Cretaceous, Late Cretaceous, and Tertiary (Figs. 2 and 3).

Fig. 2. Jurassic and earliest Cretaceous successions and deformation stages in northeast Asia. Fm = Formation.

Fig. 3. Cretaceous and Cenozoic basin fill and basin evolution in northeast Asia. WD = West Depression Group in the East China Sea basins; ED = East Depression Group in the East China Sea basins; OT = Okinawa Trough. The other abbreviations are the same as in Fig. 2.

2.1.1. Deformation period from the Jurassic to the earliest Cretaceous

The Early-Middle Jurassic and Late Jurassic-earliest Cretaceous deformation events (Figs. 1 and 2) were characterized by intracontinental shortening, which formed basement-involved fold-and-thrust and flexural basins, and the structural deformations in the Yanshan Mountains serve as models (e.g., Liu, 1998; Liu et al., 2007; Wang et al., 2008; Zhang et al., 2011; Liu et al., 2013; Zhang et al., 2014). The deformed Xingshikou Formation, which mostly consists of conglomerate, unconformably overlies Paleozoic and Proterozoic strata (Liu et al., 2007). The U-Pb ages of detrital zircons within the formation include subsidiary peaks at 198 ± 5 Ma (Liu et al., 2012) and 205 Ma (Yang et al., 2006), which indicate an Early Jurassic maximum depositional age. The Nandaling Formation, which unconformably overlies the Xingshikou Formation, consists of basalts and associated clastic rocks, with a ^{40}Ar-^{39}Ar biotite age of 180 ± 2 Ma (Davis et al., 2001) and a minimum U-Pb zircon age of 174 ± 8 Ma (Zhao et al., 2006) for the basalts. The Jiulongshan (or Haifanggou) Formation, which overlies the coal-bearing Xiahuayuan (or Yaopo) Formation, mainly consists of conglomerate, sandstone, and mudstone that is interbedded with andesitic breccia and tuff, with a ^{40}Ar-^{39}Ar age of 166.7 Ma for the tuff from the Haifanggou Formation (Chang et al., 2013; Huang, 2015) and a weighted mean U-Pb age of 154 ± 2 Ma for all the zircon grains in a sample from the Jiulongshan Formation in West Beijing (Liu et al., 2017). The Tiaojishan Formation (or Lanqi Formation) in the Yanshan Mountains, which covers the Jiulongshan and Xiahuayuan Formations, mainly comprises andesitic and basaltic breccia, conglomerate, and tuff that is interbedded with sedimentary layers. Collectively, the Ar/Ar and U-Pb ages are ca. 161-152 Ma for the Tiaojishan (the Lanqi) Formation (Davis et al. 2001; Zhao et al. 2004; Davis, 2005; Liu et al., 2007; Hu et al., 2010; Chang et al., 2013; Huang, 2015). The Tuchengzi (or Houcheng) Formation unconformably overlies the

Xiahuayuan and Tiaojishan Formations and Archean metamorphic rocks and is overlain by the Zhangjiakou Formation. The Tuchengzi Formation consists of thick, massive, or horizontally stratified conglomerate that is intercalated with massive or laminated mudstone and thin layers of pebbly sandstone. Published K-Ar, Ar-Ar, and U-Pb ages from the Tuchengzi and Zhangjiakou Formations include ca. 153-137 Ma (Davis, 2005; Davis et al., 2001; Zhang et al., 2002; Liu et al., 2015a) and ca. 136-127 Ma (Li et al., 2000; Swisher et al., 2002; Niu et al., 2003; Zhao et al., 2004; Zhang et al., 2005), respectively. Based on the geochronology and stratigraphic relations, the Xiahuayuan and Jiulongshan Formations and the Tiaojishan and Tuchengzi Formations are thought to be the depositional records of two episodic deformations during the Middle (-Late) Jurassic (ca. 174-154 Ma) and Late Jurassic-earliest Cretaceous (ca. 161-136 Ma). The overlapping ages between these two episodes may have been caused by the westward expansion of structural deformation and basin formation, which lasted longer than each deformation episode and its depositional record in the West Hills of Beijing and in the Taihang Mountains (Yang et al., 2006; unpublished data from Liu et al. (2017)).

Structurally, the NNE-trending Xinglong thrust belt in the Yanshan (Fig. 1) is represented by basement-involved thick-skinned thrusts with a typical flat-and-ramp geometry and top-to-the-northwest thrusting (Zhang et al., 1997). The northern extension of this thrust belt was unconformably covered by the stratigraphy of the Tiaojishan and Tuchengzi Formations, which demonstrates that this thrusting occurred before the Late Jurassic. The age of this episodic deformation was also constrained to be ca. 175-150 Ma by U-Pb dating and $^{40}Ar/^{39}Ar$ chronological analyses on the structure of the WNW-vergent folds and thrusts in the West Hills of Beijing and in the Taihang Mountains (Wang and Li, 2008; Wang et al., 2011). Commonly, the Late Jurassic to earliest Cretaceous thrust controlled its frontal flexural basin deposition (Liu et al., 2007; 2013; Liu et al., 2017). The deposition of the Tuchengzi Formation in the Chengde basin, which was constrained to 153-135 Ma by U-Pb zircon dating, was proven to record the south-(and north)-vergent thrusting of the Chengde thrust faults (Liu et al., 2015a). The controversial Tan-Lu fault in the

eastern North China Craton was characterized by thrust faulting or sinistral transpression during the Middle-Late Jurassic (e.g., Wan and Zhu, 1996; Zhang and Dong, 2008; Zhu et al., 2010) and is dated to ca. 165-155 Ma (Wang, 2006). The NW-trending faults in the Luxi area were characterized by dextral transpression during this period (Wang et al., 1998; Wang et al., 2008; Fig. 1). The average shortening strains were approximately 10-15% and 15-20% along the NW-trending section from the northern margin of the North China Craton to the Sulu orogen during the Early-Middle (or earliest) Jurassic and Late Jurassic to the earliest Cretaceous, respectively. However, the shortening strain before 137 Ma in the Yanshan Mountains was approximately 35-38% (Zhang et al., 2011), which was much higher than in the entire North China Craton.

After the collision between the North China and South China plates during the Late Triassic, the Qinling-Dabie orogenic belt, which was a southern margin of northeast Asia, underwent long-term suturing, intracontinental shortening and thrusting since the Jurassic (Liu et al., 2003; Liu et al., 2015b; Fig. 1). This intracontinental deformation included an orthogonal intracontinental collision and south- and north-vergent thrusting during the Early and Middle Jurassic. This deformation also included the indentation of South China into the Qinling-Dabie Orogen and arc-shaped extrusions of the southern Qinling-Dabie foreland fold-thrust belt from the Late Jurassic to the Cretaceous. The shortening rate of the first phase from ca. 200-164 Ma was approximately 15%, and the shortening rate of the second phase from ca. 163-100 Ma was approximately 50% in the Daba Mountains (Li, 2015; Li et al., 2015; Li et al., 2017; Fig. 1).

2.1.2. Cretaceous deformation period

The Cretaceous extensional deformation (Figs. 1 and 3) began at the deposition of the Zhangjiakou (or Yixian) volcanic rocks in a rift basin, which unconformably covered the underlying Tuchengzi, Tiaojishan, Jiulongshan, and Xiahuayuan Formations, among others. Published K-Ar, Ar-Ar, and U-Pb ages from the Zhangjiakou Formation are ca. 136-127 Ma (Li et al., 2000; Davis et al., 2001; Niu et

al., 2003; Cope, 2003; Zhao et al., 2004; Gao et al., 2004; Zhang et al., 2005). The time of the extension as demonstrated by the metamorphic core complexes in the Yiwulüshan, Louzidian, Yunmengshan and Hohhot areas, among others (e.g., Davis et al., 1996; Davis et al., 2002; Darby et al., 2004; Wang and Zheng, 2005) was mainly constrained to be 145-110 Ma. Zircon U-Pb and $^{40}Ar/^{39}Ar$ radiometric ages and apatite fission-track data indicated granitic intrusions from 146-125 (130) Ma and tectonic exhumation and ESE-trending stretching lineation at ca. 130-120 Ma in the Taihang Mountains (Wang et al., 2008). Thirty-four laser ablation (LA)-ICPMS zircon U-Pb dates for plutons and volcanic rocks along the Tan-Lu fault zone indicated that extension-related magmatism began as early as 136 Ma. The development of pre-eruption rift basins along the Tan-Lu fault zone during the earliest Early Cretaceous further constrained the onset time of the Tan-Lu normal faulting to ca. 145 Ma (Zhu et al., 2010). The ^{40}Ar-^{39}Ar and U-Pb dating of basalts, andesites, and rhyolites in the Tamulangou Formation from the Xing'anling Group, which is exposed at the base of the Hailar rift basin, yielded an age range of 164-147 Ma (Wang et al., 2006). The ^{40}Ar-^{39}Ar dating of rhyolite in the lower and upper portions of the Xing'anling Group in the Erlian basin produced plateau ages of 141.6 ± 1.6 Ma and 129.1 ± 1.9 Ma, respectively (Chen et al., 2009). Therefore, the transition time from early shortening to extension deformation has been suggested to be ca. 136 Ma throughout most of northeast Asia (e.g., Liu et al., 2004; Cope et al., 2010). However, the western, middle, and eastern rift-basin zones, which mainly consist of the Hailar-Erlian basins, Songliao-Bohai Bay basins, and Sanjiang-Laiyang basins, formed at ca. 157 Ma only in the north-western part of northeast Asia (Fig. 1).

The Erlian and Hailar basins (Figs. 1 and 3) in the western province were filled with sedimentary successions in the uppermost Jurassic-Lower Cretaceous syn-rifting phase, which was dominated by a fluvial-lacustrine depositional environment with andesite, tuff, rhyolite, and basalt; these basins were also filled in the uppermost Lower Cretaceous to Upper Cretaceous post-rifting phase, which was dominated by a fluvial environment (Bonnetti et al., 2014). The syn-rift event in the western province was defined to be ca. 157-115 Ma (A et al., 2013; Wang et al., 2006; Chen et al.,

2009). Structural-balance recovery modelling in the Erlian basin indicated both high- and low-strain extensional regimes, and the strains ranged from 6-15% (Qu et al., 2013). Afterward, the entire western province changed to a stage of post-rift subsidence, uplift, and compressive inversion (A et al., 2013).

The Songliao basin (Figs. 1 and 3) in the middle province was filled with sedimentary successions of coal-bearing fluvial, floodplain, lacustrine, and fan-delta strata and widespread volcanic rocks, dating to ca. 134-110 Ma, in syn-rifted grabens and half-grabens; these grabens were isolated by horst blocks and post-rift strata (110-65.5 Ma) of alluvial fan, fluvial, floodplain, lacustrine, and delta deposits (Feng et al., 2010; Wu et al., 2009). Anomalous subsidence in this basin permitted the accumulation of thick post-rift deposits, which were typically 3,000-4,000 m-thick with a maximum thickness of 6,000 m, that extended beyond the rift blocks and on-lapping across the basin margins to form a large uniform basin, in contrast to other Cretaceous basins in northeast Asia (Feng et al., 2010; Li and Liu, 2015). We found that the predicted post-rift subsidence that was based on the uniform stretching model that followed earlier lithospheric thinning events was much lower than the subsidence that was provided by back stripping. The residual subsidence, i.e., the difference between the modelled and observed (or back-stripped) subsidence, during the post-rift stage was between 200 m and 800 m (Li and Liu, 2015). This regional residual subsidence suggests a possible deficit in the negative buoyancy (mantle loading) that was induced by downward drag pressure from the subducting western Izanagi slab and asthenospheric mantle flow beneath the Songliao basin, which was similar to what occurred in the Western Interior Seaway basin of the United States (Liu and Nummedal, 2004; Liu et al., 2014). In addition, three compressional inversion episodes at ca. 87 Ma, 82-79 Ma, and 65 Ma interrupted the long-term cooling subsidence and residual subsidence, which produced folding and uplift (Song et al., 2014). Cross-section restoration in the Songliao basin indicated that the horizontal crustal extension during the syn-rifting stage was estimated to have been 10.6-25.5% (Ge et al., 2012) and that the WNW-ESE-trending shortening strains at ca. 87 Ma were approximately 8-12% in the northern Songliao basin.

In the Yanshan Mountains and the North China Craton to the west of the Tan-Lu fault, the period of basement rifting that occurred in the Early Cretaceous (136-110 Ma) rift basins coincided with the syn-rift stage of the Songliao basin (Fig. 3). However, these rift basins lacked thermal subsidence during the post-rift stage (since 100 Ma), in contrast to the abnormally rapid subsidence that occurred in the Songliao basin after ca. 100 Ma (Li and Liu 2015). We believe that this lack of thermal subsidence in the Cretaceous rift basins was caused by anomalous uplift (minimal anomalous uplift) between ca. 300 m and 400 m according to the results of a 1D strain rate inversion model (Li and Liu, 2015).

The Sanjiang, North Yellow Sea, Laiyang, and South Yellow Sea basins sporadically developed in the eastern rift-basin zone (Figs. 1 and 3). The basin-controlled normal faults on the eastern margin of the North China Craton and the northeast Yangtze showed a change from an Early Cretaceous NNE-trending distribution to a Late Cretaceous ENE-WSW (or E-W to WNW-ESE)-trending distribution, which controlled a nearly E-W-trending depocentre arrangement in the southern and northern South Yellow Sea basin, Hefei basin, and Laiyang basin (Zhu et al., 2012). These structural patterns suggest that the Early Cretaceous rifting should have been driven by a nearly WNW-ESE extension and that the Late Cretaceous rifting was driven by a nearly NNW-SSE extension from the dextral movement of the Tan-Lu and its branching faults (Shinn et al., 2010). The U-Pb detrital zircon dating of sedimentary rocks and K-Ar dating of basaltic-andesitic rocks in the Laiyang basin constrained the two rift episodes to ca. 130-109 Ma and 80-60 Ma (He et al., 2015; Wang et al., 2016; An et al., 2016). The nearly E-W-trending extensions were 9.4%, 2.95%, and 7.12%, and the nearly N-S-trending extensions were 10.29%, 4.41%, and 16.03% at ca. 130-120 Ma, 120-109 Ma, and 80-60 Ma, respectively, in the Laiyang basin (Tong, 2007). The nearly N-S-trending Late Cretaceous extension strains in the southern and northern South Yellow Sea basin were approximately 6-10% (Shinn et al., 2010; Xiao and Tang, 2014).

The Sanjiang basin (Figs. 1 and 3), which is located in the northern area of the eastern rift-basin zone, was inverted to thrusting and compression during the Late

Cretaceous. The western boundary of this basin was created by major post-depositional, east-vergent thrust faults, and the eastern section of the basin was created by west-vergent asymmetric folds and imbricated thrust faults, some backthrusts and pop-up structures, and flexural molasse depozones in front of the thrust faults (Zhang et al., 2012). Cross-section restoration shows that the shortening strains were approximately 8-18%.

2.1.3. Tertiary deformation period

Cenozoic rift basins (Figs. 1 and 3) developed across northeast Asia. Tertiary extensional deformation began with an unconformity between the Paleocene or Eocene and its underlying strata and included high-angle normal faults and their controlled horsts and rift basins (Qi and Yang, 2010). East-dipping, high-angle normal faults along the eastern margin of the Taihang Mountains formed at ca. 70-60 Ma, which was constrained by the $^{40}Ar/^{39}Ar$ dating of sericite minerals. The $^{40}Ar/^{39}Ar$ dating of syn-deformation chlorite and K-feldspar minerals that were parallel to a down-dip stretching lineation from the east-dipping normal faults along the southern segment of the Tan-Lu fault zone yielded cooling ages of ~75-70 Ma, which were interpreted as the timing of slip along the normal faults (Wang and Zhou, 2009). Here, we constrained the initial time of the Tertiary extension deformation in northeast Asia to ca. 66-60 Ma.

The Bohai Bay basin (Figs. 1 and 3) is bounded by NNE-striking normal and dextral faults at the eastern and western margins and nearly E-W-trending normal faults at the northern and southern margins (Qi and Yang, 2010), which produce an anti-“S” shape. The basin was filled with Cenozoic sedimentary successions, including the Kongdian, Shahejie, and Dongying Formations during the syn-rift stage (ca. 60-24 Ma) and the Guantao, Minghuazhen, and Pingyuan Formations during the post-rift stage (ca. 24-0 Ma) (Qi and Yang, 2010). Balanced-section analysis of seismic sections in different orientations revealed four phases of rifts and extensions in the syn-rift stage of this basin. The NW-SE-trending extension was initiated at the southern part of the Bohai Bay basin (including the south-eastern part of the Bohai

Bay basin in the Jiyang Depression) during the first phase of the Paleocene to the early Eocene (the Kongdian Formation to Member 4 of the Shahejie Formation), and the extension strains were as high as approximately 4-9% across the NW-SE-trending and S-N-trending sections. During the second phase of the Middle Eocene, the rifting migrated from south to north, and the entire basin was extended along the NNE-SSW-trending normal faults. The extension strains greatly increased to approximately 9-19% across the NW-SE-trending sections. These two rifting phases constituted the first rifting stage in the basin. The rifting during the third phase of the Late Eocene (Members 1 and 2 of the Shahejie Formation) weakened, but the extension strains remained at approximately 2% in the middle of the basin (Bohai Bay area) across the N-S-trending section. During the fourth phase of the Oligocene (Dongying Formation), the extension strains in the middle of the basin increased to approximately 2.6% along the N-S-trending section. Therefore, the middle of the Bohai Bay basin was the rift's centre, with a nearly N-S-trending extension during the second rift stage, including the third and fourth rift phases. The Cenozoic structures of the syn-rift stage mainly include NNE-trending normal fault systems and overprinted, nearly E-W-trending normal fault and NNE-trending, right-lateral strike-slip fault systems. The growth-strata characteristics in the seismic sections demonstrate that the older normal fault systems controlled the deposits of the Paleocene to Middle-Eocene Kongdian Formation and lower Shahejie Formation during the first rift stage. These characteristics also show that the younger normal and strike-slip fault systems controlled the local fills in the Late Eocene to Oligocene upper Shahejie Formation and Dongying Formation during the second rift stage. Therefore, the extension kinematics changed from a NWW-SEE or NW-SE-oriented extension and NNE-trending rift basin formation (and NE- or NEE-trending transtensional basin formation in the Jiyang Depression) during the first rifting stage (Li et al., 2012a; 2012b) to nearly a N-S-oriented extension and the formation of nearly E-W-trending normal faults and NNE-trending dextral strike-slip faults during the second rifting stage. These two stages of extension also triggered the rifting of the Weihe basin in the south-eastern Ordos and South Huabei basins. The Dabie Block migrated

southward and rotated clockwise to accommodate these extensions.

The Yellow Sea basins (Figs. 1 and 3), including the North and South Yellow Sea basins, also developed with Paleogene syn-rift grabens and Neogene post-rift depressions. The Cenozoic rifts were mostly oriented to the NEE in the South Yellow Sea basin. Structural-balance reconstruction analyses indicated that the extensional strains were approximately 4-10% during the Eocene and that the reversal shortening ratios were approximately 0.2-1% during the Oligocene and Neogene along the interpreted NW-trending seismic sections in the northern depression of the northern South Yellow Sea basin (Li et al., 2013). The nearly N-S-oriented extensional ratios in the southern South Yellow Sea basin were ca. 3-6% during the Eocene and approximately 3-4% during the Neogene (Xiao and Tang, 2014).

The East China Sea basins (Figs. 1 and 3), including the East China Sea Shelf basin and the Okinawa Trough, developed a two-layered syn-rift and post-rift architecture (Suo et al., 2013). The temporal evolution differed between the West Depression Group and the East Depression Group in the East China Sea basins. In the West Depression Group, most of the normal faults terminated before the end of the Late Paleocene, and the Paleocene Yueguifeng, Lingfeng, and Mingyuefeng Formations were rifting deposits. The Eocene Oujiang and Wenzhou Formations unconformably overlie the rifted grabens and horsts, which implies that the West Depression Group began its post-rift subsidence stage after the Eocene. In the East Depression Group, the rifted sub-basins were filled with the Eocene Pinghu Formation and the Oligocene Huagang Formation, and the entire depression was then covered by the Miocene Longjing, Yuquan, and Liulang Formations, which suggests that this depression group underwent a uniform post-rift subsidence stage during the Miocene. Finally, the Okinawa Trough acted as a rift basin during the Miocene and Pliocene. As the rifting events migrated eastward, compressional inversion structures, including folding and uplifting, successively formed in the West Depression Group during the Eocene and Oligocene and in the East Depression Group during the Miocene because of accommodation adjustments. Therefore, the East China Sea basins were characterized by three stages of rifts that migrated eastward from the

West Depression Group to the Okinawa Trough. The structurally balanced reconstruction across the Lishui and Jiaojiang Sags in the West Depression Group indicated that the highest extensional ratios were ca. 18-6% during the Early Paleocene, which recorded the first episodic rifting in the southern West Depression Group. The highest extensional ratios in the East Depression Group were ca. 6-2.5% during the Eocene, which recorded the second episodic rifting in the East Depression Group. The eastward migration of these rifting events may relate to the retreat of the subduction trench (Yoshida, 2017).

The Japan Sea basin is located behind (to the west of) the Japanese Islands (Figs. 1 and 3). The rapid rifting and subsidence of the Japan Sea basin began at 21-24 Ma, accelerated approximately 17 Ma, and reached its most rapid rate at 16-14 Ma; this basin changed to progressive compression from 15-5 Ma (e.g., Chough and Barg, 1987; Yamaji, 1990; Kato, 1992; Tamaki et al., 1992; Jolivet et al., 1994). Japan Sea ODP drilling results revealed that the basement volcanic materials were 17-21 Ma and that the oldest intersected sediments were 13-18.5 Ma (Tamaki et al., 1992; Nohda, 2009). Therefore, the basin began with its syn-rift stage at ca. 30-28 Ma, followed by the post-rift and inversion stage at ca. 15-14 Ma.

Paleomagnetic evidence has demonstrated opposite rotations for southwestern and northeastern Japan (e.g., Kawai et al., 1961; Otofuji, 1996; Hoshi and Yokoyama, 2001). SW Honshu and northern Kyushu consistently rotated clockwise. In contrast, the areas to the northeast of the Kashiwazaki-Choshi Tectonic Line in NE Honshu and western Hokkaido predominantly rotated counter-clockwise. The amount of rotation increased from less than 10° to more than 20° eastward in SW Japan and from ca. 20° to ca. 40° northward in NE Japan (Martin, 2011). Analyses of the mean declinations compared with age and fourth-order polynomials by Otofuji (1996) suggested that the rotation began by 22-25 Ma, and the fastest rotation occurred from 16-14 Ma. Between SW and NE Honshu, a major arc-orthogonal rift, the Fossa Magna, developed from 23-18 Ma to 14 Ma, which was thereafter inverted from 15 Ma to the present because of opposite terrane rotations (Martin, 2011).

The western Japan Sea basin (and eastern Korean margin) is rimmed by

fundamental elements of rift architecture, including the seaward succession of a rift basin and an uplifted rift flank that passes into the slope, which are typical of a passive continental margin. Analyses of the rift fault patterns by Kim et al. (2007) suggested that the rifting at the Korean margin, which is the SW margin of the Japan Sea basin, was primarily controlled by normal faulting from extension rather than strike-slip deformation. To the east of the Japan Sea basin, a high-temperature ductile shear zone with a large positive flower structure extends N-S to Central Hokkaido and Sakhalin. This shear zone formed during the Oligocene-Miocene as the locus of dextral-oblique subduction between the Okhotsk Sea and Eurasia, and it exhibits a dextral-transpressive sense of deformation (Kimura et al., 1983; Lallemand and Jolivet, 1986; Kimura and Tamaki, 1986). The structural pattern in the Japan Sea basin suggests that the origin of this back-arc extension exhibited a different extension ratio and orientation. Because of the counter-clockwise rotation of north-eastern Japan and the clockwise rotation of south-western Japan, the highest extensional strains in the Japan Sea were approximately 118% along the NNW-SSE-trending section and approximately 65.8% along the NW-SE-trending section from 30 to 14 Ma.

Therefore, the deformation episodes in northeast Asia occurred during the Early-Middle Jurassic (201-164 Ma), the Late Jurassic-earliest Cretaceous (163-137 Ma), the Early Cretaceous (136-110 Ma), the Late Cretaceous (80-67 Ma), and the Cenozoic (66-0 Ma; 56-0 Ma; 30-15 Ma) (Figs. 2 and 3). In some regions, the deformation timing may have extended beyond or differed from these ages, and some different kinematic deformation events may have briefly existed during these episodes because of differential deformation and local tectonic stress-field influences.

2.2. Subduction and accretion history of the western Pacific

The plate boundaries were re-intersected through time in GPlates (www.gplates.org) to continuously define closed plate polygons that included all of Asia and the western Pacific based on the methodology of Gurnis et al. (2012). The suture belts that were preserved in northeast Asia recorded the subduction of the Okhotsk Sea and the collision of North China and South China (e.g., Liu et al., 2015c).

The onshore geological record from East Asia and its eastern margin provides evidence for the opening and closure of marginal basins, plate subduction, and terrane accretion. We incorporated onshore geology evidence, particularly volcanism that was associated with suturing events, the accretion of exotic terranes, ophiolite emplacement, large-scale crustal deformation (e.g., Taira, 2001; Barnes, 2003; Wu et al., 2007; Isozaki et al., 2010a; Charvet, 2013; Wakita, 2013; and Ren et al., 2016; Table 1; Fig. 1) and seismic tomography architecture in the deep mantle. We used this evidence to interpret the plate boundaries along the northeast Asian continental margin (Fig. 4a).

Table 1

Accretionary events along East Asia's continental margin

Subduction zone	Terranes or complexes	Accretion age	References
Hida and Hitach-Takanuki belts	Oki and South Kitakami complexes	Late Triassic	Barnes, 2003; Isozaki et al., 2010a
Mudanjiang belt	Jiamusi	Jurassic-Early Cretaceous	Wu et al., 2007; Ren et al., 2016
Mino-Tanba and N. Kitakami-Oshima belts	Mino-Tanba, Ryoke, Chichibu, and N. Kitakami-Oshima complexes	Jurassic	Barnes, 2003; Isozaki et al., 2010a
Sikhote-Alin belt	Nadanhada terrane	ca. 137-130 Ma	Zhou et al., 2014
	Taukha terrane	Post-Valanginian stage	Kemkin and Taketani, 2008; Malinovsky et al., 2008
Older Sanbagawa sub-belt	Chichibu complex	Earliest Cretaceous	Wakita, 2013
Younger Sanbagawa sub-belt	Northern Shimanto complex	Mid- to Late Cretaceous	Wakita, 2013; Barnes, 2003
North Shimanto belt	Hidaka, Kamuikotan, and Tokoro complexes in Hokkaido	Mid-Cretaceous to Miocene	Wakita, 2013; Barnes, 2003
Sakhalin belt	Susunai, Tonino-Aniva, Ozersk, and West Sakhalin terranes	Aptian-Paleocene	Zharov, 2004
South Shimanto belt	Southern Shimanto complex	Paleogene to Miocene	Wakita, 2013

Fig. 4. Reconstruction of the western Pacific plate subduction zones since 200 Ma. A. Reconstructed locations of the western Pacific plate subduction zones at 174 Ma, 137 Ma, 120 Ma, 90 Ma, 30 Ma, and 0 Ma, which show advancing subduction from 200-137 Ma and trench-retreating subduction from 136-0 Ma. B. Depths (2,236 km, 1,830 km, and 1,559 km) and the corresponding ages (100 Ma, 80 Ma, and 66 Ma, respectively) of the western Pacific subduction zones, which were interpreted from seismic tomography by Li et al. (2008). Here, the mantle sinking rates are suggested to be 3 and 2 cm/yr in the upper and lower mantles, respectively (Zahirovic et al., 2016), for the western Pacific slab when it was not attached to a subduction plate. C. Vertical cross section from MIT-P (Li et al., 2008) at 39◦N from the Japan Sea to the Ordos basin. The anomaly reflects the subducted Pacific and Izanagi oceanic plates. The slab (Izanagi) in the lower mantle is interpreted to represent advancing subduction with the slab lying at a depth below 2,000 km to the east and shallowing to the west, as well as retreat subduction with the slab shallowing eastward at a depth of 2,000 km, after which the slab lay in the transition zone at depths between 660 km and 410 km.

2.2.1. Geological constraints for the western Pacific plate's subduction zones

The Jiamusi terrane (Table 1; Fig. 1) is located in the Paleozoic Central Asian Orogenic Belt or Altaid Collage (Sengör et al., 1993) in northeast China. This terrane extends northward into the Bureya Massif and eastward into the Khanka Massif in Far East Russia (Natal'in & Borukayev 1991; Cao et al. 1992). The Jiamusi Massif consists of the Mashan and Heilongjiang complexes alongside deformed and undeformed granitoids (Wu et al., 2007). The Heilongjiang complex, which is located at the western margin of the Jiamusi terrane, predominately consists of granitic gneiss, marble, mafic-ultramafic rocks, blueschist, greenschist, quartzite, muscovite-albite schist and two-mica schist that were tectonically interleaved, which indicates a mélange. The ultramafic rocks, blueschist, greenschist and quartzite (chert) were similar to components in ophiolite. Wu et al. (2007) suggested that the early-stage components of the Jiamusi terrane probably formed a component of an exotic block from Gondwana that was affected by Late Pan-African orogenesis and collided with the Asian continental margin during the Early Jurassic. The subduction of oceanic

crust between the Jiamusi block and the eastern Central Asian Orogenic Belt formed a huge volume of Jurassic granites (ca. 190-173 Ma) along the north-eastern margin of China (Xu et al., 2013). The $^{40}Ar/^{39}Ar$ dating of biotite and phengite from the granitic gneiss and mica schist yielded a late Early Jurassic metamorphic age between 184 and 174 Ma. The collision of the Jiamusi terrane with the Mongol-China block to the west along the Mudanjiang Fault was the result of circum-Pacific accretion.

The Nadanhada-Bikin terrane (Fig. 1), which is located to the east of Jiamusi in northeast Asia and was identified by Kemkin (2012), consists of at least three specific age fragments of a primary sequence of sedimentary cover that once overlaid the paleo-oceanic plate and then folded. The biostratigraphic ages of the pelagic chert/terrigenous sedimentary layers are Pliensbachian, Bajocian, and Oxfordian-Tithonian. These layers' formation involved the structural emplacement of Jurassic oceanic-crust-derived tectonostratigraphic (volcano-sedimentary) complexes of at least three different ages into the Jurassic accretionary prism of the Sikhote-Alin fold belt (Kemkin, 2012). A paleomagnetic study suggested that the accretion of these terranes did not end until the Late Cretaceous (Ren et al., 2016). The westward subduction and terrane accretion along the western Paleo-Pacific plate (Izanagi plate) drove the shortening and volcanism of calc-alkaline series (190-173 Ma) (Xu et al., 2013) along the eastern margin of northeast Asia to form a continental-arc orogenic belt from ca. 201-137 Ma.

This accretion event may have extended to the south of Japan's Honshu Island, and the area of proto-Japan along the inner edge of the trench experienced the accretion of bulldozed oceanic floor sediments and the Permian Akasaka-Kuzuu seamount cluster at ca. 150 Ma (Charvet, 2013, Isozaki et al., 2010a). The Jurassic-Early Cretaceous accretionary complexes include the Mino-Tanba, Ryoke, Chichibu and North Kitakami-Oshima belts, which constitute the current archipelagic basement (Barnes, 2003; Wakita, 2013) (Fig. 1; Table 1). Similarly, this accretional zone is paralleled by a contemporaneous Ryoke and Gosaisho granitic belt that was once situated along the edge of northeast Asia (Barnes, 2003; Isozaki et al., 2010a). Therefore, the terranes' accretion was represented in our GPlates model by building

topologies with a subduction zone (gpml feature) that subducted to the west since 200 Ma and collided with the Eurasian plate at ca. 137 Ma (Fig. 4a). This subduction zone advanced westward to accommodate the shortening deformation in northeast Asia during the Jurassic and earliest Early Cretaceous.

The Cretaceous accretional events in northeast Asia (Fig. 1; Table 1) were represented by the accretion of the Nadanhada and Taukha terranes along the Sikhote-Alin belt in north-eastern China and the far eastern part of Russia (Zhou et al., 2014; Kemkin and Taketani, 2008; Malinovsky et al., 2008), as well as the South Kitakami-Kurosegawa block along the Sanbagawa and North Shimanto accretional zones in Shikoku. These Cretaceous accretional events were also represented by the south-eastern margin of Honshu and Hokkaido (Barnes, 2003) and a parallel Kyoke granite belt that was generated in the arc and that extended to the southern margin of South Korea and Sikhote-Alin in Russia (Taira, 2001). These accretional complexes are assumed to have been continuous along the northeast Asian continental margin, but the Shimanto belt was discontinuous between western Japan and Hokkaido because of the deformation of the island arc. Zhou et al. (2014) suggested that the Raohe complex in the Sikhote-Alin belt finally accreted to northeast Asia between 137 and 128 Ma. The Sanbagawa belt was divided into two sub-belts by Isozaki et al. (2010b). The older sub-belt was characterized by the accretion of the earliest Cretaceous Chichibu belt complex, and the younger sub-belt was subjected to the accretion of the Mid-Late Cretaceous Shimanto belt complex (Wakita, 2013; Barnes, 2003). Wakita (2013) and Barnes (2003) suggested that the accretional activities of the Hidaka, Kamuikotan, and Tokoro complexes along the North Shimanto belt (to the east of Sikhote-Alin) in Hokkaido occurred from the Middle Cretaceous to the Miocene, contemporaneous with the younger Sanbagawa sub-belt. Therefore, the western Pacific subduction zone exhibited two episodes of trench-retreat accretional subduction from the Early Cretaceous to the Late Cretaceous and was represented in the GPlates model by setting the subduction zone features and topological network to migrate from the reconstructed location of the Sikhote-Alin and older Sanbagawa sub-belts in the west to the North Shimanto belt in the east from ca. 130-90 Ma (Fig.

4a).

After ca. 90 Ma, sharp geodynamic changes were recorded in the stratigraphic sequences by the regional unconformity that developed before the Coniacian in the Sanjiang basin in north-eastern China (Zhang et al., 2015). Widespread uplifting and erosion, which corresponded to the unconformity surface, matched the subsequent inversion of drainage patterns by sourcing from the eastern coastal fold-thrust belt along the continental margin. The retro-arc foreland ultimately produced episodic, short-term folding and thrusting across north-eastern China in both the Sanjiang basin and its western Songliao basin during the Late Cretaceous (Feng et al., 2010; Zhang et al., 2012). These changes were compatible with surface uplift cause by the shifting of the tectonic regime from a retro-arc extensional setting to a contracting setting and from trench retreat to short-term trench advancement. This marginal tectonic process from ca. 88-80 Ma was represented in the GPlates model by a westward-advancing subduction zone. Unfortunately, we have not found any evidence of such tectonic shifts along Asia's south-eastern margin.

The Tertiary accretional events were supplemented based on reconstructions by Seton et al. (2012) and Seton et al. (2015). The early accretion included the accretion of the Shimanto and Okinawa blocks into an early accretional margin along northeast Asia in Kyushu, Shikoku, and southern Honshu in Japan at ca. 60 Ma. Top-to-the-SE thrusts, accretionary wedge growth, and a tectonic mélange developed along the South Shimanto belt because of this accretion during the Early-Middle Eocene (Raimbourg et al., 2014). After this accretion, the sub-parallel subduction of a mid-ocean ridge between the Izanagi and Pacific plates occurred at ca. 55 Ma, which was intersected along East Asia (Seton et al., 2012; 2015). Later accretion occurred at ca. 15 Ma when eastern Hokkaido, which contained an arc from the subduction of the Pacific Plate beneath the Okhotsk Plate, collided with western Hokkaido.

Therefore, the western Pacific subduction was characterized by sub-parallel, eastward trench-retreat subduction with some trench advancement and terrane accretion since the earliest Cretaceous. This subduction was also indicated by sub-parallel accretion zones, Jurassic-to-Cretaceous granite zones, and

basin-mountain distributions. However, the clockwise rotation of the Philippine Sea plate reorganized the plate boundaries and induced the south-westward subduction of the southern Pacific plate beneath the northern Philippine basin and the perpendicular subduction (in a roughly E-W orientation) and northward migration of the Izu-Bonin Trench-Arc system along the western Pacific subduction zone after 48 Ma. The rotation of the Philippine Sea plate ceased at ca. 34 Ma. The Izu-Bonin-Mariana Trench-Arc system subducted beneath southwestern Japan (southwestern Honshu and Shikoku) and the Japan Sea, and the Philippine Sea plate continued to subduct to the northwest beneath the eastern Asian continent margin (Seton et al., 2012). This accelerated subduction of the Philippine Sea plate beneath the Eurasian plate along the Ryukyu Trench and Nankai Trough may have largely contributed to the extending, stagnated slab feature above the 670-km discontinuity (Huang et al., 2006). This accelerated subduction may also have been linked to the nearly N-S extension in the Bohai Bay basin and Japan Sea basin. This hypothesis is demonstrated by the plate motion patterns.

2.2.2. Seismic tomography constraints for the western Pacific plate's subduction zones

The accretion belts identified by geological evidence indicate their relative position with respect to the interior of northeast Asia and configuration because of the modification of later plate-tectonic displacements. Seismic tomographic images have helped to link the position of subduction zones to the deep mantle structure around eastern Asia (Zahirovic et al., 2016). Generally, the approach of estimating the longitudinal position of past oceanic subduction zones has been applied globally to derive a subduction reference frame by assuming vertical sinking and constant sinking rates (Butterworth et al., 2014). The slab sinking rates from numerical mantle convection models in Butterworth et al. (2014) suggested a global mantle sinking rate of 1.5 to 2.0 cm/yr, which is consistent with a "free sinking rate" (i.e., when not attached to a subducting plate) of 3 and 2 cm/yr in the upper and lower mantle, respectively (Zahirovic et al., 2016). Based on an assumed vertical slab sinking rate of

3 and 2 cm/yr in the upper and lower mantle, we used a global P-wave seismic tomographic model (Li et al., 2008) to infer the subduction history from post-Jurassic subduction and the longitudinal positions of previous Pacific subduction zones at 100 Ma, 80 Ma, and 66 Ma (Fig. 4b). All three subduction zones outlined the eastern boundaries of high-velocity slab remnants at tomographic depth slices of ca. 2,236 km, 1,830 km, and 1,559 km. The estimated longitudes of the subduction zones retreated eastward, which is likely consistent with the patterns provided by geological evidence. Based on the early advance of subduction and later retreat events, the positive seismic velocity anomalies that were interpreted as remnant slabs in the deep mantle represent slab lying at a depth below 2,000 km to the east, shallowing eastward at a depth of 2,000 km, and then lying at the transition zone at depths between 660 km and 410 km (Fig. 4c). Therefore, we interactively derived and modified the finite Euler rotations of subduction zone features using GPlates (Boyden et al., 2011) and placed these features in their positions through time along the eastern margin of Asia (Fig. 4b). These reconstructed, continuously closing plate polygons have covered East Asia and the western Pacific since 200 Ma based on the methodology of Gurnis et al. (2012).

2.3 Reconstructing a deforming plate

The deformation was determined in GPlates by building a reconstruction with continuously closing plates (Gurnis et al., 2012) and networks that track finite deformation (Gurnis et al., in preparation). The areas of deformation were restricted to defined boundaries in time and space, and the deformation and velocity fields were interpolated between control points. The regional reconstruction with deformation was confined to the north-eastern section of the continent within the context of a global reconstruction that comprised both deforming regions and rigid plates (dynamic plate polygons). The critical data for this reconstruction included line data to outline the deformation zone and subduction (or suture) belts, line and point data to represent the faults and geological boundaries within the deformation zone, static polygons to represent rigid micro-blocks within the deformation zone, and rotation data for the point, line, and static polygon data to represent the deformation process.

2.3.1. Creating a deformation region outline and adding features to the interior of the network

The northeast Asian continental margin has been amalgamated into a united deforming plate since the Jurassic. We created its outer boundary with a set of line features. The line data that define the outer boundary of the deformation region from 10-0 Ma include the Red River fault, the western edge of the defined deformation region, the northern edge of the defined deformation region, the Japan transform zone, the Japan subduction zone, the Okinawa Trough subduction zone, the Luzon subduction zone, and the north-western edge of the South China Sea (colour coded by feature type in Fig. 5a). Triangulations in this deformation region, which extended to southeast Asia, were used to extrapolate the velocity and model deformation across the entire deformation zone. For the duration of the model (200-0 Ma), a series of topological networks were constructed while the boundaries of the deformation region in east Asia changed.

Fig. 5. (a) Line, point, and static polygon features within the northeast Asian deformation region at 10 Ma. (b) Schematic diagram illustrating the paleo-position reconstruction of point features or points on line features from 0-24-34-42-48-60 Ma. Vectors indicate the displacement magnitude and direction of individual points (green dots) from 0-60 Ma in the Bohai Bay basin. The features with red dots indicate anchored points from 0-60 Ma. The yellow lines indicate the locations of seismic sections for defining deformation from balanced-section analysis. (c) Topological network of the northeast Asian deformation zone at 46 Ma and dilatational strain rate over the deformation network. (d) Total strain for the set of markers placed within the topological network shown at 33 Ma. Dilatational strain rates in the background, overlain with the total strain markers (accumulated during 66-33 Ma) and rendered with principle directions, with outward-facing red arrows for extension and inward-facing blue arrows for compression.

We set those sub-regions that appeared to be rigid to static polygons while the rest of the network underwent deformation. The primary rigid regions in the North

China Craton included the Ordos basin to the west and the Luxi and Jiaodong blocks in the middle, which evolved at different times (Figs. 5 and 6e). Line and point features represent primary data used to constrain deformation. They characterized faults, geological boundaries, and geological points by creating single points within each line feature or separate points for point features, which were also added to the interior of the east Asia deformation region (Fig. 5a). The deformation process within northeast Asia was defined by approximately 800 individual line and point features with different valid times.

2.3.2. Rotation of features within a deforming region

The displacements within the deforming region were transformed to rotation poles for integration with the global plate tectonic reconstructions (Gurnis et al., 2017). Each feature (point, line, or static polygon) within the network was associated with a set of rotations that described how that feature moved with respect to other (generally adjacent) features and ultimately with respect to other rigid plates and the global frame of reference. Within the deforming region, the rotations were set to be relative to the stable portion of the Eurasian plate (Plate ID: 301) from 0-150 Ma and the Asian plate from 151-230 Ma (Plate ID: 380). Consequently, the deforming region was embedded and moved with the global reconstruction. The regional reconstruction can be reused with other global plate motion models if the outer boundary of the regional reconstruction remains invariant between global reconstructions. For example, if a different global frame of reference is chosen, the regional reconstruction can be reused without modification.

Geological (1:2 500 000 geological map of China (China Geological Survey, 2004) and 1:5 000 000 Geological map of Asia (Ren et al., 2013)), geophysical and paleo-geographic data (e.g., Liu and Yang, 2000; Liu et al., 2013; Liu et al., 2015c) were used as base-maps for these reconstructions, which enabled us to trace the motions and interactions of these data through time. Our reconstructions extended from 0 to 200 Ma and were performed sequentially backward for each feature at each specified time (Fig. 5b). The paleo-position of each feature was restored using the

kinematic data for each time slice, as defined by balanced-section analysis of seismic sections in the basins, measured outcrop sections, stretching factor calculations for the rift basins, or cross-cutting sections based on geological maps in different orientations. For regions where geological data were not available, the kinematics were defined by inserting kinematic data from proximal areas or nearby deforming zones (similar to the procedure used in the regional reconstruction of western North America of McQuarrie and Wernicke, 2005). An individual point or line feature was sequentially moved backward (was rotated) from one location in time to its initial position (or initial condition) in the past along the cross-section directions based on balanced-section stretching or the shortening amounts at different stages (Fig. 5b). This kinematic reconstruction with an increment of millions of years maps onto a series of rotation poles. The deformation of any observation point was represented by its present-day coordinate, and its paleo-position was determined by interpolating rotations from nearby points with known rotations. We chose the Ordos block (basin) to be stable, and deformation or movement of any features in northeast Asia was integrated by individual rotations relative to the rigid block. This process was also used to determine the paleo-positions of the western Pacific subduction zone. Sequential backward integration of features in time through the interpolation of rotations allowed the determination of their position and "paths" in the past (Gurnis et al., 2017). Based on these reconstructions, we also obtained a set of rotation poles for each feature, which could be used for other purposes. The displacement vector constrained the regional deformation, which is shown as a dilatational strain rate interpolated with a Delaunay triangulation (Figs. 5a, 5c, and 5d).

2.3.3. Deformation strain markers

The finite strain for a set of markers was computed. Starting with their present-day positions, we sequentially reconstructed their paths through the deformation network and then forward-integrated the accumulated finite strain at each point in time (Gurnis et al., 2017). To model the deformation fields in northeast Asia

at the different stages (200-164 Ma, 163-137 Ma, 136-101 Ma, 100-67 Ma, and 66-0 Ma), we created a set of strain marker features (points) and recorded their accumulated strain and principle axes (Fig. 5d).

3. Deformation field of northeast Asia from a reconstruction of intracontinental deformation and plate subduction

Reconstruction of western Pacific subduction, continental accretion or collision and basin-mountain deformation in northeast Asia since 200 Ma, which was based on the newly revised global plate model (Müller et al., 2016), revealed the deformation field of northeast Asia (Figs. 6, 7, and 8). This forward or backward kinematic scenario with an increment of one million years reproduced the large range of strain rates, principal components of accumulated strain, and plate subduction and collision as interpreted from geological observations. Here, we describe the deformation reconstruction and the kinematics of northeast Asia sequentially backward from 0-200 Ma.

Fig. 6. Tectono-paleogeographic maps of the Middle Jurassic (a), Late Jurassic-earliest Cretaceous (b), Early Cretaceous (c), Late Cretaceous (d), and Tertiary (Late Eocene) (e) in northeast Asia. The positions of the units were not palinspastically restored, except for the subduction zones along the western Pacific. These maps were modified from the China Geological Survey (2004) and Ren et al. (2013). The basin and structural data from the Middle Jurassic and Late Jurassic-earliest Cretaceous were modified from Liu et al. (2005b) and Liu et al. (2013). The data from the Bohai Bay basin area were modified from Qi et al. (2003). The data from the Songliao basin were modified from Feng et al. (2010). The data from the Sanjiang, Hailar, and Erlian basins were modified from Zhang et al. (2012) and A et al. (2013). The data from the East China Sea basins were modified from Suo et al. (2013). The data for the reconstruction of the subduction zones along the western Pacific were cited from the references in the text. Basins: YX = Yuxian basin; XH = Xuanhua basin; Ch = Chicheng basin; CD = Chengde basin; BP = Beipiao basin; WB = western Beijing basin. Faults: JL = Jining-Longhua thrust; SP = Shangyi-Pingquan thrust; LD =

Lingyuan-Dongguanyingzi thrust.

3.1. Cenozoic (0-66 Ma) extensional deformation

Cenozoic rift basins developed across northeast Asia (Fig. 6e). The reconstruction of the Cenozoic extensional deformation was determined through sequential backward integration by interpolating the rotations of line and point features from 0-10 and 10-24 Ma in the Okinawa Trough; from 24-56 Ma and 56-66 Ma in the East Depression Group and 56-66 Ma in the West Depression Group within the East China Sea basins; from 15-30 Ma, 30-66 Ma in the Japan Sea basin; from 0-60 Ma in the Yellow Sea basins; from 0-60 Ma in the Bohai Bay basin; and from 0-46 Ma in the satellite basins around the Ordos basin (Fig. 7a). Because rifting mostly occurred around the Ordos block and east of the Taihang Mountains during the Cenozoic, the deformation restoration was conducted by interpolating rotations from the rigid Ordos block and the western margin of the Bohai Bay basin. Next, successive rotations from nearby point and line features with known rotations were performed from west to east (Fig. 7a). Therefore, the western Pacific zone accumulated more north-western movement from 0-66 Ma.

Fig. 7. Network maps of the northeast Asian deformation zone at 0 Ma (a), 67 Ma (b), 101 Ma (c), 137 Ma (d), 164 Ma (e) showing the incorporation of the kinematic data into the rotation models during the Cenozoic (0-66 Ma), Late Cretaceous (67-100 Ma), Early Cretaceous (101-136 Ma), Late Jurassic-earliest Cretaceous (137-163 Ma), and Early-Middle Jurassic (164-200 Ma), respectively. Blue dots indicate rotating points for computing deformation; red dots indicate anchored points at specific times in the study region; vectors indicate the magnitude and direction of individual relative displacements between points; vectors are labelled in the form “t1-t2 (N)” where t1 is the beginning age, t2 is the end age, and N is the feature number (see Supplementary Table 1 for the kinematic data).

Rifting occurred in the Bohai Bay basin from ca. 60 to 24 Ma and turned into post-rift subsidence after 24 Ma. Extensional deformation from ca. 60-24 Ma was

reconstructed by detailed balanced-section data (e.g. Liang et al., 2016) relative to the western margin of the basin. In the southern part of the basin, the point feature (point 1; Fig. 7a) was displaced north-westward along the NW profile by approximately 8 km, 14 km, 3 km, and 1 km from 60-48 Ma, 48-42 Ma, 42-34 Ma, and 34-24 Ma, respectively. In the middle part of the Bohai Basin from 60-24 Ma, the three balanced sections along the NS, NW, and E-W profiles (points 2, 3, and 4; Fig. 7a) respectively indicated accumulated displacements of approximately 43 km, 42 km, and 35 km. In the northern part of the basin, the displacements along the NW profiles were approximately 19 km (point 5) and 26 km (point 6) from 48-24 Ma.

The Yellow Sea basins were located to the southeast of the Bohai Bay basin and the Tan-Lu fault and were entirely moved eastwards or south-eastwards relative to the Bohai Bay basin. The deforming restoration of the Yellow Sea basins was performed by interpolating rotations relative to points (for example, 8, 9, and 11; Fig. 7a) at the north-western margins of the basins that were based on balanced-section data (Li et al., 2013; Xiao and Tang, 2014). From 24-56 Ma, points 7 and 10 at the line feature on the southern margin of the northern South Yellow Sea basins were respectively displaced 16 km north-westwards and 9 km northwards. Point 12, at the southern margin of the southern South Yellow Sea basins, was moved northward by approximately 20 km relative to point 11 during the same time period.

The East China Sea basins rifted from west to east. In addition to the rotation related to deformation at its western extent, the balanced-section analyses for the eastern margin line feature (13) of the West Depression Group show that from 66-56 Ma, this feature was displaced north-westward by approximately 13-15 km relative to the western margin line feature (14). From 56-24 Ma, line feature 15, at the eastern margin of the East Depression Group, moved by approximately 14-15 km relative to line feature 14 (Fig. 7a). Since 24 Ma, the West and East Depression Groups in the East China Sea basins have been in a post-rifting stage with less extension and shortening through inversion (Cukur et al., 2011). From ca. 10 Ma to the present day, the Okinawa Trough underwent extension of approximately 80-170 km with the subduction zone retreat (feature 16; Fig. 7a) (Miki et al., 1990).

The forward-computed strain field in the Bohai Bay basin and its adjacent regions indicated that the principal accumulative extensional strain axes from 66-0 Ma were oriented in a NW-SE direction with dilatation strain rates ranging from approximately $4x10^{-9}$/yr to $8x10^{-9}$/yr at 48 Ma and from $2x10^{-9}$/yr to $4x10^{-9}$/yr at 28 Ma. The Yellow Sea basins were extended in a NNW-SSE (or N-S) sense with dilatation strain rates that ranged from approximately $4x10^{-9}$/yr to $6x10^{-9}$/yr at 48 Ma and from $2x10^{-9}$/yr to $3x10^{-9}$/yr at 28 Ma. The East China Sea basins extended eastward along the NWW-SEE-trending principal strain axes. The strain rates reached their maximum value of approximately $6x10^{-9}$/yr in the West Depression at 56 Ma. Next, the region of maximum strain rate migrated to the East Depression during the Eocene and Oligocene and to the Okinawa Trough during the Miocene and Pliocene; the dilatation strain rates during the Eocene ranged from approximately $3x10^{-9}$/yr to $7x10^{-9}$/yr at 48 Ma; during the Oligocene, they ranged from $>5x10^{-9}$/yr at 28 Ma. The Japan Sea basin began to extend at ca. 30 Ma in response to the anti-clockwise rotation of eastern Japan and the clockwise rotation of western Japan on both sides of the Fossa Magna basin (e.g., Chough and Barg, 1987; Yamaji, 1990; Kato, 1992; Tamaki et al., 1992; Jolivet et al., 1994) (Figs. 8IX and 8X). The principal axes from the cumulative strain primarily trended in a NW-SE direction, and the dilatation strain rates were greater than $10x10^{-9}$/yr from 28-15 Ma. Therefore, the Cenozoic basins in northeast Asia were characterized by zones of high dilatation strain that shifted eastward, with the highest extension occurring in the back-arc region from 56-15 Ma. These observations suggest that these tectonic processes were related to the trench retreat and ridge subduction along the western Pacific.

3.2. Late Cretaceous (67-100 Ma) extensional deformation with post-rifting uplift or inversion

Late Cretaceous deposits in northeast Asia locally occur in the Huainan, Jiaolai, Songliao, Sanjiang, northern and southern South Yellow Sea, and Gyeongsang basins (Fig. 6d). The centre of the North China Craton to the west of the Tan-Lu fault mostly

lacks deposits because of uplifting. No new episodes of rifting occurred across the Yinshan and Yanshan Mountains in northeast China, and the Songliao basin converted to a post-rifting stage at 110 Ma with episodic compressional inversion from 88-79 Ma (Song et al., 2014). Similarly, the Sanjiang basin to the east shifted to a thrusting and compressional regime. Therefore, the Early Cretaceous back-arc extension in the Jiamusi and Sikhote-Alin regions terminated and changed to a short-term compressional thrusting and continental-margin igneous arc phase during the Late Cretaceous. This igneous arc extended southward to the western Honshu, northern Kyushu, and Gyeongsang basins (Barnes, 2003). The volcano-sedimentary complex in the Gyeongsang basin indicates a rock association in a Late Cretaceous island arc (Zhang et al., 2012). The Gyeongsang arc, together with (from west to east) the Late Cretaceous fore-arc basin, the Late Cretaceous Sanbagawa metamorphic belt, the Jurassic Chichibu accretionary complex with Cretaceous strike-slip basin sediments, and the Late Cretaceous Shimanto mélange in southwestern Japan, likely constitute a continuous subduction-related island arc system from southeast Korea to southwest Japan (Isozaki et al., 2010a; Zhang et al., 2012) (Fig. 1 and Table 1). Considering this history, we performed the Late Cretaceous reconstruction by interpolating rotations from 67-80 Ma, 80-88 Ma (or 67-90 Ma), and 90-100 Ma, relative to the western part of the North China block, to the west of the southern Tan-Lu fault and the Songliao basin (Fig. 7b).

The shortening in response to inversion during the post-rift stage of the Songliao basin was reconstructed by balanced-section data of interpreted seismic sections (Song et al., 2014). Line feature 21 (Fig. 7b) at its eastern margin was displaced eastwards by approximately 24 km from 67-90 Ma in the middle part of the basin relative to its western margin (feature 20, Fig. 7b). Based on balanced-sections from the Sanjiang basin, we interpolated rotations by approximately 91 km for the south-eastern movement of the subduction zone (feature 23, Fig. 7b) relative to feature 22 (Fig. 7b), and reconstructed the shortening from inversion in the Sanjiang basin and its eastern extension to the subduction zone. To the south of the Korean peninsula, we used balanced section data to reconstruct the nearly NS extensional

deformation from 67-80 Ma by northward movement of feature 25 (by approximately 9 km relative to feature 24 in the Laiyang basin), of feature 27 (by approximately 14 km relative to feature 26 in the northern South Yellow Sea basin), of feature 29 (by approximately 8 km relative to feature 28 in the southern South Yellow Sea basin) (Tong, 2007; Shinn et al., 2010; Xiao and Tang, 2014). From 67-100 Ma, the southern part (feature 30) of the western Pacific subduction zone was displaced approximately 64 km westwards according to geological and seismic tomography constraints for its location and extensional strain levels less than approximately 10% in the South Yellow Sea basins.

The reconstructed results indicate that northeast Asia was subjected to a NWW-SEE-trending extension with a strain rate of $8x10^{-9}$/yr to $10x10^{-9}$/yr along the western Pacific subduction zone from 100-90 Ma (Figs. 8f and 8VI). This shifted to a nearly NW-SE-trending compression regime with a dilatation strain rate ranging from approximately $0x10^{-9}$/yr to $-4x10^{-9}$/yr in the northern section and a NW-SE (NNW-SSE)-trending extension regime with a dilatation strain rate of $2x10^{-9}$/yr to $4x10^{-9}$/yr in the south-eastern sections from 88-67 Ma (Figs. 8g and 8VII). This differential kinematic field may have been triggered by the westward subduction of the paleo-Pacific plate along the Sanbagawa-North Shimanto accretional zone to the north and the eastward retreat subduction along the Okinawa Trough to the south.

3.3. Early Cretaceous (101-136 Ma) extensional deformation

Following the final collision of the Mongol-Okhotsk Ocean in the Late Jurassic to the Early Cretaceous, the regions boarding the Mongol-Okhotsk suture and the Hailar-Erlian-eastern Gobi region in Mongolia and Inner Mongolia shifted from contraction to extension from the Late Jurassic to the Cretaceous. This occurred with the development of the western rift-basin zone to the west of the Great Xing'an Range and to the north of the Ordos basin (Fig. 6c). The Erlian and Hailar basins in the western rift-basin zone continuously experienced a NNW-SSE-trending extension from 136-110 Ma. However, the Yinshan Mountains experienced a

NNW-SSE-trending compression until 137 Ma, when this regime changed to NW-SE-trending extension from 136-120 Ma. The extensional recovery of the Hailar basin, the Erlian basin, and the Yinshan Mountains occurred by north-westward or northward movement. The south-eastern margin line features of the basins moved by approximately 10 km and 9 km from 110-136 Ma, and the Yinshan Mountains moved by 8 km from 120-136 Ma (features 40, 42, and 43; Fig. 7c) relative to the north-western margin line features (the fixed line feature, feature 41, and feature 42). Computing the dilatation strain rates of the Erlian and Hailar basins and the Yinshan Mountains gives a value of approximately $3x10^{-19}$/yr during the syn-rifting stage from 136-110 Ma. The formation of this rift-basin zone may reflect a rapid shift from orogenic crustal thickening to extensional collapse during the latest Jurassic-Cretaceous or an accommodation zone with a Mesozoic strike-slip component along the Mongol-Okhotsk suture zone, the East Gobi fault zone, and the Solonker suture zone (Johnson et al., 2015; Yang et al., 2014).

The middle rift-basin zone during the Early Cretaceous was distributed from the basement of the Bohai Bay basin in the south to the Yanshan Mountains and the Songliao basin in the north (e.g., Ren et al., 2002; Cope et al., 2010) (Fig. 6C). The Tan-Lu fault located along the eastern margin was activated as a normal fault and extended during the middle-late Early Cretaceous (e.g., Wang et al., 2000; Zhu et al., 2010). Alongside these rift basins, metamorphic core complexes formed in the Liaonan, Yiwulüshan, Louzidian, Yunmengshan and Hohhot areas, among others, because of a WNW-ESE-trending extension from ca. 140-120 Ma (e.g., Davis et al., 1996; Darby et al., 2004; Liu et al., 2005a; Lin et al., 2008; Davis and Darby, 2010; Zhu et al., 2012 and references therein). The extensional deformation in this rift-basin zone was recovered by moving line feature 45 westward by approximately 10 km (at the south) to 36 km (at the north) relative to feature 44 (Fig. 7c) based on the extension of approximately 18-20% (Ge et al., 2012). These reconstructed and modelled results indicate that the principal compressive strains were oriented in the NWW-SEE direction (Fig. 8V) and had dilatation strain rates ranging from approximately $2x10^{-19}$/yr to $5x10^{-19}$/yr (Fig. 8e).

U-Pb zircon ages, K-Ar ages, and geochemical and isotopic data indicated that Late to Early Cretaceous (133-106 Ma) volcanic rocks were widely distributed in northeast Asia (Xu et al., 2013; Kim et al., 2012; Kim et al., 2015). The volcanic materials in the eastern Heilongjiang-Jilin provinces of China (Xu et al., 2013), in Sikhote-Alin in western South Korea (Kim et al., 2012), and in southwest Japan (Taira, 2001) formed in an active continental-margin setting related to the subduction of the paleo-Pacific Plate beneath the Eurasian continent. The bimodal volcanic materials formed in an extensional environment (Xu et al., 2013; Kim et al., 2012) (Fig. 6c). Behind this subduction zone, the Laiyang, northern South Yellow Sea, and southern South Yellow Sea basins in the eastern rift-basin zone rifted and extended. The deformation paths of these basins from 110-136 Ma were determined by interpolating rotations through westward or north-westward motions of features at their southern margins (features 47, 49, and 51 moved by approximately 6 km, 12 km, and 17 km, respectively) relative to the features at their northern margins (46, 48, and 50; Fig. 7c) (e.g., Tong, 2007; Shinn et al., 2010; Xiao and Tang, 2014). The paleo-position of the western Pacific subduction zone was also constrained by geological data and seismic tomography (see section 2.2) and the extension of 20% in the eastern rift-basin zone. The paleo-position from 101-136 Ma was determined based on approximately 110-128 km of westward movement of the subduction zone line feature 52 relative to feature 51. The computed kinematic field indicates that the eastern rift-basin zone was characterized by a NW-SE-trending principal axis of accumulation strain (Fig. 8V) and dilatation strain rates from approximately $3x10^{-19}$/yr to $4x10^{-19}$/yr, and the eastern continental margin was characterized by a NWW-SEE-trending principal axis (Fig. 8V) with strain rates from approximately $1x10^{-9}$/yr to $2x10^{-9}$/yr (Fig. 8e).

Therefore, the rift-basin patterns and the high extensional strain rates in the middle and eastern provinces from 136-101 Ma demonstrate that the tectonic kinematics of northeast Asia transformed to an extensional regime during this time. The related paleo-Pacific subduction zone retreated eastward to the Sanbagawa-North Shimanto accretional zone, which triggered back-arc extension and volcanism along

South Korea, western Honshu, and Sikhote-Alin (Xu et al., 2013) (Figs. 6c and 8V).

3.4. Jurassic-earliest Early Cretaceous (137-200 Ma) shortening deformation

The plate tectonics of northeast Asia were characterized by the westward subduction of the western paleo-Pacific plate, the north-westward subduction of the Mongol-Okhotsk Ocean, a nearly N-S oriented continental-continental collision in the Qinling-Dabie orogenic belt, and a NW-SE- or W-oriented shortening within the continent at the present-day geographic coordinates (Seton et al., 2012; Liu et al., 2013; Liu et al., 2015c) (Figs. 6a and 6b). The western subduction zone of the paleo-Pacific plate was reconstructed to be located along Mudanjiang, central Honshu Island in Japan, and the central uplift zone of the East China Sea basin from ca. 200-137 Ma by closing the later-extended Japan Sea and the East China Sea basins and removing the Cretaceous accreted terranes and backward recovering the compressional deformation to the east of the Ordos rigid block (Figs. 6a and 6b). The paleo-position of the western subduction zone was determined by eastward displacement of subduction zone line feature 61 by approximately 91 km from 137-163 Ma, and by 59 km from 164-200 Ma relative to feature 60 (Figs. 7d and 7e). The approximately 6-10% shortening was consistent in the nearby Sulu region. The reconstructed position of the subduction zone is consistent with inferences made using seismic images of the mantle (Fig. 4).

3.4.1. Late Jurassic-earliest Cretaceous (137-163 Ma)

The Late Jurassic to earliest Cretaceous deformation in the North China Craton was mainly characterized by a NW-SE-trending contraction and the development of large-scale thrust faults, folds, and intermontane basins (Fig. 6b). The Late Jurassic to earliest Cretaceous fold-and-thrust belts were mainly distributed in the Yinshan and Yanshan belts along the northern North China Craton, the Taihang Mountains, the Helan area at the western margin of the Ordos basin, the southern and south-eastern margins of the North China Craton, and the Liaodong area and Jiaodong Peninsula in

the eastern North China Craton (e.g., Zhang et al., 2014 and references therein; Liu, 1998; Darby and Ritts, 2002; Liu et al., 2001). The Late Jurassic to earliest Cretaceous basins migrated northward and north-westward to the margins of the Jining-Longhua, Shangyi-Pingquan and Lingyuan-Dongguanyingzi thrust belts in the Yanshan, north Taihang, and Yinshan Mountains, and locally developed in front of the Helan thrust fault in the western Ordos and in front of the North Qinling thrust faults on the southern margin of the North China Craton (Fig. 6b). These basins were filled with gravel braided channel and braided channel delta depositional systems, and fan-conglomerates (Fig. 2) were predominantly distributed along the thrust-controlled margins of the basins. The conglomerates thickened towards the front of the thrusts because of thrust belt loading, folding, and footwall tilting (Liu et al., 2007; Liu et al., 2003). The reconstructed deformation of the North China Craton from the Jurassic to earliest Cretaceous was characterized by NW-SE-trending shortening deformation with a convergent contraction from the surrounding mountains to the craton's centre. The Ordos basin was interpreted to be rigid, and the Tan-Lu fault was interpreted to be a sinistral strike-slip fault that only developed in the southern section between the Dabie and Sulu orogenic belts during the Jurassic to earliest Early Cretaceous, but later extended northward.

Fig. 8. Modelled results for the northeast Asian deformation field. The figures in the right column show the northeast Asian deformation network (with interior rigid blocks); colours indicate the dilatation strain rate (red is extension, blue is compression) based on the colour palette in Fig. 5. Also shown are the principal components of the strain that accumulated at 200-175 Ma (I) and 164 Ma (II); at 163-152 Ma (III) and 137 Ma (IV); at 136-110 Ma (V); at 100-90 Ma (VI) and 67 Ma (VII); and at 66-42 Ma (VIII), 24 Ma (IX), and the present (X). The outward-facing red arrows indicate extension, and the inward-facing blue arrows indicate compression. The red lines with arrows represent subduction zones, and the purple lines represent ocean ridges. The figures in the left column display the cross-sections of the dilatation strain rate at 182 Ma (a), 168 Ma (b), 152 Ma (c), 140 Ma (d), 113 Ma (e), 94 Ma (f), 72 Ma (g), 48 Ma (h), and 28 Ma (i). DSR: dilatation strain rate. The locations of sections a, b, c, and d are shown in the outline figure of the

deformation region at 28 Ma (j), which depicts the western Pacific subduction zone (red toothed lines) and the Ordos and Sichuan rigid blocks (grey areas). QD = Qinling-Dabie Mountains; HA = Hailar basin; ER, Erlian basin; HT = Hetao basin; YI = Yinshan Mountains; YA = Yanshan Mountains; TH = Taihang Mountains; SU = Sulu Mountains; SL = Songliao basin; BH = Bohai Bay basin; SH = South Huabei basin; LY = Laiyang basin; NY = North Yellow Sea basin; SY = southern South Yellow Sea basins; EC = East China Sea basins; JP = Japan Sea basin.

The deformation reconstruction for the Late Jurassic and earliest Cretaceous was performed from west to east by anchoring the Ordos block and the western boundary of the northeast Asian deformation zone. The Hailar and Erlian basins in the western deformation zone experienced NNW-SSE-trending extension beginning at approximately 157 Ma. Deformation in both basins from 137-157 Ma was conducted by north-westward rotation of feature 63 by approximately 10 km and feature 65 by 26 km relative to features 62 and 64, respectively (e.g., Qu et al., 2013; Fig. 7d). The computed strain field shows NNW-SSE-trending extension, and the extensional dilatation strain rates ranged from approximately $4x10^{-19}$/yr to $2x10^{-19}$/yr (Fig. 8c). From 137-163 Ma, the compressional deformation in the Taihang-Yanshan Mountains was recovered by south-eastward rotation of Feature 67 by approximately 16 km and Feature 69 by 15 km, relative to Features 66 and 68, respectively. For the Sulu Mountains, Feature 71 was rotated south-eastward by approximately 10 km relative to Feature 70, at approximately 10-25% of the shortening strain level (e.g., Zhang et al., 2011; Wang et al., 1998; Wang et al., 2008; unpublished data of Liu et al.). Bohai Bay and the Songliao basins are located between these two mountain belts; their deformation was recovered by interpolating rotations with approximately 15% shortening (Fig. 7d). The computed strain field from 137-163 Ma suggests that the principal compression accumulation axes of the strain were oriented in a NW-SE direction in the eastern zone; this direction was NNW-SSE in the Taihang-Yanshan Mountains and Yinshan Mountains (Figs. 8III and 8IV). The dilatation strain rates ranged from approximately $-10x10^{-19}$/yr to $-7x10^{-19}$/yr in the Yanshan Mountains and from $-10x10^{-19}$/yr to 0/yr in the Taihang Mountains (Figs. 8c and 8d).

The high shortening strain rates were focused in the Yanshan-Taihang (or Yinshan) Mountains; these rates may have been driven by convergent compression from both the western Pacific plate's subduction and the closing of the Mongol-Okhotsk Ocean. This observation suggests that the Taihang-Yanshan Mountains were the frontal belt of the East Asia orogen, which resulted from the western Pacific plate's subduction.

3.4.2. Early-Middle Jurassic (164-200 Ma)

The deformation pattern in the North China Craton was mainly characterized by NW-SE shortening during the Early-Middle (or early Late) Jurassic, similar to that of the Late Jurassic-earliest Cretaceous. The recovered Early-Middle (or early Late) Jurassic Ordos basin was originally nearly N-S trending with contracting mountain margins to both the west and east (Fig. 6a) and thrust belts to the north and south (Liu et al., 2013). A regional unconformity developed between the Triassic Yanchang Formation and the overlying Lower Jurassic Fuxian Formation or Middle Jurassic Yanan Formation in the western Ordos basin (Fig. 2). The Lower-Middle Jurassic basin strata in the western Ordos consisted of predominantly coal-bearing fluvial and lacustrine strata, reached 1,600 m in thickness, and were sourced from the uplifted western Helan flanks (Liu and Yang, 2000; Ritts et al., 2009). Relative to the present-day Ordos basin, the eastern margin of the Early-Middle Jurassic Ordos basin extended eastward to the Taihang Mountains, including the later isolated small basins. The Middle Jurassic Yan'an Formation in the eastern margin of the basin showed a facies change from marginal fluvial in the north and northeast to deltaic and lake in the basin's centre (Liu et al., 2013). Structural investigations, U-Pb dating, and $^{40}Ar/^{39}Ar$ chronological analyses indicated that the Taihang Mountains initially uplifted and formed fold-thrust structures at 175-150 Ma (Wang and Li, 2008). The extensive WNW-vergent thrust faults and folds that formed during the Middle-Late Jurassic indicated WNW-oriented contraction (Wang and Li, 2008). In the Yinshan belt (Fig. 6a) to the north of the Ordos basin, deformation began with right-lateral

strike-slip faulting and basin development along east-striking structures during the Early Jurassic (Ritts et al., 2001; Darby et al., 2001). This structure remained until the earliest Middle Jurassic and then changed into a contractile foreland-style basin formation (Darby et al., 2001). South of the Ordos basin, the North Qinling belt (Fig. 6a) thrust and expanded northward and deformed the Late Triassic wedge-top basin strata (Liu et al., 2013). The Dabie Mountains were a doubly vergent thrust system during the Jurassic, and its northern thrusts controlled the deposition of the Hefei foreland basin (Liu et al., 2003; Liu et al., 2010). Therefore, the Early-Middle Jurassic Ordos basin formed a walled intracratonic basin that was surrounded by orogenic uplifts (geomorphic walls), which was related to predominantly WNW-ESE- and N-S-directed intraplate contraction (Liu et al., 2013). Two Early-Middle (or earliest Late) Jurassic intermountain basin zones, namely, the Xuanhua, Chicheng, Luanping-Chengde, and Beipiao basin zones and the western Beijing and Niuyingzi basin zones, developed in the Yanshan belt (Fig. 6a) and were bound by thrust faults or folds (Liu et al., 2004). Whether the sinistral strike-slip motion of the Tan-Lu fault in south-eastern North China was initiated during the Late Triassic-Early Jurassic because of the collision between the South and North China blocks (e.g., Zhu et al., 2009) or no earlier than the Middle-Late Jurassic (e.g., Wang, 2006) remains highly controversial. However, the Tan-Lu sinistral strike-slip movement developed during the Early-Middle (or earliest Late) Jurassic because of trending NW-SE shortening. This shortening event was accompanied by the formation of a series of NNE (or NEE)-striking shortening structures, fold-and-thrust faults and intermontane basins in the basement of the Tertiary Bohai Bay basin, the south-eastern North China Craton and the eastern Jiaodong Peninsula (Li et al., 2009; Zhang et al., 2007).

The reconstructed deformation in northeast Asia indicated three NE-SW-trending deforming zones, namely, the eastern, middle, and western deformation zones; from 200-164 Ma, the eastern deformation zone was adjacent to the subduction zone, the middle deformation zone was across the Taihang-Yanshan Mountains (including the present-day Bohai Bay basin basement), and the western deformation zone was in Inner Mongolia (Fig. 6a). The deformation reconstruction was performed by

two-stage backward integration by interpolating feature rotations from 164-174 Ma and from 175-200 Ma based on the difference between strains (Fig. 7e). For the western deformation zone, from 164-174 Ma, we rotated features 82 and 84 south-eastward by approximately 5-10 km with less than 2% shortening. From 175-200 Ma, we rotated feature 81 by approximately 92 km relative to feature 80, with approximately 12% shortening. For the Yanshan-Taihang Mountains, from 164-174 Ma, we moved features 83, 85, and 86 south-eastward by approximately 18 km, 10 km, and 25 km relative to features 82, 84, and 91, with approximately 3-10% shortening strain (e.g., Zhang et al., 2011; unpublished data of Liu et al.). Very few feature rotations were performed around Bohai Bay and the Songliao basins because of this region's weak deformation during the Early Jurassic (Liu et al., 2013). The reconstruction in the Sulu deformation zone from 164-200 Ma was determined by rotating feature 88 by approximately 8 km relative to feature 87 with approximately 8% shortening strain (e.g., Wang et al., 1998; Wang et al., 2008). The computed kinematic field suggests that the principal compression accumulation strain axes trended NW in the area west of the Tan-Lu fault in the middle and western deformation zones and trended nearly E-W along the eastern deformation zone of northeast China (Figs. 8I and 8II). The principal compression accumulation axes trended NNE in the Qinling-Dabie orogenic belt south of northeast Asia. The total accumulated strains lacked any principal extension components throughout most of northeast Asia, except for its eastern margin. The coexisting strain field of extension and compression components may have been driven by the dextral strike-slip subduction of the Pacific plate. The dilatation strain rates were mostly minor (compressional). The dilatation compressional strain rates ranged from $-1x10^{-19}$/yr to $-5x10^{-19}$/yr, from $-6x10^{-19}$/yr to $0x10^{-19}$/yr, from $-4x10^{-19}$/yr to $1x10^{-19}$/yr, and from $-4x10^{-19}$/yr to $-6x10^{-19}$/yr, respectively, in the eastern, middle and western deformation zones and the Qinling-Dabie orogenic belt (Figs. 8A and 8B). Clearly, the higher strain rate in the eastern deformation zone was driven by the western Pacific plate's subduction to the east, and the higher strain rate in the western deformation zone was driven by the closing of the Mongol-Okhotsk Ocean to the north.

4. Linkage of intracontinental deformation to plate motion

The configuration and motion of plates on Earth's surface are intrinsic manifestations of plate-mantle coupling and the evolving configuration of mantle convection. The complex interactions of plate boundary forces result in plate motions dominated by interactions among far-field plate velocities, hinge migration direction, subduction polarity (Doglioni et al., 2007; Doglioni and Panza, 2015), slab pull and ridge push forces (Forsyth and Uyeda, 1975; Stadler et al., 2010), the dynamics driven by mantle drag (Conrad and Lithgow-Bertelloni, 2006), and radial (Phillips and Bunge, 2005) and lateral viscosity contrasts (Stadler et al., 2010). The kinematics of subduction zones suggest a close relationship between the velocities of subduction hinge migration, lower plate motion, and subduction relative to the anchored upper plate. The far-field velocities of the upper and lower plates and the trench migration (or the transient subduction hinge) control plate subduction (Doglioni et al., 2007; Doglioni and Panza, 2015). Global or regional plate motion changes are likely related to tectonic events through changes in plate boundary forces which may further drive intracontinental deformation, back-arc spreading or shortening.

Developing a global plate model involves four main components: the reconstruction of relative plate motions, an absolute reference frame, the choice of a timescale, and the construction of continuously-closing plate polygons (Seton et al., 2012; Müller et al., 2016). The anchor for a global plate motion model is an absolute reference frame that expresses how the entire system of plates moves relative to a fixed reference, such as the mantle or the spin. Global plate models allow the computation of fundamental variables such as measures of both relative and absolute plate velocity magnitudes and directions; these can help elucidate global changes in the plate system through time (Müller et al., 2016). Relative plate motions are intimately related to absolute plate motions, which are relative to Earth's deep interior, or mantle. Generally, relative plate motions are much more tightly constrained than absolute plate motions, as the latter are limited by many uncertainties in geodynamic models of hotspot motion, decoupling between the lithosphere and subasthenospheric

mantle, or seismic tomography imaging of the lower mantle (Doglioni et al., 2005; Cuffaro and Doglioni, 2007; Crespi et al., 2007; Afonso et al., 2008; and Müller et al., 2016). The global absolute plate motions displayed in GPlates (Müller et al., 2016) are linked to Africa via the post-Pangea seafloor spreading or rifting record back to 200 Ma (Seton et al. 2012). After 83 Ma, the Pacific is linked to the plate circuit based on the establishment of seafloor spreading between the Pacific and West Antarctic Plates, and for earlier times by using a fixed Pacific hotspot reference frame (Wessel and Kroenke 2008).

Global plate motion models have been created with continuously closing plate boundaries and global tectonic events from the Triassic (at 230 Ma) to the present day (Müller et al., 2016). Based on these global plate motion models (Müller et al., 2016), we re-intersected the plate boundaries to define continuously closed plate polygons including all of Asia and the western Pacific; we then reconstructed the plate motion, the accretion of exotic terranes, and large-scale crustal deformation. The western Pacific subduction zone, constrained by geological evidence and seismic tomography, advanced westward or retreated eastward to accommodate the deformation in northeast Asia and plate subduction since 200 Ma. Our revised global plate motion models (Fig. 11) offer insights into the tectonic events that have affected Eurasia and its adjacent continents. These insights are based on the absolute plate motions (APMs; that is, motion relative to the mantle) for the Mongol-China, Eurasian, Meso- (and Neo-) Tethys, Indian, Izanagi, and Pacific plates, especially when paired with their plate motion azimuths through time computed at the centroid points of the continents. Using this approach, we demonstrate three periods of plate motion measured for the plates: those with intermediate rates (mean APM rates of 6-11 cm yr^{-1}) from ca. 200-140 Ma, high rates (mean APM rates of 4-13 cm yr^{-1}) from 139-50 Ma, and slow rates (mean APM rates of 2-11 cm yr^{-1}) after 50 Ma (Fig. 9). To analyse regional plate motion changes in northeast Asia and its adjacent plates, we focused on relative plate motions, including the rates and directions of convergence between regionally key plate pairs (including the Eurasian relative to the China-Mongol plate, Izanagi relative to China-Mongol, Izanagi relative to Eurasian, Pacific relative to Eurasian, and Indian

relative to Eurasian) along representative flow lines (Fig. 10). In addition to the plate motion changes experienced in northeast Asia from 200-0 Ma, we also consider the lithospheric age of the down-going plate (Fig. 12), which also showed a multi-stage evolution.

Fig. 9. Continental absolute plate motion velocity (APM) rates (left column) and directions (azimuth clockwise from north) that were computed at a given continent's centroid point (right column) for the (a) Mongol-China and Eurasian, (b) Meso-Neo-Tethys, (c) Izanagi, and (d) Pacific plates. These plate motion velocities were computed from Müller et al.'s (2016) global plate motion model.

Fig. 10. Rates and directions of convergence between key plate pairs, which reveal the tectonic events of circum-plates compared with the Eurasian plate. The plates are as follows, the first plate being the moving plate and the second plate being the fixed plate: (a) the Eurasian plate compared with the Mongol-China plate (200 Ma-151 Ma); (b) the Izanagi plate compared with the Mongol-China plate (200 Ma-151 Ma); (c) the Izanagi plate compared with the Eurasian plate (150 Ma-101 Ma); (d) the Izanagi plate compared with the Eurasian plate (100 Ma-56 Ma); (e) the Pacific plate compared with the Eurasian plate; (f) the Meso-Tethys plate compared with the Mongol-China plate; (g) the Neo-Tethys plate compared with the Mongol-China plate; (h) the Indian plate compared with the Eurasian plate; and (i) the Philippine Sea plate compared with the Eurasian plate. The globes show the locations of the coloured tectonic flowlines along which the convergence rates and directions are plotted. The colours in the rate and direction plots match the colours of the flowlines. The tectonic events that are reflected in the above plate pairs occurred around ~189 Ma, ~180 Ma, 170-155, ~140 Ma, 120-105, ~85, ~55, and ~35 Ma as major changes in either the convergence rates or directions.

4.1. Multi-plate convergence and advanced slab subduction from ca. 200-140 Ma

Prior to the Mesozoic, the continents were amalgamated into one large

supercontinent, Pangaea, surrounded by two oceans, Panthalassa (also referred to as the Panthalassic Ocean) and the smaller Tethys Ocean. The Panthalassa was encircled by subduction during the Mesozoic. The plates in the Panthalassa behaved as a simple three-plate system (e.g., with the Izanagi, Farallon and Phoenix plates), and a new Pacific plate grew from the centre of their triple junction; when the Pacific Ocean began to grow, it led to convergence of the Izanagi toward the Eurasian plate. The Pangaea supercontinent consisted of Mongol-China, Laurasia, North America, West Gondwana, and East Gondwana (Fig. 11). The breakup of Pangaea commenced with the rifting of Gondwana from Laurasia and Mongol-China along the Neo-Tethys ridge, a ridge between the Madagascar and Somalian plates, and the Caribbean-Central Atlantic ridge. This breaking process drove the motion of North America and Laurasia (or Eurasia) towards the northern Mongol-China plate, northeast Asia at east. The Mongol-Okhotsk Ocean (an ocean basin that formed between Mongol-China, northeast Asia, Laurasia, and Siberia) was closed through north-east subduction along the southern Siberia margin. In the Tethys Sea, north-verging subduction along the southern Laurasian and Mongol-China margins drove the consumption of the Paleo-Tethys and the collision of the remnant continental blocks (the Cimmerian terranes including Iran, Afghanistan, Pakistan, South Tibet, and Sibumasu) with the Mongol-China plate (Seton et al., 2012). Therefore, the plates and continents converged toward Mongol-China or Laurasia during the Jurassic and earliest Cretaceous. We computed the relative plate motion by choosing plate pairs (Eurasian and Mongol-China, Meso-Tethys, Neo-Tethys, and Mongol-China; and Izanagi and Mongol-China) with a fixed Mongol-China plate. The mean relative convergent motions of the circum-plates towards the Mongol-China plate ranged from 4.8 to 10.2 cm yr^{-1}, which corresponds to an intermediate APM period in the Eurasian and western Pacific regions (Figs. 10a-c and 10f and Fig. 11). During this convergent motion period, five minor changes in the convergence rates and directions occurred between the Izanagi and Mongol-China plates (Fig. 10a-c) at ca. 189 Ma, 179-170 Ma, 169-160 Ma, and 159-140 Ma.

Fig. 11. Global plate reconstructions from 200 Ma to the present day in 10 Ma intervals, which show the age-area distribution of oceanic crust at the time of formation, the absolute plate motion, and the tectonic evolution of East Asia (modified from Müller et al., 2016). The black-toothed lines delineate subduction zones, and the other black lines indicate mid-ocean ridges and transform faults. The grey polygons indicate continental regions, with the present-day coastlines shown in dark grey. A Hammer projection with a 100◦E central meridian is used. Abbreviations: A = Aluk plate; AFR = African plate; ANT = Antarctic plate; AR = Arabian plate; AUS = Australian plate; C = Cocos plate; CA = Caribbean plate; CAT = Catequil plate; CC = Cache Creek oceanic plate; CHZ = Chasca plate; CIM = Cimmerian-Tethys plate; CP = Capricorn plate; EGD = East Gondwana; EUR = Eurasian plate; FAR = Farallon plate; GON = Gondwana; GRN = Greenland plate; HIK = Hikurangi Plateau; IND = Indian plate; IZA = Izanagi plate; K = Kula plate; LHR = Lord Howe Rise; M = Manihiki Plateau; MCH = Mongol-China; MT = Meso-Tethys Ocean; NAM = North American plate; NAZ = Nazca plate; NEA = Northeast African plate; NT = Neo-Tethys Ocean; NWA = Northwest African plate; P = Philippine Sea plate; PAC = Pacific plate; PHO = Phoenix plate; SAF = South African plate; SAM = South American plate; SOM = Somali plate; SP = Sepik plate; V = Vancouver plate; VA = Vardar plate; WAN = West Antarctic plate; WGD = West Gondwana; and WMT = West Meso-Tethys Ocean.

4.1.1. First tectonic event: plate motion change at ca. 189-180 Ma

From 200-190 Ma, Laurasia moved rapidly eastward and south-eastward towards the Mongol-China plate, which drove the closing of the Mongol-Okhotsk Ocean. To the east, the Izanagi plate subducted north-westward beneath the margin of the Mongol-China plate, but the Meso-Tethys plate subducted north-north-eastward (Figs. 9b-c). All the features in northeast Asia mostly moved south-eastward (Fig. 11). The relative plate motion with respect to Mongol-China indicates that northeast Asia was compressed by the Meso-Tethys subduction zone from the SW, the Mongol-Okhotsk subduction zone from the NW, and the western Pacific subduction zone from the east (Figs. 10a-b). Under this background, northeast Asia mostly uplifted and was exhumed under compression, and formed mostly SE- (or E-W-) trending folds and thrusts and their frontal fore-deep deposits in the Yanshan Mountains (Fig. 2) (Liu et

al., 2007; Liu et al., 2012).

From 189-180 Ma, the Izanagi plate exhibited northwest-verging subduction, the Meso-Tethys plate extruded south-eastward, and the Mongol-China and Eurasian plates changed their motion to the south (Figs. 9a-c and 11). The Mongol-China plate was compressed by the surrounding plates; the relative motions between the Izanagi and Mongol-China plates decreased from approximately 9 cm/yr to 2 cm/yr (Fig. 10b). This decrease in relative convergence between the Izanagi and Mongol-China plates and the changes in the APM directions of the two plates with a very low velocity of subduction hinge advancement (approximately 0.2 cm/yr) and relatively high plate subduction may explain the first decrease in the shortening strain. This induced the intracontinental volcanic activity recorded in the Nandaling Formation in the North China Craton (Fig. 2).

4.1.2. Second tectonic event: plate motion change at ca. 179-170 Ma

Earlier opening by ultra-slow spreading occurred in the Central Atlantic, with ongoing rifting in the northern Atlantic and Caribbean at ca. 179 Ma, and the Eurasian plate's motion slowed and shifted towards the southeast. The Mongol-China plate rotated counter-clockwise and slowly moved north westward with continuous closure of the Mongol-Okhotsk Ocean. The high-speed northwest vergence and subduction of the Izanagi plate accommodated the accelerated growth of the Pacific plate at the centre of Panthalassa (Figs. 9a-b and 11). In the northern Tethys, the closure of the Paleo-Tethys Ocean and accretion of the Cimmerian terrane occurred along the southern Laurasian margin at 179 Ma, and spreading in the Meso-Tethys Ocean accelerated its north-eastward subduction after 179 Ma (Fig. 10f). Under this tectonic setting, the relative plate motion rate and direction changes occurred for the Izanagi and Mongol-China plate pair (from approximately 11 to 12 cm/yr and 290° to 256°) and the Meso-Tethys and Mongol-China plate pair (at approximately 10 cm/yr and from approximately 38° to 41°; Figs. 10b and f). The WNW-vergent subduction of the Izanagi plate with approximately 0.4 cm/yr of subduction hinge westward advancement triggered NNE-SSW-trending folding and thrusting and intermontane

flexural basin formation in northeast Asia, including the Taihang and Yanshan Mountains (Figs. 6a and 8I).

4.1.3. Third tectonic event: plate motion change at ca. 169-160 Ma

After 169 Ma, the movement of the Mongol-China and Eurasian plates quickly shifted westward, and the Meso-Tethys and Izanagi plates continued to move north-eastward and north-westward, respectively (Figs. 9 and 11). Between the Izanagi and Mongol-China plates, the relative plate motion direction changed from west-verging (258°) to SW- or SSW-verging (234°) and the convergent motion rate changed from 12 cm/yr to 2.2 cm/yr with approximately 0.6 cm/yr of westward advancement of the subduction hinge relative to the anchored Mongol-China plate, which greatly decreased the compression from the Izanagi plate to the East Asian continental margin through the western Pacific subduction zone (Fig. 10b). The third change in plate motion may have been related to the shortening strain decrease in northeast Asia, which induced the intracontinental volcanic activity that was recorded in the Tiaojishan Formation (ca. 165-160 Ma) in the North China Craton (Fig. 2).

4.1.4. Fourth tectonic event: plate motion change at ca. 159-140 Ma

From 159-140 Ma, several minor changes in the plate kinematics occurred. The Central Atlantic continued to spread between 159 and 140 Ma. Spreading occurred in a NW-SE direction and began approximately 149 Ma, which caused the North American and Eurasian plates to move eastward. The Mongol-Okhotsk Ocean between the Eurasian and Mongol-China plates closed at 150 Ma to form a united Eurasian plate. The Eurasian plate, including the Mongol-China plate, began to move SSE after 149 Ma. The Meso-Tethys Ocean continued to spread and moved NNE (Fig. 11). The spreading and growth of the Pacific plate continued in Panthalassa, but with a gradual increase in the spreading rate. Therefore, northeast Asia maintained a multi-plate convergent setting. Between the Izanagi and Mongol-China (or Eurasian) plates, the relative plate motion direction changed to WNW or NW (280°-300°), and the convergent motion rate changed to 100-190 mm/yr (Figs. 10b and 10c) with

approximately 5 mm/yr of westward advancement of the subduction hinge and a high plate subduction rate relative to the anchored Mongol-China plate. These changes greatly increased the compression from the Izanagi plate to East Asia's continental margin by the westward subduction of the Izanagi plate. This plate motion change may have induced the intracontinental folding and thrusting and the formation of the intermountain flexural basin in the Tuchengzi Formation (156-137 Ma) in the North China Craton (Figs. 6b and 8IV).

4.2. Obduction of Eurasia across the Izanagi plate's centre and trench retreat from ca. 139-67 Ma

During the Cretaceous, the Gondwana continent began to complete its rifting. The Central Atlantic and the proto-Caribbean Sea continued their growth through a differential motion between North and South America (Seton et al., 2012). Coincidently, spreading along the Neo-Tethys ridge extended from the Argo Abyssal Plain to the north of Greater India, which accommodated the northward consumption and subduction of the Meso-Tethys (Fig. 11). Therefore, the different spreading and subduction motion speeds along the Central Atlantic, Caribbean Sea, and Meso-Tethys induced the clockwise rotation of the North American and Eurasian plates and the obduction of the Eurasian continent across the Izanagi plate's centre, which consisted of older oceanic lithosphere. The Early-Middle Cretaceous marked a significant increase in the seafloor spreading rates in Panthalassa among the Pacific, Farallon, Izanagi and Phoenix plates and the subduction rate of the Izanagi plate under East Asia's margin. Under this plate-tectonic background, the APM rates during the Cretaceous in the Eurasian plate and its surrounding plates doubled between 140 and 120 Ma and at ca. 80 Ma (Fig. 9).

4.2.1. First period of high-speed plate motion from 139 to 120 Ma

From 139-121 Ma, the Eurasian, North American, and Neo-Tethys plates consistently began to move N, NNE or NE, but the Izanagi plate moved westward, nearly perpendicular to the western Pacific subduction zone. The eastern Eurasian

plate margin migrated onto the Izanagi oceanic plate, and the western Pacific subduction zone became a convergent centre (Fig. 11). The primary age of the subducting oceanic plate, which was computed along the western Pacific subduction zone along a 7,000-km-long profile, matched the age of relatively old ocean crust (approximately 70-90 to 110-140 million years). Cruciani et al.'s (2005) measurements and analyses suggest that a combination of slab age and subduction rate account for the slab dip, though the correlation is moderate. This age along the subduction zone corresponds to the subducting Izanagi plate (Fig. 12), with high plate subduction velocity; other supplemental forces or constraints (Cruciani et al., 2005) likely increased the slab dip and trench retreat with accelerated spreading along the triple junctions in Panthalassa. The interpretation of continuous slab retreat during the Cretaceous is supported by the geological evidence used to reconstruct the subduction zones.

After 130 Ma, the Eurasian plate rotated clockwise, and the Izanagi plate moved WSW. Southeast Asia shifted onto the Neo-Tethys oceanic plate as the Neo-Tethys plate moved NW (Figs. 9 and 11). The relative plate motion directions between the Izanagi and Eurasian plates were mostly NW (315-327°), and the convergent motion rate increased to 206 mm/yr at 127 Ma, which drove the counter-clockwise strike-slipping subduction of the Izanagi plate beneath northeast Asia (Fig. 10c). After 119 Ma, the westward subduction rate of the Izanagi plate slightly decreased, and the motion direction of East Asia changed to the W from ca. 119-106 Ma. The relative plate motion directions between the Izanagi and Eurasian plates remained NW, but the rates slightly decreased (90-120 mm/yr from 119-106 Ma). The relative motion between the Neo-Tethys and Eurasian plates changed to ENE (Fig. 10g). This plate motion mechanism continued to drive the counter-clockwise strike-slipping subduction of the Izanagi plate, as well as strong trench retreat and rapid south-eastward migration of the subduction hinge relative to the anchored Eurasian plate (0.4 cm/yr from 139 to 120 Ma) due to the westward divergent motion of the overthrusted Eurasian plate. Therefore, high-speed north-westward subduction and trench retreat along the western Pacific subduction zone during the Early Cretaceous

resulted in broad intracontinental extension and NNE-SSW-trending rifts in northeast Asia (Kusky et al., 2014; Figs. 6c and 8V).

4.2.2. Second period of high-speed plate motion at ca. 80 Ma

The Mid- and South Atlantic Ridges were well established by 100 Ma, and the Mid-Atlantic ridge propagated northward between North America and Eurasia. Rifts were still active around Greenland. The divergent motions of the North American and Eurasian plates were associated with North Atlantic spreading, clockwise Eurasian plate rotation and motion to the east or northeast (Fig. 11). The eastern margin of Eurasia, namely, eastern Asia, exhibited southward motion from 104-83 Ma and eastward or south-eastward motion from 82-60 Ma (Fig. 9). This change in the direction of eastern Asia coincided with the observed changes in rift-basin development and extension directions and formed ENE-WSW- or NE-SW-trending rift basins in northeast Asia (Fig. 6d).

In Panthalassa, spreading occurred along the Pacific-Izanagi, Pacific-Farallon, and Farallon-Izanagi ridges. A change in plate motion rate was recorded in the Izanagi plate, and its westward motion was consistent at approximately 170 mm/yr from ca. 95 to 84 Ma, after which it rapidly increased to approximately 230 mm/yr^{-1} at ca. 80 Ma (Fig. 9c). The relative plate motion between the Izanagi and Eurasian plates accelerated to approximately 260-190 mm/yr^{-1} from 82-60 Ma (Fig. 10d). Since ca. 90 Ma, the subducting ocean along the northern part of the western Pacific subduction zone gradually became younger (decreasing from 80 to 20 million years between 90 and 67 Ma), but the age in the southern part remained slightly older (decreasing from 90 to 60 million years between 90 and 67 Ma; Fig. 12). Young ocean crust and relative low subduction velocities could have lessened the trench retreat (Goes et al., 2008). Therefore, the advancing subduction (the average velocity of the relative westward advancement of the subduction hinge was greater than 10 mm/yr) occurred in the northern section of the subduction zone, exerting compressional force and inducing shortening deformation on the overriding plate along the north-eastern margin of Asia from ca. 90-80 Ma. In addition, the Late Cretaceous accretion of the

Northern Shimanto and East Sakhalin complexes (or terranes) in north-eastern Asia along this part of the subduction zone could also have induced retro-arc compression (Wakita, 2013; Barnes, 2003; Zyabrev, 2011). However, the south-eastern margin did not exhibit the same clear shortening deformation as did the north-eastern margin.

Therefore, the southward motion of the East Asian margin and the trench retreat of the western Pacific subduction zone, which are related to subduction hinge divergence relative to the upper Eurasia plate, drove the extension in the northeast Asian intra-continent and back-arc system (Kusky et al., 2014). The eastward, north-eastward or south-eastward motion of the eastern Asian margin and the possible advancing subduction at the north-western Pacific subduction zone, which may have been induced by younger oceanic lithosphere, the change in subduction rate, and the accretionary complex, triggered short-term basin inversion in northeast Asia during the Late Cretaceous (Figs. 6d, 8VI, and 8VII).

Fig. 12. Subducting ocean crustal age at the trench along a 7,000-km long profile of the western Pacific subduction zone since 230 Ma. See text for explanations.

4.3. Obduction of East Asia across the oceanic plate's edge and ridge from ca. 66-0 Ma

Seafloor spreading propagated into the Eurasia-Greenland margin along the Reykjanes Ridge by 58 Ma and formed a triple junction among North America, Greenland, and Eurasia. Spreading in the Eurasian basin to the north that began approximately 55 Ma along the Gakkel/Nansen Ridge resulted in the clockwise rotation of Eurasia and the southward motion of the eastern Asian margin across the edges of the Izanagi-Pacific plate, which consisted of younger oceanic lithosphere (Fig. 11). In the Pacific, the Pacific-Izanagi ridge began to subduct under the East Asian margin between 55 and 50 Ma and signalled the death of the Izanagi plate, which coincided with a dramatic change at 47 Ma in the spreading direction of the Kula-Pacific ridge from N-S to NW-SE and the direction of the Pacific plate from nearly N-S to E-W (Figs. 9d and 11). With the complete spreading of the Indian

Ocean, the disintegrated plates or continents from East Gondwana, such as the Philippine and Indian continents, moved to the east and converged toward Eurasia. Spreading in the proto-South China Sea in the western Pacific ceased at 50 Ma, which coincided with the clockwise rotation of the neighbouring Philippine Sea plate. At ca. 55 Ma, the northern tip of Greater India began to collide with Eurasia, and the closure of the Tethys Ocean in this area occurred by approximately 47 Ma (Fig. 11) (Müller et al., 2016). The event at approximately 50 Ma, when expressed in terms of the relative and APM changes around northeast Asia (Figs. 9, 10h, and 11), indicates that an increase in collisional forces (such as the Indian-Eurasian collision) and ridge subduction events in the Pacific (such as the Izanagi-Pacific ridge) played a significant role in modulating plate velocities (Müller et al., 2016).

4.3.1. Izanagi-Pacific Ridge subduction from 59-48 Ma

After the Pacific-Izanagi ridge began its parallel subduction under the eastern Asian margin at 55 Ma, the relative plate motion rates between the Indian and Eurasian plates and between the Pacific and Eurasian plates slightly increased to 16 cm/yr^{-1} and 6.4 cm/yr^{-1}, respectively (Figs. 10e and h). From 59-48 Ma, the Pacific plate continued to move westward and nearly perpendicular to its western subduction zone. Coincidently, the Eurasian plate moved SSW, and the Indian plate moved NNW at much higher speeds than the Eurasian plate, which moved SSW (Figs. 9a-b and 11). Obviously, the high-speed indentation from the Indian plate and the spreading of the subducted Izanagi-Pacific ridge triggered the spreading and rifting in the East Asian margin.

4.3.2. Clockwise rotation of the Philippine Sea plate and the Pacific plate's clockwise strike-slip subduction from 47-35 Ma

From 47-35 Ma, the Indian plate continuously moved NE and began to collide with the SSW-moving Eurasian plate. The plate motion changes during this period mainly included the Philippine Sea plate's nearly N-S spreading and clockwise NE migration and the Pacific plate's clockwise strike-slip subduction (Fig. 11). The

relative plate motion of the Philippine Sea plate with the Eurasian plate was oriented to the NE and parallel to the Ryukyu subduction zone (Fig. 10i). The relative motion of the Pacific plate with the Eurasian plate was oriented to the west (Fig. 10e), with clockwise strike-slip subduction under the north-eastern Asian margin and counter-clockwise strike-slip subduction along the Izu-Bonin-Mariana trench (Fig. 11). Lesser amounts of convergent motion were centred along the western Pacific and Ryukyu subduction zones and lengthwise relative motion (motion in the opposite direction) between the Indian (or Australian) and Eurasian plates (Fig. 10h). Along with approximately 0.5 cm/yr of subduction hinge divergent motion, this convergent motion triggered trench retreat and back-arc extension along the northeast Asian margin and eastward rifting in the East China Sea (Figs. 6e and 8VIII).

4.3.3. North-South Philippine Ridge subduction from ca. 34-25 Ma

From 32-25 Ma, the Australian plate continued to move north, but the Eurasian plate remained almost stationary (Fig. 11). The direction of the Pacific plate's subduction under the northeast Asian margin remained to the west (Fig. 9d). The trending NW-SE spreading ridge between the North and South Philippine Sea plates changed to fast subduction to the northwest and towards the Bohai Bay and South Yellow Sea basins, which was perpendicular to the East China Sea and SW Japan margin (Fig. 11k). Therefore, this subducted slab window triggered trending NNE-SSW spreading and rifting in northeast Asia and resulted in the nearly N-S-trending extension in the Bohai Bay and East China Sea basins.

4.3.4. Izu-Bonin-Mariana back-arc spreading and Nankai-Ryukyu-East Sakhalin trench retreat from ca. 24-15 Ma

The western Pacific was dominated by the opening of a series of back-arc basins from 25-15 Ma due to the retreat of the subduction hinge of the Tonga-Kermadec and Izu-Bonin-Mariana trenches. Spreading in the Shikoku and Parece Vela basins and South China Sea ceased at 15 Ma (Fig. 11). After 19 Ma, East Asia moved NE, and the Indian plate continuously compressed behind Eurasia (Fig. 11). Responding to the

back-arc extension of the Shikoku basin, the Philippine Sea plate began to move south to accommodate the western Nankai-Ryukyu trench's retreat (Fig. 1). The western Pacific plate continued to subduct westward. The age of the subducting plate and subduction rate gradually increased from the Hokkaido to the Izu-Bonin-Mariana trenches (at 50-90 Ma; Fig. 11), which likely drove the trenches (and subduction hinges) to retreat with steep subduction. However, the East Sakhalin zone, the northern extension of the Hokkaido trench, exhibited the advancing subduction of the newly spreading Okhotsk oceanic crust. Therefore, the back-arc differential extensions, which were driven by the retreat of the Nankai and Hokkaido subduction zones or hinges, were the primary origin of the Japan Sea basin. The trench retreat and weak clockwise subduction of the Ryukyu zone triggered the third rifting episode in the Okinawa Trough (Fig. 8IX).

4.3.5. Subduction of the Philippine Sea and Izu-Bonin-Mariana arc-basin system from ca. 14-0 Ma

At ca. 14 Ma, the spreading of the Izu-Bonin-Mariana arc-basin system decreased, and the Philippine Sea plate and its eastern arc-basin system began to subduct NW under the East China Sea and south-western Japan (Fig. 11). This arc subduction triggered the weak, nearly E-W-trending extension of the Japan Sea basin, and the continuous retreat of the Ryukyu zone triggered back-arc extension. At ca. 4 Ma, the Shikoku back-arc basin, which comprised young oceanic lithosphere, may have obstructed the north-vergent subduction of the Izu-Bonin-Mariana arc-basin system and induced the north-westward subduction of the Philippine Sea plate, which resulted in brief compression in SW Japan instead of extension, the continuous rifting of the Ryukyu arc, and the extension of the Mariana arc (Fig. 11).

It is difficult to determine a plate motion reconstruction for the Philippine Sea plate, or discern its interactions with nearby plates. The plate is surrounded by subduction zones with a triple-trench junction. The Philippine Sea plate motion and its effect on the tectonics of the Japanese archipelago have been debated. Plate reconstructions presented by Mahony et al. (2011) suggest that prior to 15 Ma, Pacific

plate subduction dominated Kyushu tectonics, and the Philippine Sea plate started to subduct beneath Kyushu due to the northward migration of the triple junction between the Pacific plate, the Philippine Sea plate, and southwest Japan from 15 to 6 Ma. From 6 to ca. 1.5 Ma, changes in the Philippine Sea plate motion led to more rapid, nearly trench-normal subduction of the Philippine Sea plate (Seno and Maruyama 1984; Mahony et al., 2011). At ca. 1.5 Ma, the Philippine Sea plate was eventually rotated counter-clockwise from northwest to west-northwest (Seno 1985). Based on analyses of the focal mechanism after the 2016 Kumamoto Earthquake, Yoshida (2017) suggested that the regional stress field of Honshu Island could be extended to Kyushu Island and that the kinematics of the Philippine Sea Plate could have been affecting the stress field in Kyushu since the late Miocene. Therefore, key points were reassessed, such as the timing of the Izu-Bonin-Mariana arc-basin system collision with central Japan and the history of motion of the Philippine Sea plate. The resulting model favours the Izu-Bonin-Mariana-central Japan collision from ca. 8-6 Ma rather than the more widely accepted date of ca. 15-14 Ma (Mahony et al., 2011; Ma et al., in preparation).

5 Conclusion

(1) We reconstructed the northeast Asian tectonic regime with continuously closing and deforming plates that were based on a newly built global plate motion model. The plate boundaries, subduction zones and suture zones in northeast Asia were reconstructed through time; these include the Jurassic advancing subduction, the Cretaceous-Tertiary retreat subduction of the western Pacific oceanic plate, and the terrane accretion along the margin of northeast Asia. The deformation within deforming regions bound by rigid plates was determined by reconstructing individual features (including faults, basin boundaries, and outcrop points) progressively backward in time. Deforming areas were restricted to defined boundaries in time and space, and the deformation field was interpolated between control points.

(2) Northeast Asia underwent multiple episodes of deformation with different kinematic features. The deformation patterns in northeast Asia were mainly

characterized by two episodes of NW-SE shortening, which occurred during the Early-Middle (or early Late) Jurassic and the Late Jurassic-earliest Cretaceous. The related western Pacific subduction zone, the Mudanjiang and Mino-Tanba zone, advanced westwards.

After the final collision of the Mongol-Okhotsk Ocean, northeast China shifted to a WNW-ESE-trending extension regime with the development of the western, middle, and eastern rift-basin zones. The related western Pacific subduction zone moved back eastward to the Sanbagawa-North Shimanto accretional zone.

During the Late Cretaceous, the north-easternmost part of Asia experienced short-term shortening with NW-SE-trending maximum strain axes, but the area to the south mostly experienced extensional strain with NW-SE- and NNW-SSE-trending maximum strain axes. This difference in deformation may have been related to the westward-advancing subduction along the Sanbagawa-North Shimanto accretional zone to the north and the eastward retreat along the East Asian subduction zone to the south.

Cenozoic deformation in northeast Asia was characterized by intracontinental and back-arc rifting due to WNW-ESE- and nearly N-S-oriented extensions. The related western Pacific subduction zone moved back to the east or southeast, with ridge and arc subduction.

(3) Relative and absolute plate motions of the Eurasian plate and its surrounding plates indicate three motion periods: one with intermediate motion rates (mean APM of 6-11 cm/yr^{-1}) from ca. 200-140 Ma, one with high motion rates (mean APM of 4-13 cm/yr^{-1}) from 139-50 Ma, and one with reduced motion rates (mean APM of 2-11 cm/yr^{-1}) after 50 Ma. From ca. 200-140 Ma, the Eurasian, Tethys, and Izanagi plates converged towards the Mongolia-China continent, which triggered advancing subduction along the western Pacific, intracontinental folding and thrusting, and the formation of an intermountain flexural basin. The two instances of APM lows and changes in the plate motion direction between the Izanagi and Mongolia-China plates may have been related to two episodes of weak deformation from intracontinental volcanic activity, which were recorded in the Nandaling and Tiaojishan Formations in

the North China Craton.

During the Cretaceous, different spreading centres and subduction zones in the Central Atlantic, Caribbean Sea, and Tethys and high-speed seafloor spreading in Panthalassa induced the clockwise motion and obduction of the Eurasian continent across the Izanagi plate's centre. Two instances of high-speed north-westward plate subduction and trench retreat along the western Pacific subduction zone from 139-120 Ma and from 82-60 Ma resulted in intra-continent and back-arc extension and rifting in northeast Asia. Advancing subduction along the Shimanto zone from ca. 88-80 Ma triggered basin inversion along the north-eastern margin of Asia.

Spreading in the northern Atlantic drove the clockwise rotation of Eurasia and the obduction of its eastern margin across the edges of the Izanagi-Pacific plate during the Cenozoic. High-speed indentation from the Indian plate and the spreading of the subducted Izanagi-Pacific ridge from 59-48 Ma triggered spreading and rifting in East Asia. We suggest that diminished convergence along the western Pacific subduction zone from 37-35 Ma triggered trench retreat, back-arc extension, and rifting. From 32-25 Ma, the NW-SE-trending ridge in the Philippine Sea plate quickly subducted to the northwest, which triggered a nearly N-S-oriented extension in the Bohai Bay basin and East China Sea basins. The back-arc extensions in different directions, which were driven by the retreat of the Nankai and Hokkaido subduction zones from 24-15 Ma, and the subduction of the Izu-Bonin-Mariana arc from 14-5 Ma may have been the primary mechanisms leading to the development of the Japan Sea basin.

Acknowledgements

The work was funded by National Key R&D Plan (Grant No. 2017YFC0601405), Chinese Natural Science Foundation grants (Nos. 91114203 and 41572189), and the Strategic Priority Research Program (B) of the Chinese Academy of Sciences (Grant No. XDB18000000).

Appendix A. Supplementary data

Supplementary data to this article can be found online at

References

A, M.N., Zhang, F.Q., Yang, S.F., Chen, H.L., Batt, G.E., Sun, M.D., Meng, Q.A., Zhu, D.F., Cao, R.C., Li, J.S., 2013. Early Cretaceous provenance change in the southern Hailar Basin, northeastern China and its implication for basin evolution. Cretaceous Research 40, 21-42.

Afonso, J.C., Fernàndez, M., Ranalli, G., Griffin, W.L., Connolly, J.A.D., 2008. Integrated geophysical-petrological modeling of the lithosphere and sublithospheric upper mantle: Methodology and applications. Geochemistry Geophysics Geosystems 9(5): 303-307.

An, W., Kuang, H.W., Liu, Y.Q., Peng, N., Xu, K.M., Xu, H., Zhang, P., Wang, K.B., Chen, S.Q., Zhang, Y.X., 2016. Detrital zircon dating and tracing the provenance of dinosaur bone beds from the Late Cretaceous Wangshi Group in Zhucheng, Shandong, East China. Journal of Paleogeography 5, 72-99.

Barnes, L.G., 2003. Origins of the Japanese Islands: The New "Big Picture". Japan Review 15, 3-50.

Beaman, M., Sager, W.W., Acton, G.D., Lanci, L., Pares, J., 2007. Improved Late Cretaceous and Early Cenozoic paleomagnetic apparent wander path for the Pacific plate. Earth and Planetary Science Letters 262, 1–20.

Bonnetti, C., Malartre, F., Huault, V., Cuney, M., Bourlange, S., Liu, X.D., Peng, X.B., 2014. Sedimentology, stratigraphy and palynological occurrences of the late Cretaceous Erlian Formation, Erlian Basin, Inner Mongolia, People's Republic of China. Cretaceous Research 48, 177-192.

Boyden, J.A., Müller, R.D., Gurnis, M., Torsvik, T.H., Clark, J.A., Turner, M., Ivey-Law, H., Watson, R.J., Cannon, J.S., 2011. Next-generation plate-tectonic reconstructions using GPlates. In: Keller, G.R., Baru, C. (Eds.), Geoinformatics: Cyberinfrastructure for the Solid Earth Sciences. Cambridge University Press, pp: 95–114.

Butterworth, N., Talsma, A., Müller, R., Seton, M., Bunge, H.-P., Schuberth, B.,

Shephard, G., Heine, C., 2014. Geological, tomographic, kinematic and geodynamic constraints on the dynamics of sinking slabs. Journal of Geodynamics 73, 1–13.

Cao, X., Dang, Z.X., Zhang, X.Z., Jiang, J.S., Wang, H.D., 1992. The Composite Jiamusi Terrane. Jilin Publishing House of Science and Technology, Changchun (in Chinese with English and Russian abstracts).

Chang, SC., Zhang, H., Hemming, S.R., Mesko, G.T., Fang, Y., 2014. $^{40}Ar/^{39}Ar$ age constraints on the Haifanggou and Lanqi formations: When did the first flowers bloom? Geological Society, London, Special Publications, 378(1), pp. 277-284.

Charvet, J., 2013. Late Paleozoic–Mesozoic tectonic evolution of SW Japan: A review – Reappraisal of the accretionary orogeny and revalidation of the collisional model. Journal of Asian Earth Sciences 72, 88-101.

Chen, Z.G., Zhang, L.C., Wu, Y.H., Zhou, X.H., Liu, Q., 2009. Ar–Ar age, geochemistry and petrogenesis of Late Mesozoic volcanic rocks in the northern marginal region of Erlian basin, Inner-Mongolia. Acta Petrologica Sinica 25, 297–310 (in Chinese with English Abstract).

China Geological Survey, 2004. Geological map of People's Republic of China, 1:2 500 000, China Cartographic Publishing House, Beijing.

Chough, S.K., Barg, E., 1987. Tectonic history of Ulleung basin margin, East Sea (Sea of Japan). Geology 15, 45-48.

Conrad, C.P., Lithgow-Bertelloni, C., 2006. Influence of continental roots and asthenosphere on plate-mantle coupling. Geophysical Research Letters 33, 308-314.

Cope, T., 2003. Sedimentary Evolution of the Yanshan Fold-thrust Belt, Northeast China. Dissertation of Stanford University for Doctoral Degree, California, pp: 1-230.

Cope, T., Ping, L., Zhang, X.Y., Zhang, X.J., Song, J., Zhou, G., Shultz, M.R., 2010. Structural controls on facies distribution in a small half-graben basin: Luanping basin, NE China. Basin Research 22, 33–44.

Crespi, M., Cuffaro, M., Doglioni, C., Giannone, F., and Riguzzi, F., 2007. Space geodesy validation of the global lithospheric flow. Geophysical Journal International 168: 491-506.

Cruciani, C., Carminati, E., Doglioni, C., 2005. Slab dip vs. lithosphere age: no direct

function. Earth Planetary Science Letters 238: 298– 310.

Cuffaro, M., and Doglioni, C., 2007. Global Kinematics in the deep versus shallow hotspot reference frames. In: Foulger, G.R., and Jurdy, D.M., eds., Plates, plumes, and planetary processes, Geological Society of America Special Paper 430: 359–374.

Cukur, D., Horozal, S., Lee, G.H., Kim, D.C., Han, H.C., Kang, M.H., 2011. Structural evolution of the northern East China Sea Shelf Basin interpreted from cross-section restoration. Mar Geophys Research 32, 363–381

Darby, B.J., Davis, G.A., Zhang, X.H., Wilde, S., Yang, J.H., 2004. The newly discovered Waziyu metamorphic core complex, Yiwulü Shan, western Liaoning province, northwest China. Earth Science Frontier 11, 145–155 (in English with Chinese abstract).

Darby, B.J., Davis, G.A., Zheng, Y., 2001. Structural evolution of the southwestern Daqing Shan, Yinshan belt, Inner Mongolia, China. In: Hendrix, M.S., Davis, G.A. (Eds.), Paleozoic and Mesozoic tectonic evolution of central and eastern Asia – from continental assembly to intracontinental deformation, Boulder, CO, Geological Society of America Memoir 194, pp. 199–214.

Darby, B.J., Ritts, B.D., 2002. Mesozoic contractional deformation in the middle of the Asian tectonic collage: the intraplate Western Ordos fold–thrust belt, China. Earth and Planetary Science Letter 205, 13–24.

Davis, G.A., 2005. The Late Jurassic "Tuchengzi/Houcheng" Formation of the Yanshan fold-thrust belt: an analysis. Earth Science Frontiers 12, 331–345.

Davis, G.A., Darby, B.J., 2010. Early Cretaceous overprinting of the Mesozoic Daqing Shan fold-and-thrust belt by the Hohhot metamorphic core complex, Inner Mongolia, China. Geoscience Frontier 1, 1–20.

Davis, G.A., Darby, B.J., Zheng, Y., Spell, T.L., 2002. Geometric and temporal evolution of an extensional detachment fault, Hohhot metamorphic core complex, Inner Mongolia, China. Geology 30, 1003–1006.

Davis, G.A., Qian, X., Zheng, Y., Tong, H., Yu, H., Gehrels, G., Shafiqullah,M., Fryxell, J., 1996. Mesozoic deformation and plutonism in the Yunmeng Shan: a metamorphic core complex north of Beijing, China. In: Yin, A., Harrison, T.M. (Eds.),

The Tectonic Evolution of Asia. Cambridge University Press, Cambridge, U.K., pp. 253–280.

Davis, G.A., Zheng, Y.D., Wang, C., Darby, B.J., Zhang, C.H., Gehrels, G.E., 2001. Mesozoic tectonic evolution of the Yanshan fold and thrust belt, with emphasis on Hebei and Liaoning Provinces, Northern China. In: Hendrix, M.S., Davis, G.A. (Eds.), Paleozoic and Mesozoic Tectonic Evolution of Central Asia: From Continental Assembly to Intracontinental Deformation. Geological Society of America Memoir, 194, pp. 171–197.

Doglioni, C., Carminati, E., Cuffaro, M., Scrocca, D., 2007. Subduction kinematics and dynamic constraints. Earth-Science Reviews 83: 125-175.

Doglioni, C., Green, D.H., Mongelli, F., 2005. On the shallow origin of hotspots and the westward drift of the lithosphere. Special Paper of the Geological Society of America 388(42): 735-749.

Doglioni, C. and Panza, G.F., 2015. Polarized plate tectonics. Advances in Geophysics, 56, 3, 1-167.

Engebretson, D.C., Cox, A., Gorden, R.G., 1985. Relative motions between oceanic and continental plates in the Pacific basin. The Geological Society of America, Special Paper 206, 1–59.

Feng, Z.Q., Jia, C.Z., Xie, X.N., Zhang, S., Feng, Z.H., Cross, T.A., 2010. Tectonostratigraphic units and stratigraphic sequences of the nonmarine Songliao Basin, NE China. Basin Research 22, 79–95.

Flament, N., Gurnis, M., Williams, S., Seton, M., Skogseid, J., Heine, C., Müller, R. D., 2014. Topographic asymmetry of the South Atlantic from global models of mantle flow and lithospheric stretching, Earth and Planetary Science Letter 387, 107–119.

Forsyth, D.W., Uyeda, S., 1975. On the relative importance of the driving forces of plate motions. Geophysical Journal 43, 163-200.

Gao, S., Rudnick, R.L., Yuan, H.L., Liu, X.M., Liu, Y.S., Xu, W.L., Ling, W.L., Ayers, J., Wang, X.C., Wang, Q.H., 2004. Recycling lower continental crust in the North China craton. Nature 432, 892–897.

Ge, R.F., Zhang, Q.L., Wang, L.S., Chen, J., Xie, G.A., Wang, X.L., 2012. Late

mesozoic rift evolution and crustal extension in the central songliao basin, northeastern china: constraints from cross-section restoration and implications for lithospheric thinning. International Geology Review 54, 183-207.

Goes, S., Capitanio, F.A., Morra, G., 2008. Evidence of lower mantle slab penetration phases in plate motions. Nature 451, 981–84.

Gurnis, M., Turner, M., Bower, D., 2013. Advancing cyberinfrastructure for plate reconstructions: Present day mantle structure and the stratigraphic architecture of continents assignals of a dynamic Earth. Geological Society of America Abstract Programs. Denver, Colorado USA, 45(7): 233.

Gurnis, M., Turner, M., Zahirovic, S., Dicaprio, L., Spasojevic, S., Müller, R.D., Boyden, J., Seton, M., Manea, V., Bower, D., 2012. Plate tectonic reconstructions with continuously closing plates. Computers and Geosciences 38, 35–42.

Gurnis, M., Yang, T., Cannon, J., Turner, M., Williams, S., Flament, N., Müller, R.D., in preparation. Global tectonic reconstructions with continuously evolving deforming and rigid plates.

He, B.Z., Qiao, X.F., Zhang, Y.L., Tian, H.S., Cai, Z.H., Chen, S.Q., Zhang, Y.X., 2015. Soft-sediment deformation structures in the Cretaceous Zhucheng depression, Shandong Province, East China; their character, deformation timing and tectonic implications. Journal of Asian Earth Sciences 110, 101-122.

Hoshi, H., Yokoyama, M., 2001. PaleomagnetismofMiocene dikes in the Shitara basin and the tectonic evolution of central Honshu, Japan. Earth Planets Space 53, 731–739.

Hu, J.M., Zhao, Y., Liu, X.W., Xu, G., 2010. Early Mesozoic deformations of the eastern Yanshan thrust belt, northern China. International Journal of Earth Sciences (Geologische Rundschau) 99, 785–800.

Huang, D.Y., 2015. Yanliao biota and Yanshan movement. Acta Palaeontologica Sinica 54, 501-546.

Huang, J., Zhao, D., 2006. High-resolution mantle tomography of China and surrounding regions. Journal of Geophysical Research 111, B09305, doi:10.1029/2005JB004066.

Isozaki, Y., Aoki, K., Nakama, T., Yanai, S., 2010a. New insight into a subduction-related orogen: A reappraisal of the geotectonic framework and evolution of the Japanese Islands. Gondwana Research 18, 82–105.

Isozaki, Y., Maruyama, S., Aoki, K., Nakama, T., Miyashita, A., Otoh, S., 2010b. Geotectonic subdivision of the Japanese Islands revisited: categorization and definition of elements and boundaries of pacific-type (Miyashiro-type) Orogen. Journal of Geography 119, 999–1053 (in Japanese with English abstract).

Johnson, C.L., Constenius, K.C., Graham, S.A., Mackey, G., Menotti, T., Payton, A., Tully, J., 2015. Subsurface evidence for late Mesozoic extension in western Mongolia: tectonic and petroleum systems implications. Basin Research 27, 272–294.

Jolivet, L., Tamaki, K., Fournier, M., 1994. Japan Sea, opening history and mechanism: a synthesis. Journal of Geophysical Research 99, 22,237–22,259.

Kato, H., 1992. Fossa magna: a masked border region separating southwest and northeast Japan. Bulletin of Geological Survey of Japan 43, 1–30.

Kawai, N., Ito, H., Kume, S., 1961. Deformation of the Japanese Islands as inferred from rock magnetism. Geophysical Journal Royal Astronomical Society 6, 124–130.

Kemkin, V.I., 2012. Microfaunal biostratigraphy and structural framework of the Nadanhada–Bikin terrane within a Jurassic accretionary prism of the Sikhote-Alin Fold Belt, eastern Russia. Journal of Asian Earth Sciences 61, 88-101.

Kemkin, V.I., Taketani, Y., 2008. Structure and age of lower structural unit of Taukha terrane of Late Jurassic–Early Cretaceous accretionary prism, southern Sikhote–Alin. Island Arc 17, 517–530.

Kim, H. J., Lee, G. H., Jou, H. T., Cho, H. M., Yoo, H. S., Park, G. T., Kim J.S., 2007. Evolution of the eastern margin of korea: Constraints on the opening of the east sea (japan sea). Tectonophysics 436, 37-55.

Kim, S.W., Kwon, S., Ryu, I.-C., Jeong, Y.-J., Choi, S.-J., Kee, W.-S., Yi, K., Lee, Y.S., Kim, B.C., Park, D.W., 2012. Characteristics of the early Cretaceous igneous activity in the Korean Peninsula and tectonic implications. Journal of Geology 120, 625–646.

Kim, Y.H., Lee, C., Kim, S.S., 2015. Tectonics and volcanism in East Asia: Insights

from geophysical observations. Journal of Asian Earth Sciences 113, 842-856.

Kimura, G., Miyashita, S., Miyasaka, S., 1983. Collision tectonics in Hokkaido and Sakhalin. In: Hashimoto, M., Uyeda, S. (Eds.), Accretion Tectonics in the Circum-Pacific Regions. Terra Science Publication, Tokyo, pp: 123–134.

Kimura, G., Tamaki, K., 1986. Collision, rotation, and back-arc spreading in the region of the Okhotsk and Japan Seas. Tectonics 5, 389–401.

Kusky, T.M., Windley, B.F., Wang, L., Wang, Z.S., Li, X.Y., Zhu, P.M., 2014. Flat slab subduction, trench suction, and craton destruction: Comparison of the North China, Wyoming, and Brazilian cratons. Tectonophysics 630, 208-221.

Lallemand, S., Jolivet, L., 1986. Japan Sea: A pull-apart basin? Earth and Planetary Science Letter 76, 375–389.

Li, C., Liu, S.F., 2015. Cretaceous anomalous subsidence and its response to dynamic topography in the Songliao Basin, Northeast China. Journal of Asian Earth Sciences 109, 86-99.

Li, C., van der Hilst, Engdahl, E.R., Burdick, S., 2008. A new global model for P wave speed variations in Earth's mantle. Geochemistry, Geophysics, Geosystems 9, Q05018, doi:10.1029/2007GC001806.

Li, J., Dong, S., Yin, A., Zhang, Y., Shi, W., 2015. Mesozoic tectonic evolution of the Daba Shan Thrust Belt in the southern Qinling orogen, central China: Constraints from surface geology and reflection seismology, Tectonics 34, 1545–1575, doi:10.1002/2014TC003813.

Li, N., Li, W.R., Long, H.Y., 2013. Study of positive inversion structures in the north depression of the South Yellow Sea Basin. Marine Geology and Quaternary Geology 33, 95-100.

Li, S.Z., Jahn, B.M., Zhao, S.J., Dai, L.M., Li, X.Y., Suo, Y.H., Guo, L.L., Wang, Y.M., Liu, X.C., Lan, H.Y., Zhou, Z.Z, Zheng, Q.L., Wang, P.C., 2017. Triassic southeastward subduction of North China Block to South China Block: Insights from new geological, geophysical and geochemical data. Earth-Science Reviews 166: 270-285.

Li, S.Z., Liu, X., Suo, Y.H., Liu, L.P., Qian, C.C., Liu, X.C., Zhang, G.W., Zhao,

G.C., 2009. Triassic folding and thrusting in the eastern block of the North China Craton and the Dabie–Sulu orogen and its geodynamics. Acta Petrologica Sinca 25, 2031–2049 (in Chinese with English abstract).

Li, S.Z., Zhao, G.C., Dai, L.M., Liu, X., Zhou, L.H., Santosh, M., Suo, Y.H., 2012a. Mesozoic basins in eastern China and their bearing on the deconstruction of the North China Craton. Journal of Asian Earth Sciences 47: 64-79.

Li, S.Z., Zhao, G.C., Dai, L.M., Zhou, L.H., Liu, X., Suo, Y.H., Santosh, M., 2012b. Cenozoic faulting of the Bohai Bay Basin and its bearing on the destruction of the eastern North China Craton. Journal of Asian Earth Sciences 47: 80-93.

Li, S.Z., Zhao, S.J., Liu, X., Cao, H.H., Yu, S., Li, X.Y., Somerville, I., Yu, S.Y., Suo, Y.H., in press. Closure of the Proto-Tethys Ocean and Early Paleozoic amalgamation of microcontinental blocks in East Asia. Earth-Science Reviews.

Li, W.P., 2015. Analysis of structural deformation and evolution in the Dabashan arc-shaped belt, the northern margin of the Upper Yangtze Plate, Dissertation of China University of Geosciences for Doctoral Degree, Beijing, pp. 1-121.

Li, W.P., Liu, S.F., Wang, Y., Qian, T., and Gao T.J., 2017. Duplex thrusting in the South Dabashan arcuate belt, central China. Journal of Structural Geology (submitted).

Li, W.P., Lu, F.X., Sun, S.P., Li, J.Z., 2000. Discussion on the origin of volcanic rocks of Donglingtai Formation in Beijing Xishan Mountain and its geological setting. Acta Petrologica Sinica 16, 345–352 (in Chinese).

Liang, J., Wang, H.L., Bai, Y., Ji, X.Y., Duo, X.M., 2016. Cenozoic tectonic evolution of the Bohai Bay Basin and its coupling relationship with Pacific Plate subduction. Journal of Asian Earth Sciences 127, 257-266.

Lin, W., Faure, M., Monie, P., Scharer, U., Panis, D., 2008. Mesozoic extensional tectonics in eastern Asia: The South Liaodong Peninsula Metamorphic Core Complex (NE China). Journal of Geology 116, 134–154.

Liu, J., Zhao, Y., Liu A.K., Ye H., Late Jurassic to Early Cretaceous sedimentary-tectonic development in the Chengde Basin, Yanshan fold-thrust belt, North China Craton, Journal of Asian Earth Sciences, 2015a, 144: 611-622.

Liu, J., Zhao, Y., Liu, X., Wang, Y., Liu, X., 2012. Early Jurassic rapid exhumation of the basement rocks along the northern margin of the North China Craton: evidence from the Xiabancheng basin in the Yanshan Tectonic Belt. Basin Research 24, 544–558.

Liu, J.L., Davis, G.A., Lin, Z., Wu, F., 2005a. The Liaonan metamorphic core complex, Southeastern Liaoning Province, North China: a likely contributor to Cretaceous rotation of Eastern Liaoning, Korea and contiguous areas. Tectonophysics 407, 65–80.

Liu, S.F., 1998. The coupling mechanism of basin and orogen in the western Ordos Basin and adjacent regions of China. Journal of Asian Earth Sciences 16, 369-383.

Liu S.F., Heller, L.P, Zhang, G.W., 2003. Mesozoic basin development and tectonic evolution of the Dabieshan orogenic belt, central China. Tectonics 22, 1038, doi: 10.1029/2002TC001390

Liu, S.F., Li, W.P., Wang, K., Qian, T., Jiang, C.X., 2015b. Late Mesozoic development of the southern Qinling-Dabieshan foreland fold-thrust belt, Central China, and its role in continent-continent collision. Tectonophysics 644-645, 220-234, 10.1016/j.tecto.2015.01.015.

Liu, S.F., Li, Z., Zhang, J.F., 2004. Mesozoic basin evolution and tectonic mechanism in Yanshan, China. Science in China, Series D 47 (Supp. II), 24-38.

Liu, S.F., Lin, C.F., Liu, X.B., and Zhuang, Q.T., 2017. Syn-tectonic sedimentation and its linkage to fold-thrusting in the region of Zhangjiakou, North Hebei, China. Science China Earth Sciences (submitted).

Liu, S.F., Liu, W.C., Dai, S.W., Huang, S.J., Lu, W.Y., 2001. Thrust and exhumation processes of bounding mountain belt: constrained from sediment provenance analysis of Hefei Basin, China. Acta Geologica Sinica 75, 144–150.

Liu, S.F., Nummedal, D., 2004. Late Cretaceous subsidence in Wyoming: Quantifying the dynamic component. Geology 32, 397-400.

Liu, S.F., Nummedal, D., Gurnis, M., 2014. Dynamic versus flexural controls of Late Cretaceous Western Interior Basin, USA. Earth and Planetary Science Letters 389, 221-229.

Liu, S.F., Qian, T., Li, W.P., Dou, G.X., Wu, P., 2015c. Oblique closure of the northeastern Paleo-Tethys in central China. Tectonics 34, doi:10.1002/2014TC003784.

Liu, S.F., Steel, R., Zhang, G.W., 2005b. Mesozoic sedimentary basin development and tectonic implication, northern Yangtze Block, eastern China: record of continent-continent collision. Journal of Asian Earth Sciences 25, 9-27.

Liu, S.F., Su, S., Zhang, G.W., 2013. Early Mesozoic basin development in North China: Indications of cratonic deformation. Journal of Asian Earth Sciences 62, 221-236.

Liu, S.F., Yang, S.G., 2000. Upper Triassic-Jurassic sequence stratigraphy and its structural controls in the western Ordos Basin, China. Basin Research 12, 1-18.

Liu, S.F., Zhang, G.W., Ritts, B., Zhang, H.P., Gao, M.X., Qian, C.C., 2010. Tracing exhumation of the Dabie Shan UHP metamorphic complex using the sedimentary record in the Hefei basin, China. Geological Society of America Bulletin 122, 198-218.

Liu, S.F., Zhang, J.F., Hong, S.Y., Ritts, B., 2007. Early Mesozoic basin development and its response to thrusting in the Yanshan fold and thrust belt, China. International Geology Review 49, 1025-1049.

Ma, P.F., Liu, S.F., Gurnis, M., in preparation. Flat-slab subduction and tearing within the transition zone in East Asian continental margin.

Malinovsky, I.A., Golozoubov, V.V., Simanenko, P.V., Simanenko, F.L., 2008. Kema terrane: A fragment of a back-arc basin of the early Cretaceous Moneron–Samarga island-arc system, East Sikhote–Alin range, Russian Far East. Island Arc 17, 285–304

Martin, A.K., 2011. Double saloon door tectonics in the Japan Sea, Fossa Magna, and the Japanese Island Arc. Tectonophysics 498, 45–65.

Metcalfe, I., 2006. Palaeozoic and Mesozoic tectonic evolution and palaeogeography of East Asian crustal fragments: The Korean Peninsula in context. Gondwana Research 9, 24–46.

Miki, M., Matsuda, T., and Otofuji, Y., 1990. Opening mode of the Okinawa Trough:

paleomagnetic evidence from the South Ryukyu Arc. Tectonophysics 175: 335-347.

Müller, R.D., Seton, M., Zahirovic, S., Williams, E.S., Matthews, J.K., Wright, M.N., Shephard, E.G., Maloney, T.K., Barnett-Moore, N., Hosseinpour, M., Bower, J.D., Cannon, J., 2016. Ocean Basin Evolution and Global-Scale Plate Reorganization Events Since Pangea Breakup. Annual Review of Earth & Planetary Sciences 44, 107-138.

Natal'in, B. A., Borukayev, C.B., 1991. Mesozoic sutures in the southern Far East of USSR. Geotectonics 25, 64–74.

Niu, B.G., He, Z.J., Song, B., Ren, J.S., 2003. SHRIMP dating of volcanic rocks of t he Zhangjiakou Formation and it s significance. Geological Bulletin of China 22, 140–141 (in Chinese).

Nohda, S., 2009. Formation of the Japan Sea basin: reassessment from Ar–Ar ages and Nd–Sr isotopic data of basement basalts of the Japan Sea and adjacent regions. Journal of Asian Earth Sciences 34, 599–609.

Otofuji, Y., 1996. Large tectonic movement of the Japan Arc in Late Cenozoic times inferred from palaeomagnetism: Review and synthesis. Island Arc 5, 229–249.

Phillips, B.R., Bunge, H.P., 2005. Heterogeneity and time dependence in 3D spherical mantle convection models with continental drift. Earth and Planetary Science Letters 233, 121-135.

Qi, J.F., Yang, Q., 2010. Cenozoic structural deformation and dynamic processes of the Bohai Bay basin province, China. Marine and Petroleum Geology 27, 757–771.

Qu, X.Y., Yang, M.H., Luo, X.H., Ding, C., Zhou, D., Gong, T., Yang, G., 2013. Extensional tectonic feature and its control on hydrocarbon accumulation of Saihanta Sag in Erlian Basin. Geoscience 27, 1023-1032 (in Chinese with English Abstract).

Raimbourg, H., Augier, R., Famin, V., Gadenne, L., Palazzin, G., Yamaguchi, A., Kimura, G., 2014. Long-term evolution of an accretionary prism: The case study of the Shimanto Belt, Kyushu, Japan. Tectonics 33, 936–959, doi:10.1002/2013TC003412.

Ren, J., Niu, B.G., Wang, J., Jin, X.C., Xie, L.Z., 2013. 1:5 000 000 International Geological Map of Asia. Geological Publishing House, Beijing.

Ren, J., Tamaki, K., Li, S., Junxia, Z., 2002. Late Mesozoic and Cenozoic rifting and its dynamic setting in Eastern China and adjacent areas. Tectonophysics 344, 175–205.

Ren, Q., Zhang, S.H., Wu, H.C., Liang, Z.K., Miao, X.J., Zhao, H.Q., Li, H.Y., Yang, T.S., Pei, J.L., Davis, A.G., 2016. Further paleomagnetic results from the ~ 155 Ma Tiaojishan Formation, Yanshan Belt, North China, and their implications for the tectonic evolution of the Mongol–Okhotsk suture. Gondwana Research 35, 180-191.

Ritts, B.D., Darby, B.J., Cope, T., 2001. Early Jurassic extensional basin formation in the Daqing Shan segment of the Yinshan belt, northern North China Block, Inner Mongolia. Tectonophysics 339, 235–253.

Ritts, D.B., Weislogel, A., Graham, A.S., Darby, J.B., 2009. Mesozoic Tectonics and Sedimentation of the Giant Polyphase Nonmarine Intraplate Ordos Basin, Western North China Block. International Geology Review 51, 95–115.

Sager, W.W., 2006. Cretaceou paleomagnetic apparent polar wander path for the Pacific plate calculated from Deep Sea Drilling Project and Ocean Drilling Program basalt cores. Physics of the Earth and Planetary Interiors 156, 329–349.

Sengör, A.M.C., Cin, A., Rowley, D.B., S-Y, N., 1993. Space-time patterns of magmatism along the Tethysides: A Preliminary Study. Journal of Geology 101, 51–84.

Seno, T., 1985. "Northern Honshu microplate" hypothesis and tectonics in the surrounding region: When did the plate boundary jump from Central Hokkaido to the eastern margin of the Japan Sea? Journal of the Geodetic Society of Japan, 31: 106-123.

Seno, T., and Maruyama, S., 1984. Paleogeographic reconstruction and origin of the Philippine Sea. Tectonophysics 102: 53-84.

Seton, M., Flament, N., Whittaker, J., Müller, R.D., Gurnis, M., Bower, D.J., 2015. Ridge subduction sparked reorganization of the Pacific plate-mantle system 60–50 million years ago. Geophysical Research Letter 42, 1732–1740, doi:10.1002/2015GL063057.

Seton, M., Müller, R.D., Zahirovic, S., Gaina, C., Torsvik, T., Shephard, G., Talsma,

A., Gurnis, M., Turner, M., Maus, S., Chandler, M., 2012. Global continental and ocean basin reconstructions since 200 Ma. Earth-Science Reviews 113, 212–270.

Shinn, Y.J., Chough, S.K., Hwang, I.G., 2010. Structural development and tectonic evolution of Gunsan Basin (Cretaceous–Tertiary) in the central Yellow Sea. Marine and Petroleum Geology 27, 500-514.

Song, Y., Ren, J., Stepashko, A.A., Li, J.G., 2014. Post-rift geodynamics of the Songliao Basin, NE China: Origin and significance of T11 (Coniacian) unconformity. Tectonophysics 634, 1-18.

Stadler, G., M. Gurnis, C. Burstedde, L. C. Wilcox, L. Alisic, and O. Ghattas, 2010. The dynamics of plate tectonics and mantle flow: From local to global scales, Science, 329, doi: 10.1126/science.1191223, 1033-1038.

Suo, Y.H., Li, S.Z., Zhao, S.J., Somerville, I.D., Yu, S., Dai, L.M., Xu, L.Q., Cao, X.Z., Wang, P.C., 2013. Continental margin basins in East Asia: Tectonic implications of the Meso-Cenozoic East China Sea pull-apart basins. Geological Journal DOI: 10.1002/gj.

Swisher III, C.C., Wang, X.L., Zhou, Z.H., Wang, Y.Q., Jin, F., Zhang, J.Y., Xu, X., Zhang, F.C., Wang, Y., 2002. Further support for a cretaceous age for the feathered dinosaur beds of Liaoning, China: New $^{40}Ar/^{39}Ar$ dating of the Yixian and Tuchengzi. Chinese Science Bulletin 47, 135–138.

Taira, A., 2001. Tectonic evolution of the Japanese Island arc system. Annual Review of Earth and Planetary Sciences 29, 109–34

Tamaki, K., Suyehiro, K., Allan, J., Ingle, Jr., J.C., Pisciotto, K.A., 1992. Tectonic synthesis and implications of Japan Sea ODP Drilling. Proceedings of the Ocean Drilling Program Scientific Results, 127/128, 1333-1348.

Tong, Y.M., 2007. The paleotectonic stress field at Laiyang Stage in Jiaolai Basin and the simulation. Petroleum Geology and Oilfield Development in Daqing 26, 6-9.

Wakita, K., 2013. Geology and tectonics of Japanese islands: A review – The key to understanding the geology of Asia. Journal of Asian Earth Sciences 72, 75-87.

Wan, T.F., Zhu, H., 1996. The maximum sinistral strike-slip displacement and formation time of the Tan–Lu fault zone. Geological Journal of China University 2,

14–27 (in Chinese with English abstract).

Wang, F., Zhou, X.H., Zhang, L.C., Ying, J.F., Zhang, Y.T., Wu, F.Y., Zhu, R.X., 2006. Late Mesozoic volcanism in the Great Xing'an range (NE China): Timing and implications for the dynamic setting of NE Asia. Earth and Planetary Science Letters 251, 179–198.

Wang, G., Jiang, B., Cao, D., Zhou, H., Jin,W., 1998. On the Xuzhou–Suzhou arcuate duplex–imbricate fan thrust system. Acta Geologica Sinica 72, 228–236 (in Chinese with English abstract).

Wang, J., Chang, S.C., Lu, H.B., Zhang, H.C., 2016. Detrital zircon provenance of the Wangshi and Laiyang groups of the Jiaolai basin: Evidence for Early Cretaceous uplift of the Sulu orogen, Eastern China. International Geology Review DOI: 10.1080/00206814.2015.1105728

Wang, X., Zhong, D., Wang, Y., 2008. Geometry, kinematics and thermochronology study of the Late Mesozoic movement of NW-trending faults, western Shandong. Acta Geologica Sinica 82, 1258–1273 (in Chinese with English abstract).

Wang, X.F., Li, Z.J., Chen, B.L., Chen, X.H., Dong, S.W., Zhang, Q.,Wu, H.L., Xin, L.S., Zhang, H., Dong, F.X., Wu, H.M., Huo, G.H., Lin, C.Y., Bai, J.Q., Liu, X.C., 2000. On Tan–Lu Fault Zone. Geological Publishing House, Beijing, pp: 1-374 (in Chinese with English abstract).

Wang, X.S., Zheng, Y.D., 2005. $^{40}Ar/^{39}Ar$ ages constraints on the ductile deformation of the detachment system of the Louzidian core complex, southern Chifeng, China. Geological Review 51, 574–582 (in Chinese with English abstract).

Wang, Y., 2006. The onset of the Tan-Lu fault movement in eastern China: Constraints from zircon (SHRIMP) and $^{40}Ar/^{39}Ar$ dating. Terra Nova 18, 423-431.

Wang, Y., Li, H.M., 2008. Initial formation and Mesozoic tectonic exhumation of an intracontinental tectonic belt of the northern part of the Taihang mountain belt, Eastern Asia. The Journal of Geology 116, 155–172.

Wang, Y., Zhou, L.Y., Li, J.Y., 2011. Intracontinental superimposed tectonics—A case study in the Western Hills of Beijing, eastern China. GSA Bulletin 123, 1033-1055.

Wang, Y., Zhou, S., 2009. $^{40}Ar/^{39}Ar$ dating constraints on the high-angle normal faulting along the southern segment of the Tan-Lu fault system: An implication for the onset of eastern China rift-systems. Journal of Asian Earth Sciences 34, 51-60.

Wessel, P., Kroenke, L., 2008. Pacific absolute plate motion since 145 Ma: an assessment of the fixed hot spot hypothesis. Journal of Geophysical Research 113: B06101

Wu, F.Y., Yang, J.H., Lo, C.H., Wilde, A.S., Sin, D.Y., Jahn, B.M., 2007. The Heilongjiang Group: A Jurassic Accretionary complex in the Jiamusi Massif at the western Pacific margin of northeastern China. Ialand Arc 16, 156-172.

Wu, H., Zhang, S., Jiang, G., Huang, Q., 2009. The floating astronomical time scale for the terrestrial Late Cretaceous Qingshankou Formation from the Songliao Basin of Northeast China and its stratigraphic and paleoclimate implications. Earth Planetary Science Letter 10, 308–323.

Xiao, W.D., Tang, X.N., 2014. Development of balanced cross-section technique and its application to Qintong Depression of North-Jiangsu Basin. Marine Geology Frontiers 30, 58-63 (in Chinese with English Abstract).

Xu, W.L., Pei, F.P., Wang, F., Meng, E., Ji, W.Q., Yang, D.B., Wang, W., 2013. Spatial–temporal relationships of Mesozoic volcanic rocks in NE China: Constraints on tectonic overprinting and transformations between multiple tectonic regimes. Journal of Asian Earth Sciences 74, 167-193.

Yamaji, A., 1990. Rapid intra-arc rifting in Miocene northeast Japan. Tectonics 9, 365–378.

Yang, J.H., Wu, F.Y., Shao, J.A., Wilde, S.A., Xie, L.W., Liu, X.M., 2006. Constraints on the timing of uplift of the Yanshan fold and thrust belt, north Chian. Earth and Planetary Science Letters 246, 336–352.

Yang, Y.T., Guo, Z.X., Song, C.C., Li, X.B., He, S., 2014. A short-lived but significant Mongol–Okhotsk collisional orogeny in latest Jurassic–earliest Cretaceous. Gondwana Research 28, 1096–1116.

Yoshida, M., 2017. Re-evaluation of the regional tectonic stress fields and faulting regimes in central Kyushu, Japan, behind the 2016 M_w 7.0 Kumamoto Earthquake.

Tectonophysics 712-713: 95-100.

Yoshida, M., 2017. Trench dynamics: Effects of dynamically migrating trench on subducting slab morphology and characteristics of subduction zones systems. Physics of the Earth and Planetary Interiors 268, 35-53.

Zahirovic, S., Matthews, K.J., Flament, N., Müller, R.D., Hill, K.C., Seton, M., Gurnis, M., 2016. Tectonic evolution and deep mantle structure of the eastern Tethys since the latest Jurassic. Earth-Science Reviews 162, 293-337.

Zahirovic, S., Müller, R.D., Seton, M., Flament, N., 2015. Tectonic speed limits from plate kinematic reconstructions. Earth and Planetary Science Letters 418, 40–52.

Zahirovic, S., Seton, M., Müller, R. D., 2014. The Cretaceous and Cenozoic tectonic evolution of Southeast Asia. Solid Earth 5: 227–273.

Zhang, C.H., Chen, A.G., Bai, Z.D., 1997. Thick-skinned thrust tectonics and its significance to exploration of concealed coalfield in Xinglong coalfield and adjacent area, Hebei Province, Geoscience 11, 305-312(in Chinese with English abstract).

Zhang, C.H., Li, C.M., Deng, H.L., Liu, Y., Liu, L., Wei, B., Li, H.B., Liu, Z., 2011. Mesozoic contraction deformation in the Yanshan and northern Taihang mountains and its implications to the destruction of the North China Craton. Science in China Earth Science 54, 798–822.

Zhang, C.H.,Wang, G.H.,Wang, G.S.,Wu, Z.W., Zhang, L.S., Sun,W.H., 2002. Thrust tectonics in the eastern segment of the intraplate Yanshan orogenic belt, western Liaoning Province, North China. Acta Geologica Sinica 76, 64–76 (in Chinese with English abstract).

Zhang, F. Q., Chen, H. L., Batt, G. E., Dilek, Y., Min-Na, A., Sun, M. D., Yang, S.F., Meng, Q.A., Zhao, X.Q., 2015. Detrital zircon U-Pb geochronology and stratigraphy of the cretaceous Sanjiang basin in NE china: provenance record of an abrupt tectonic switch in the mode and nature of the NE Asian continental margin evolution. Tectonophysics 665, 58-78.

Zhang, F.Q., Chen, H.L., Yang, S.F., Feng, Z.Q., Wu, H.Y., Batt, G.E., Zhao, X.Q., Sun, M.D., A, M.N.,Wang, S.H., Yang, J.G., 2012. Late Mesozoic–Cenozoic evolution of the Sanjiang Basin in NE China and its tectonic implications for the West

Pacific continental margin. Journal of Asian Earth Sciences 49, 287–299.

Zhang, H., Liu, X.M., Gao, S., Zhang, L.J., Li, Z.T., Yang, F.L., Wang, X.C., 2005. Redefinition of the Zhangjiakou formation in Lingyuan, western Liaoning, and it's significance—constraints from laser ICP-MS zircon U–Pb ages. Geological Bulletin of China 24, 110–117.

Zhang, H.Y., Hou, Q.L., Cao, D.Y., 2007. Study of thrust and nappe tectonics in the eastern Jiaodong Peninsula, China. Science in China Earth Science 50, 161–171.

Zhang, S.H., Zhao, Y., Davis, A.G., Ye, H., Wu, F., 2014. Temporal and spatial variations of Mesozoic magmatism and deformation in the North China Craton: Implications for lithospheric thinning and decratonization. Earth-Science Reviews 131, 49-87.

Zhang, Y.Q., Dong, S.W., 2008. Mesozoic tectonic evolution history of the Tan–Lu fault zone, China: advances and new understanding. Geological Bulletin of China 27, 1371–1390 (in Chinese with English abstract).

Zhao, Y., Song, B., Zhang, S.H., 2006. Geochronology of the inheritic zircon from Jurassic Nandaling Basalt of the Western Hills of Beijing, North China: its implications. Earth Science Frontiers 13, 183–190 (in Chinese with English abstract).

Zhao, Y., Xu, G., Zhang, S.H., Yang, Z.Y., Zhang, Y.Q., Hu, J.M., 2004. The Jurassic major tectonic events of the Yanshan intraplate deformation belt. Geology Bulletin of China 23, 854–863 (in Chinese with English abstract).

Zharov, A.E., 2004. Accretionary tectonics and geodynamics of southern Sakhalin. Geotectonics 38, 277-293.

Zhou, J.B., Cao, J.L., Wilde, A.S., Zhao, G.C., Zhang, J.J., Wang, B., 2014. Paleo-Pacific subduction-accretion: Evidence from geochemical and U-Pb zircon dating of the Nadanhada accretionary complex, NE China. Tectonics 33, 2444-2466.

Zhu, G., Jiang, D.Z., Zhang, B.L., Chen, Y., 2012. Destruction of the eastern North China Craton in a backarc setting: Evidence from crustal deformation kinematics. Gondwana Research 22, 86-103.

Zhu, G., Liu, G.S., Niu, M.L., Xie, C.L., Wang, Y.S., Xiang, B.W., 2009. Syn-collisional transform faulting of the Tan-Lu fault zone, East China. Int J Earth

Sci (Geol Rundsch) 98, 135–155.

Zhu, G., Niu, M.L., Xie, C.L.,Wang, Y.S., 2010. Sinistral to normal faulting along the Tan–Lu fault zone: evidence for geodynamic switching of the east China continental margin. Journal of Geology 118, 277–293.

Zhu R.X., Chen L, Wu F.Y., and Liu J.L., 2011. Timing, scale and mechanism of the destruction of the North China Craton. Science China, Earth Sciences 54, 789-797.

Zyabrev S.V., 2011. Stratigraphy and structure of the central east Sakhalin accretionary wedge (eastern Russia). Russian Journal of Pacific Geology 5, 313-335.

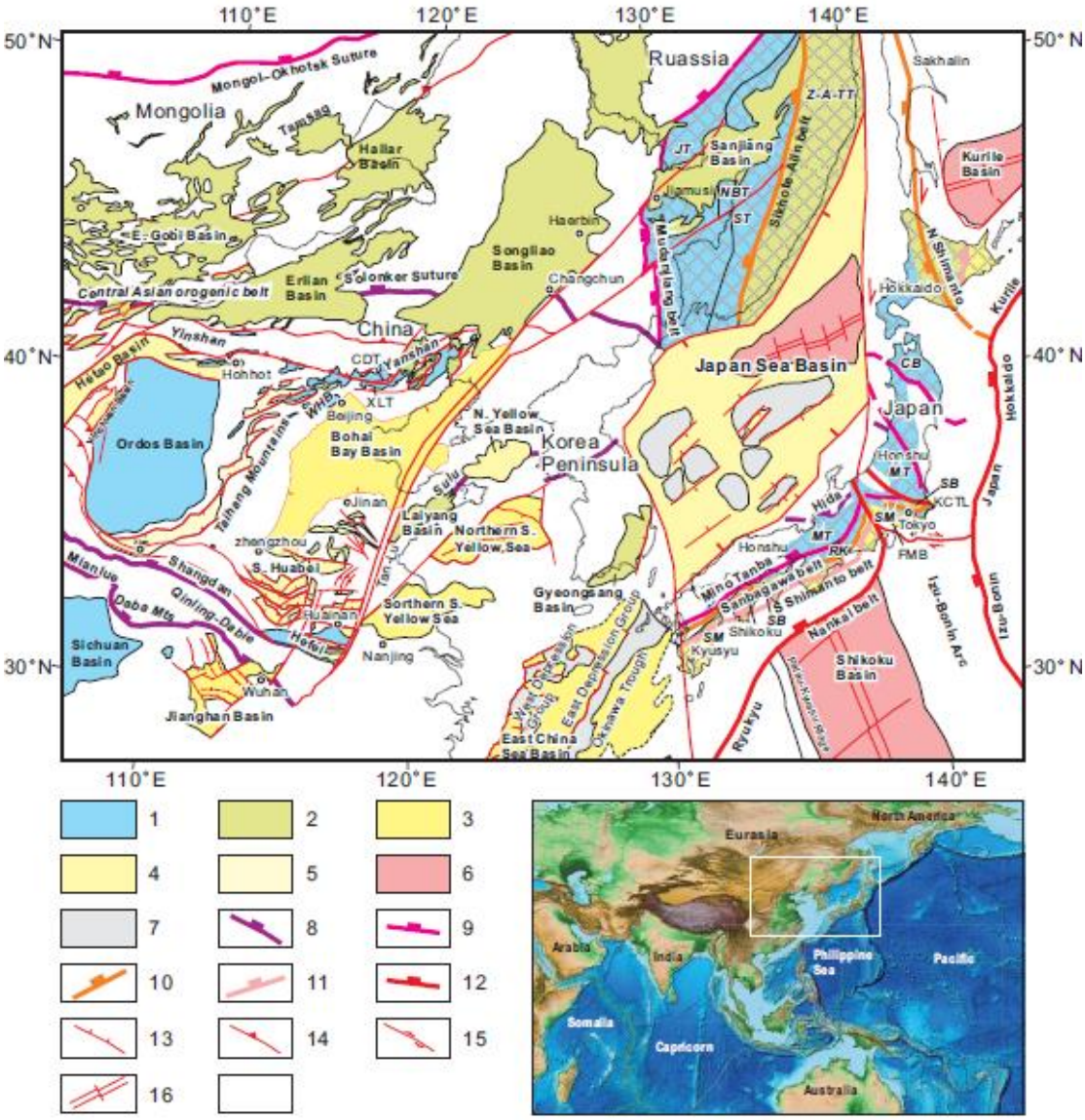

Figure 1

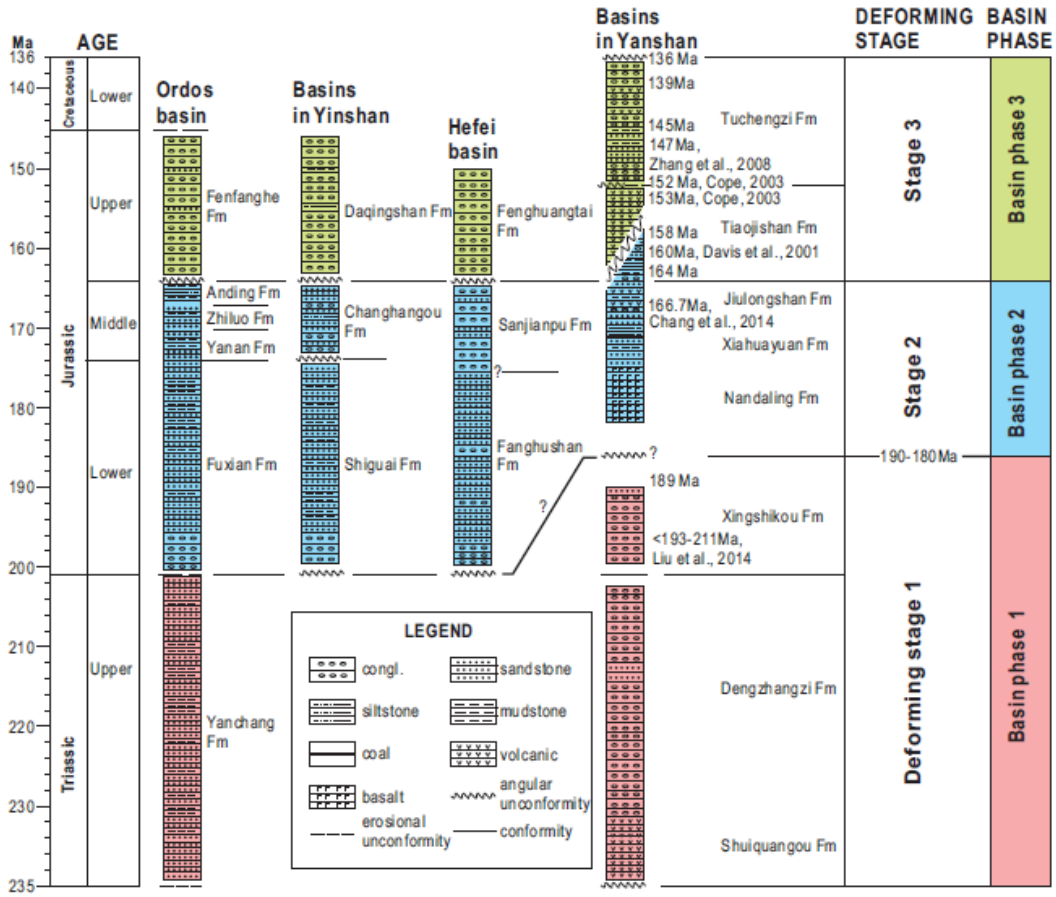

Figure 2

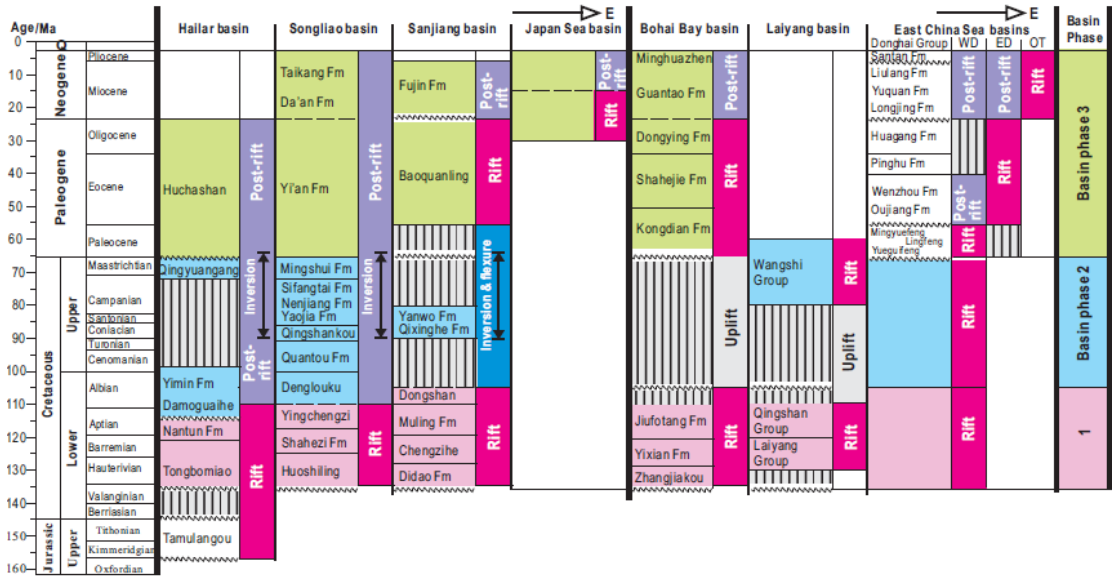

Figure 3

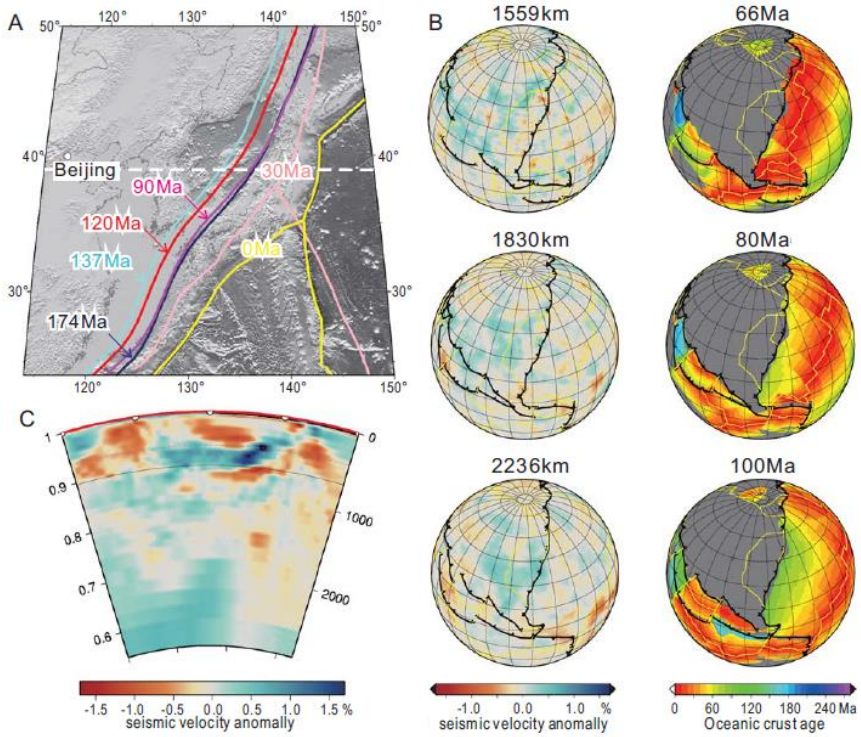

Figure 4

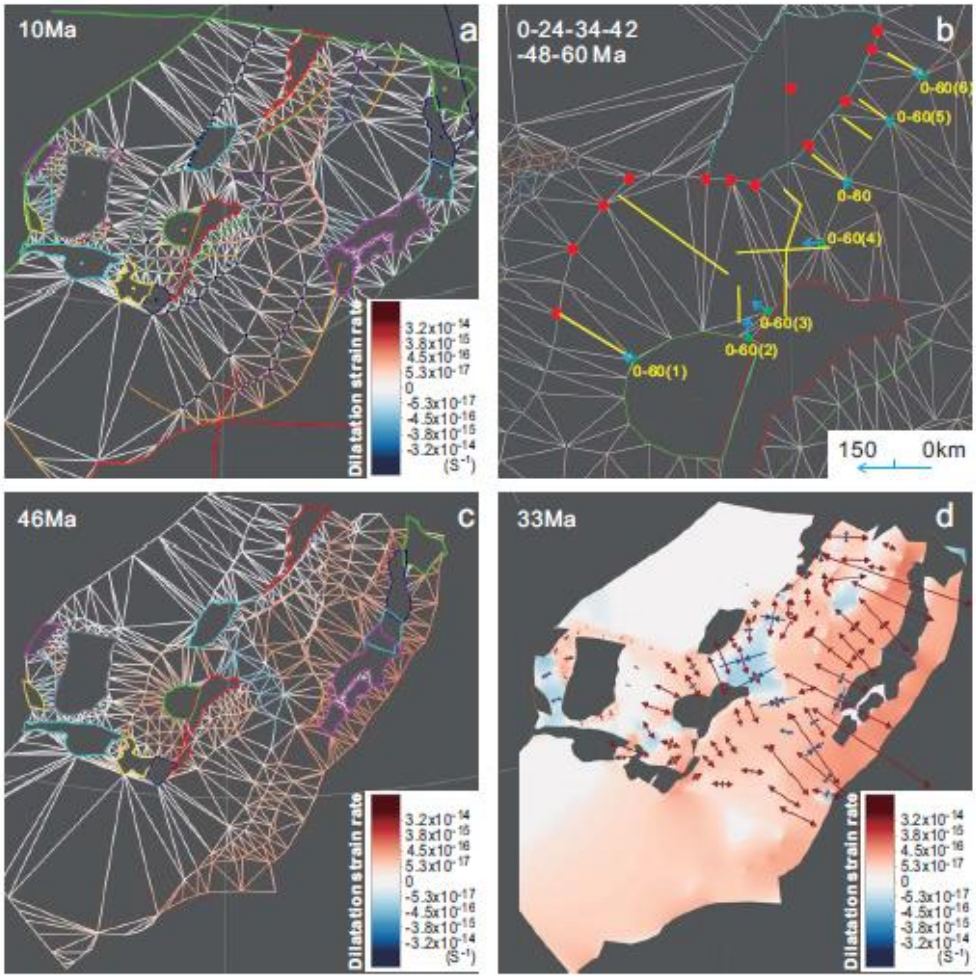

Figure 5

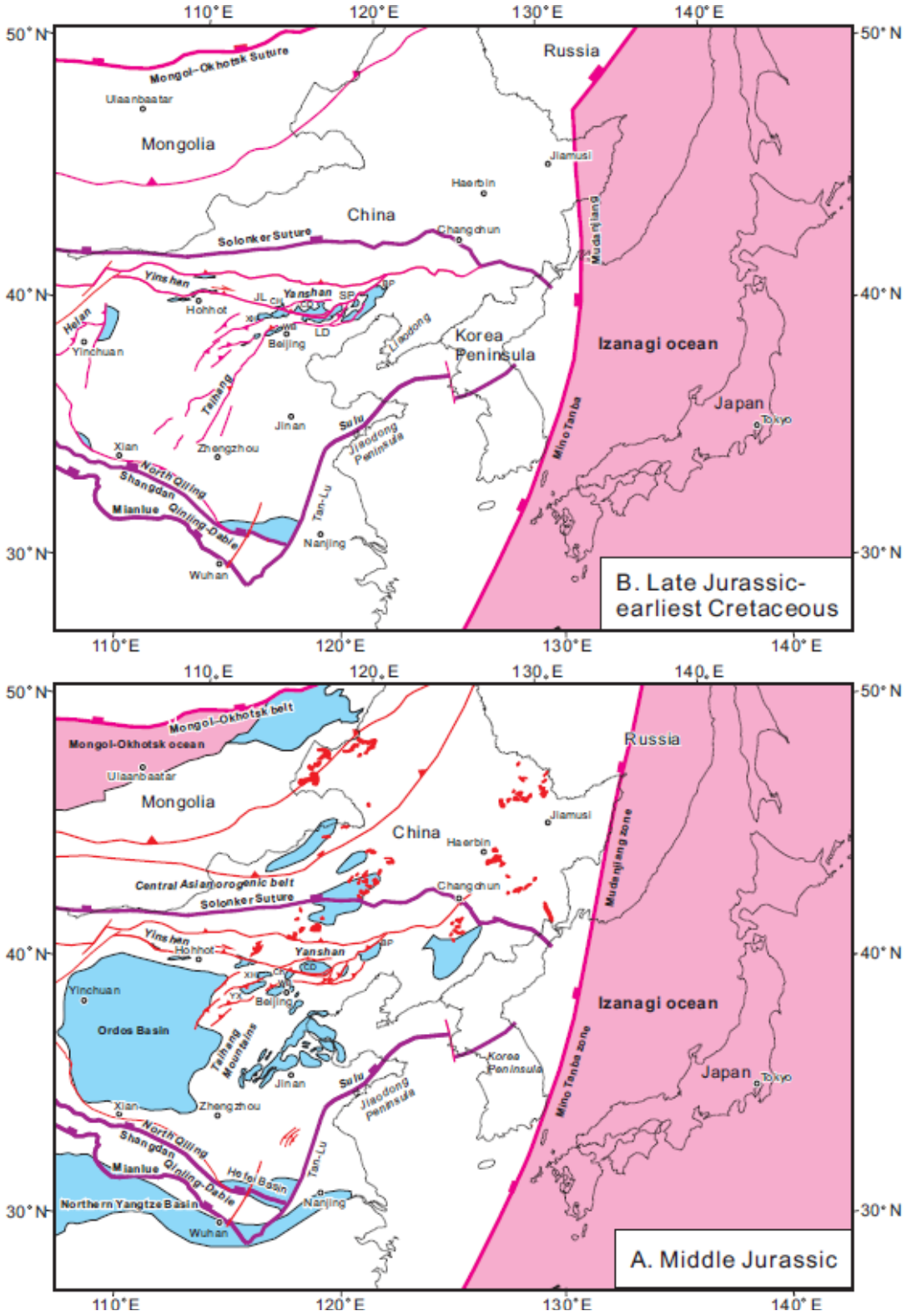

Figure 6AB

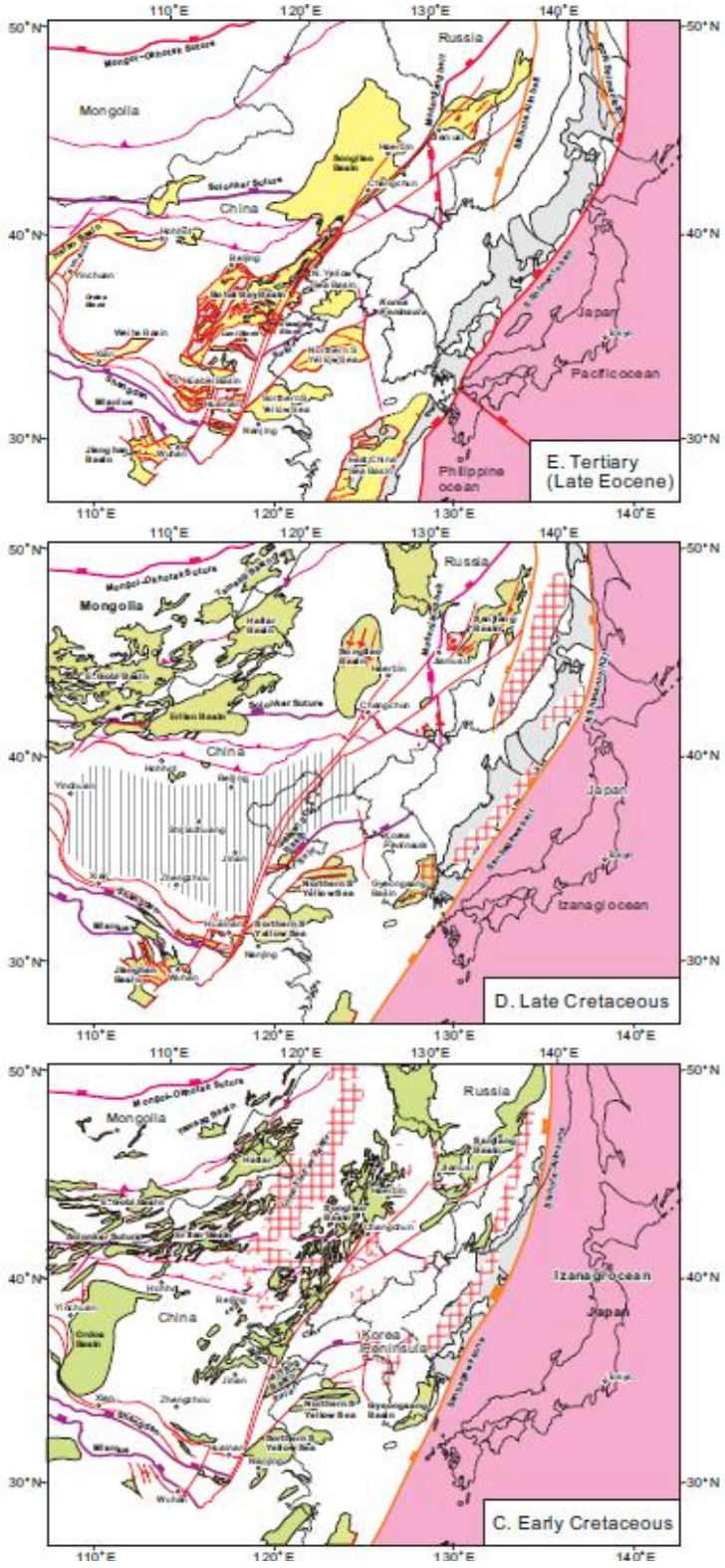

Figure 6CDE

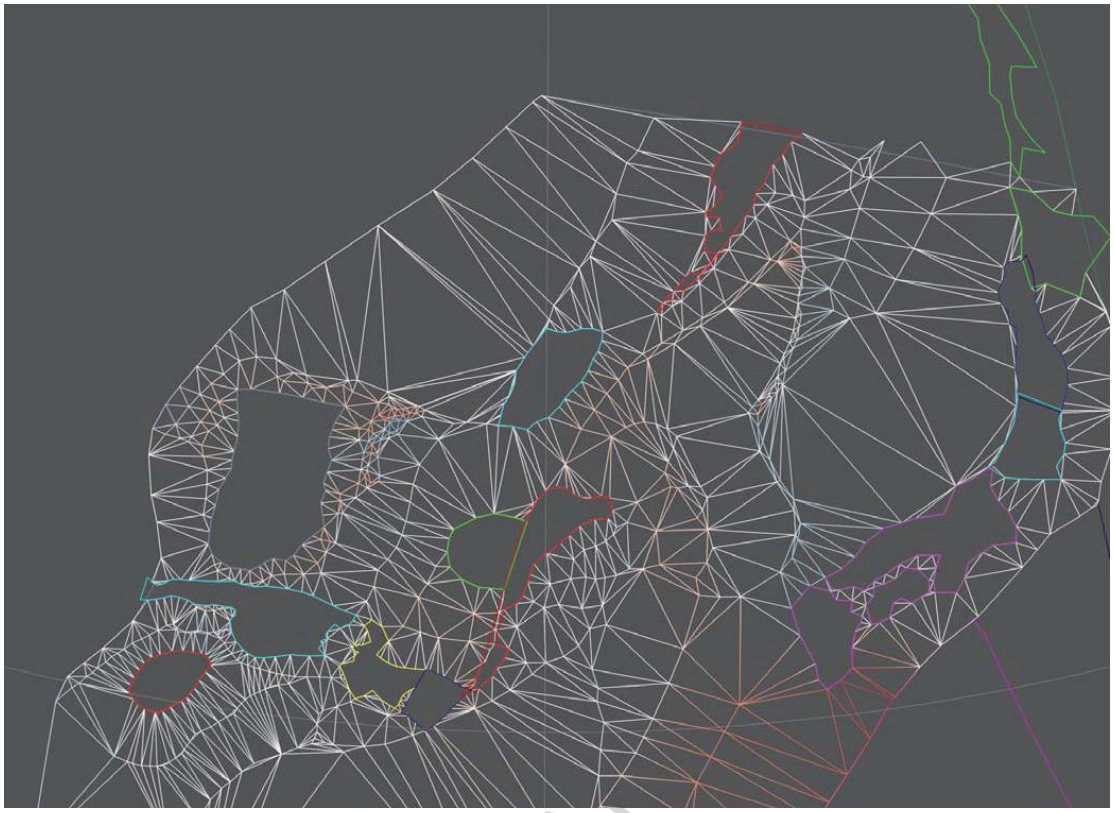

Figure 7A

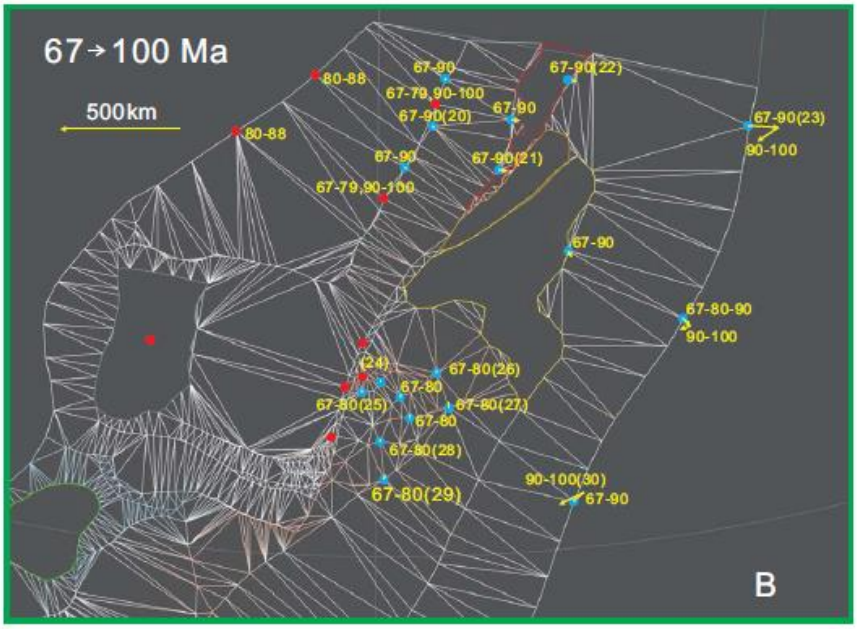

Figure 7B

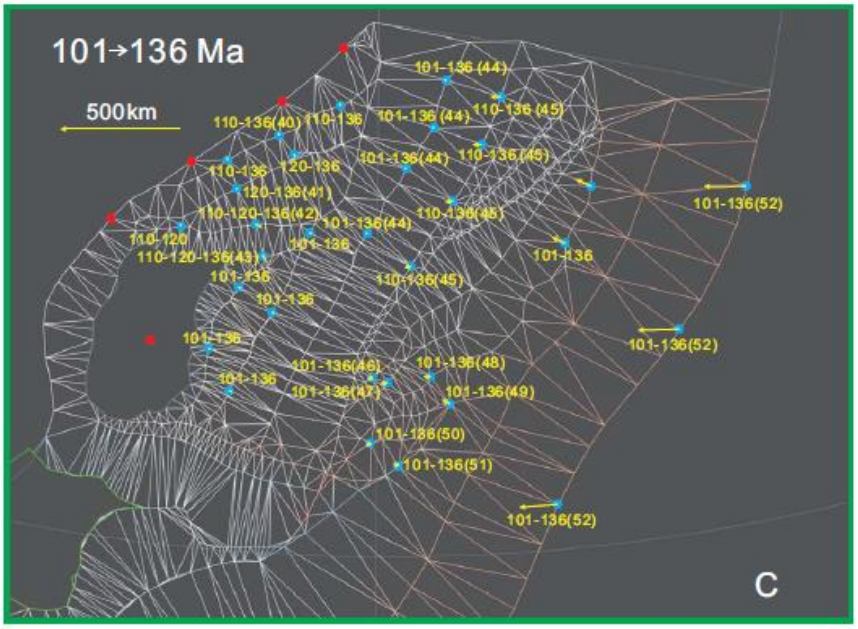

Figure 7C

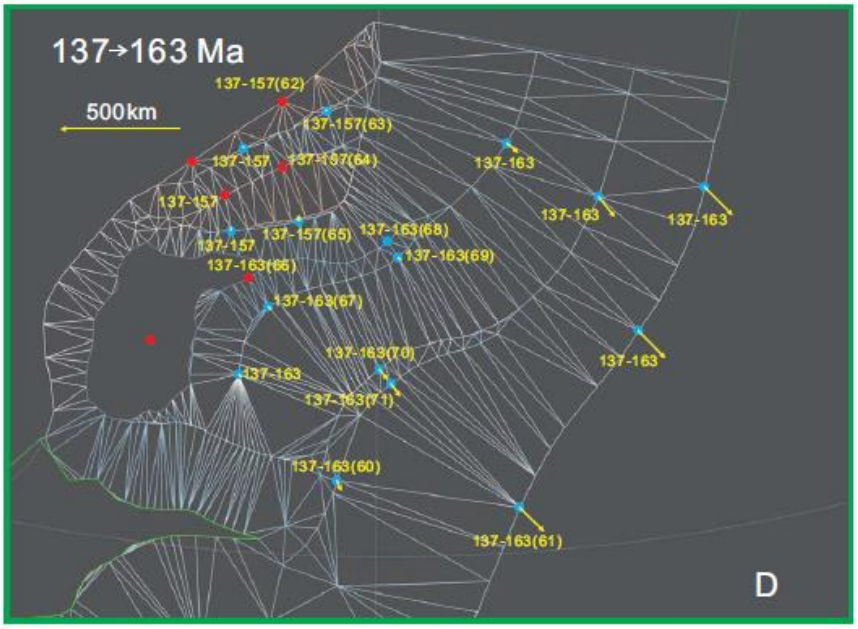

Figure 7D

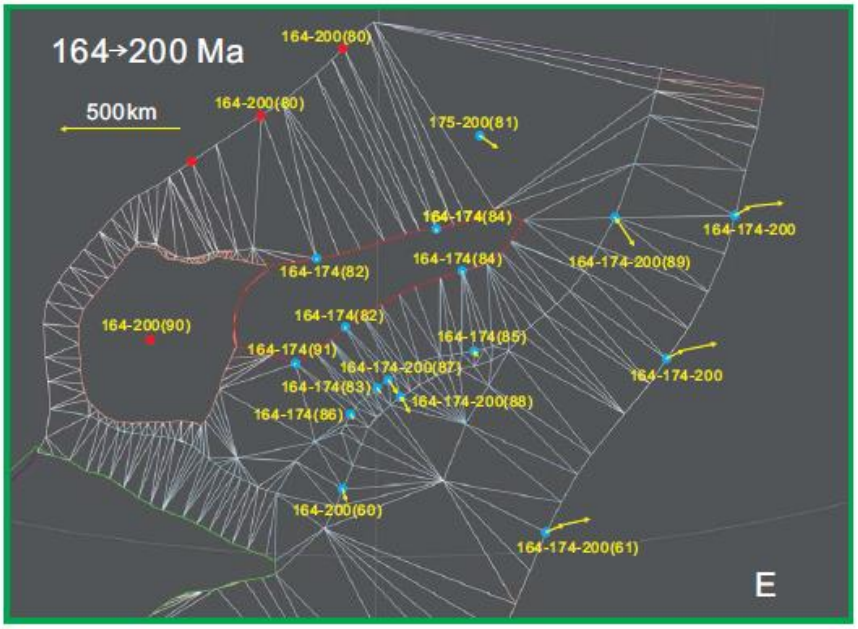

Figure 7E

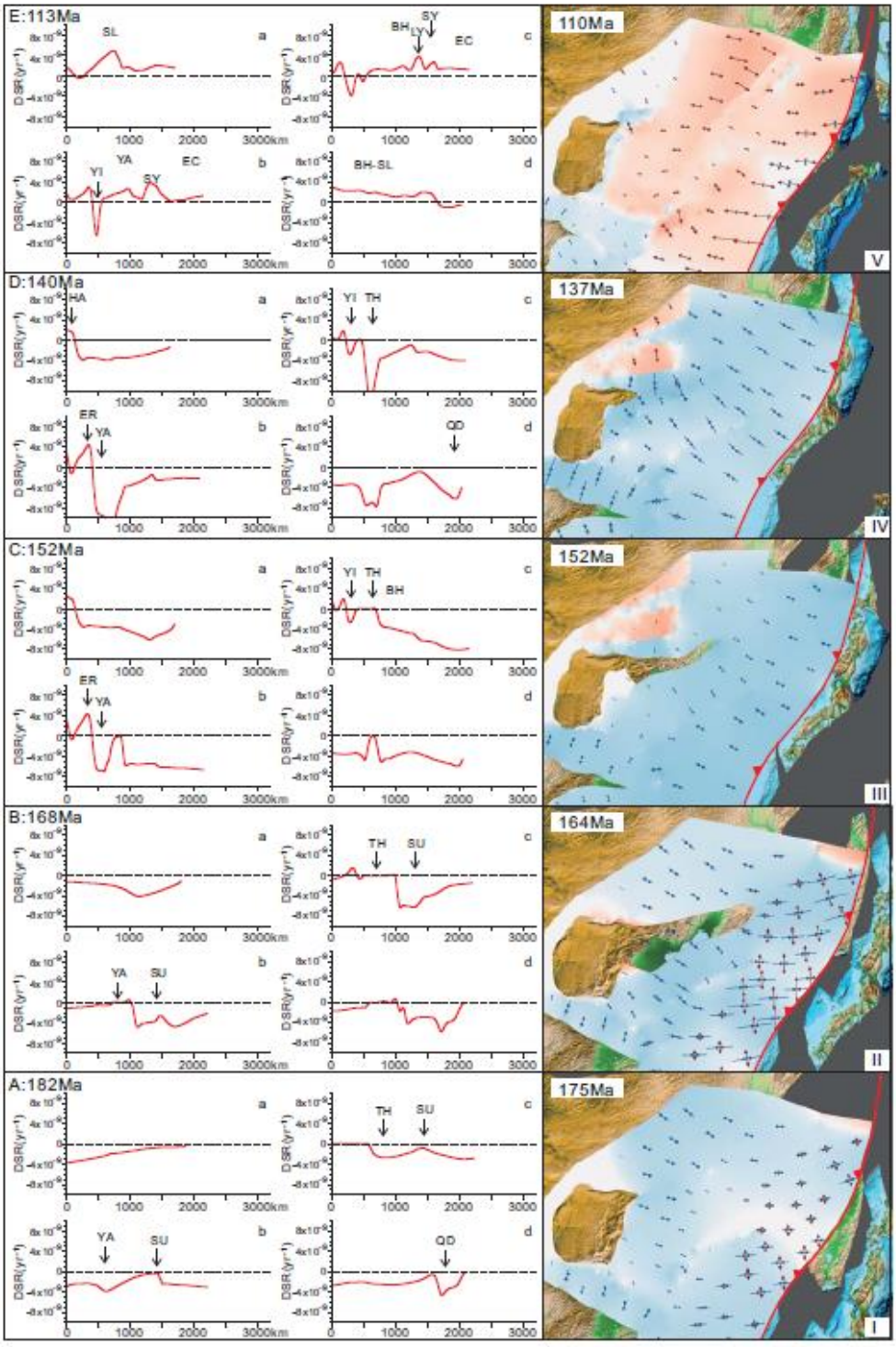

Figure 8A

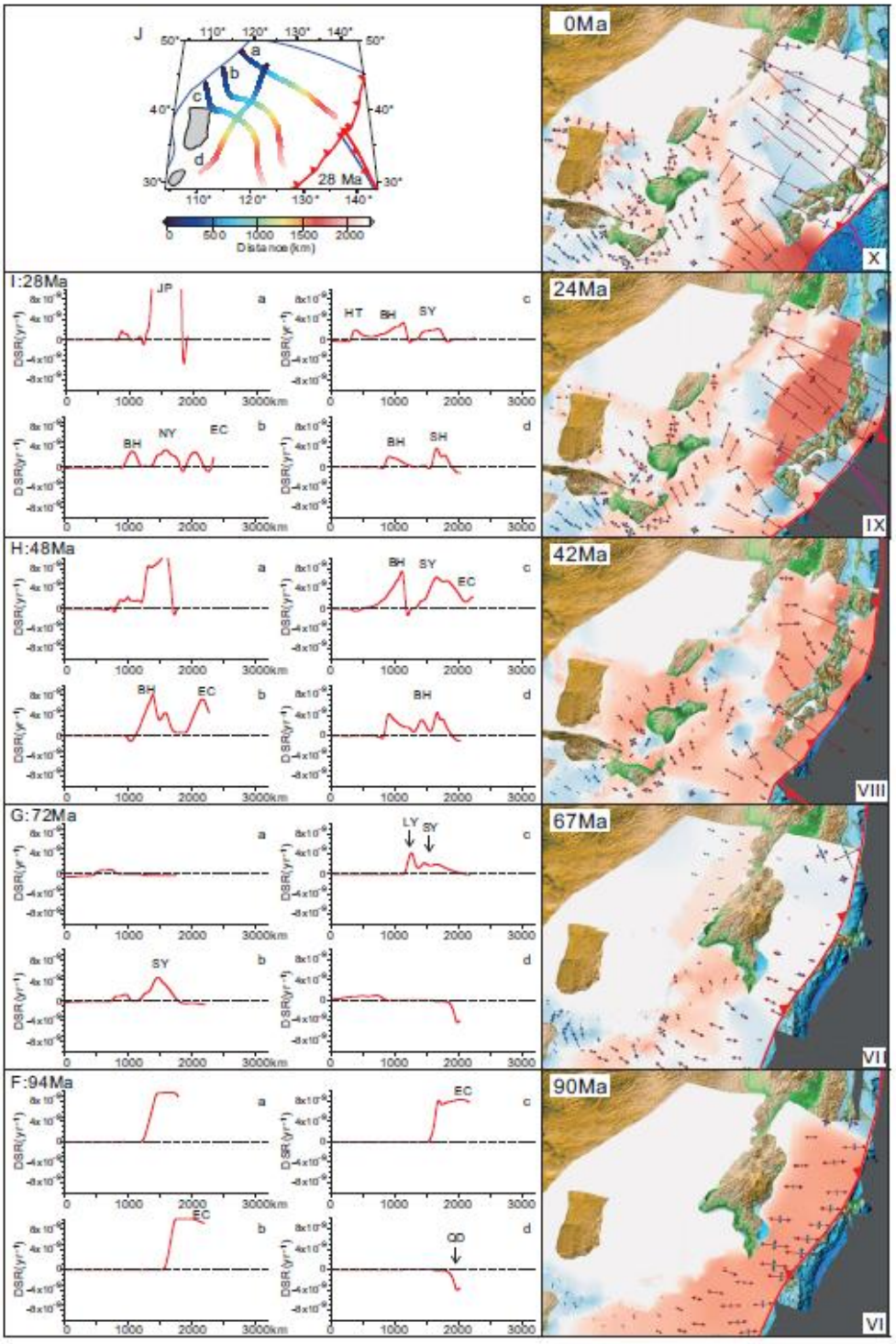

Figure 8B

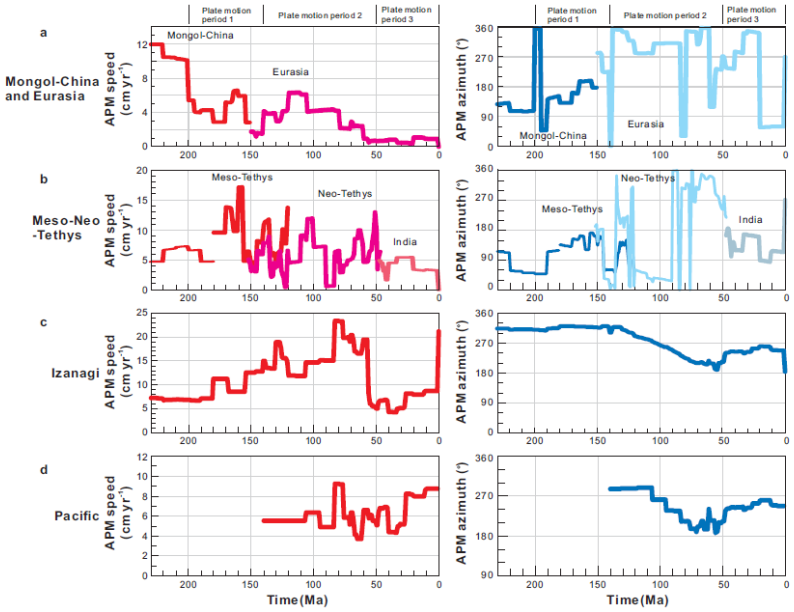

Figure 9

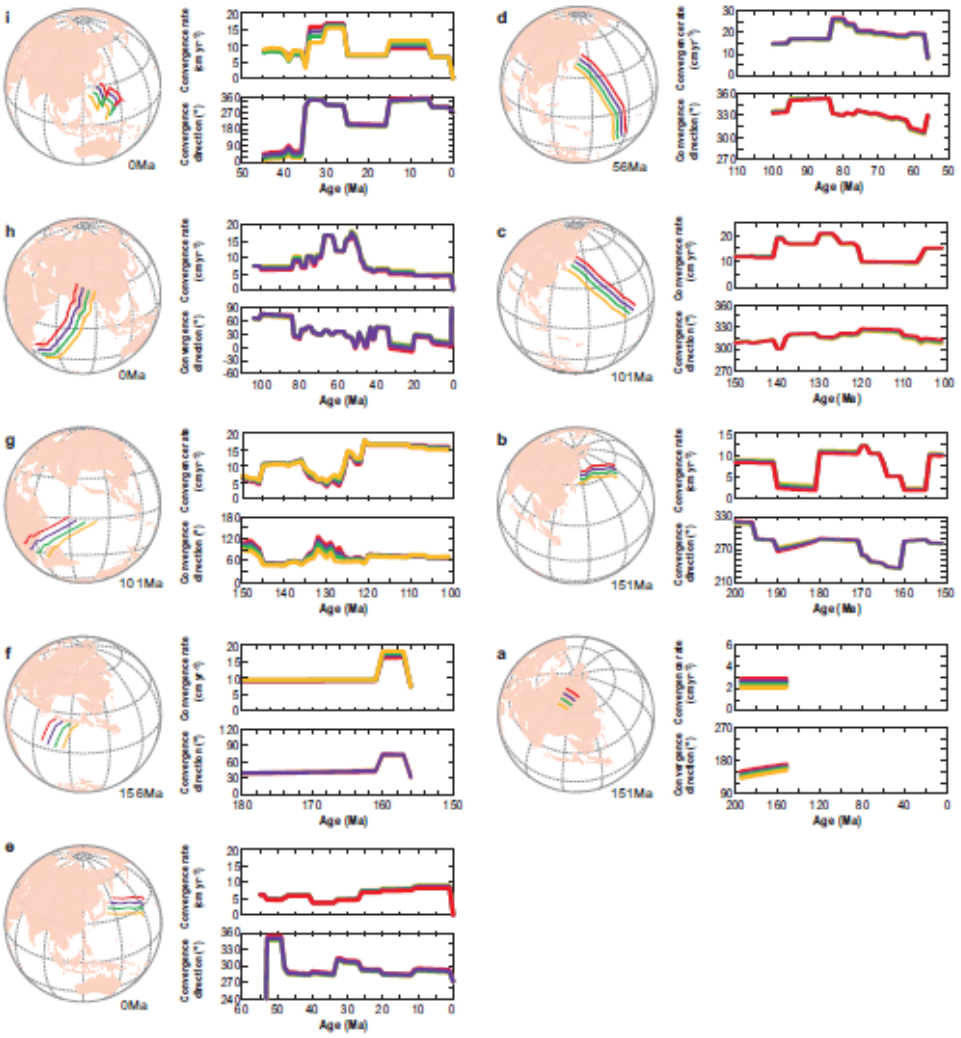

Figure 10

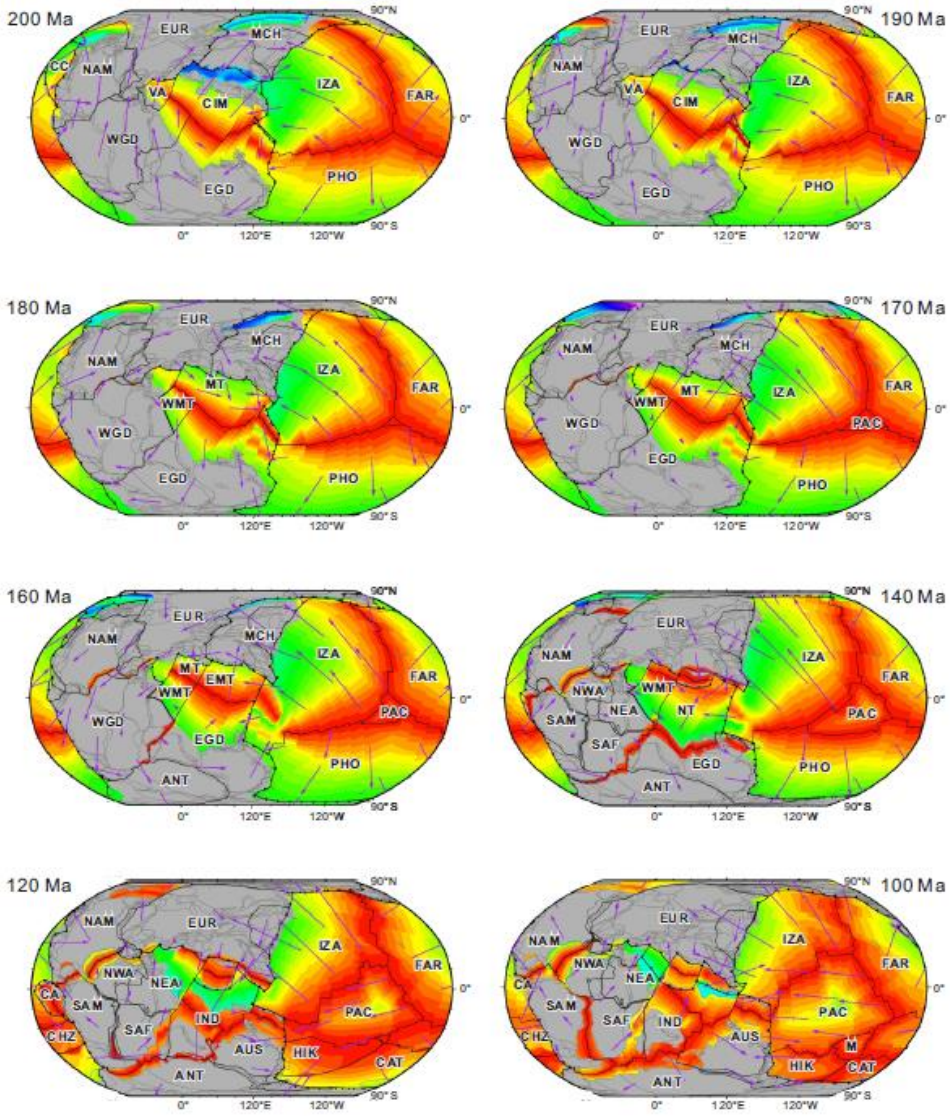

Figure 11A

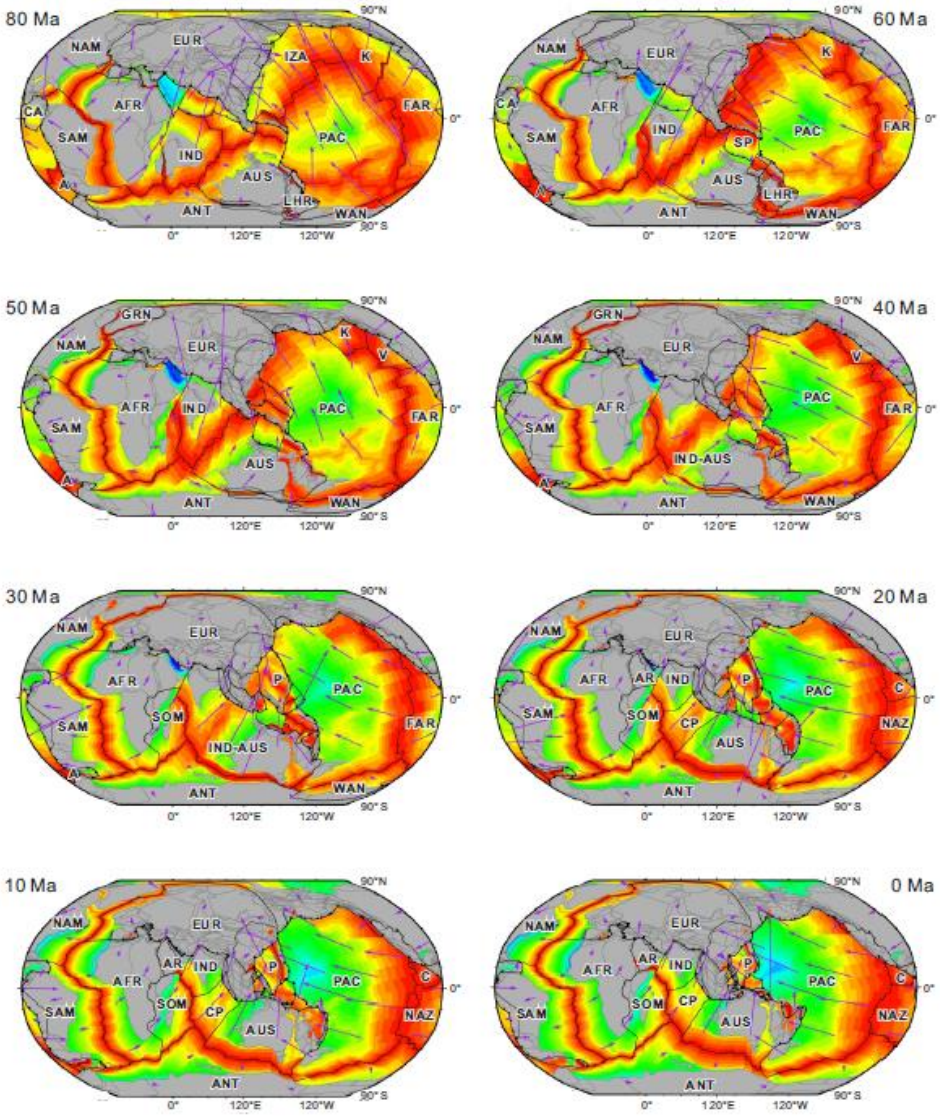

Figure 11B

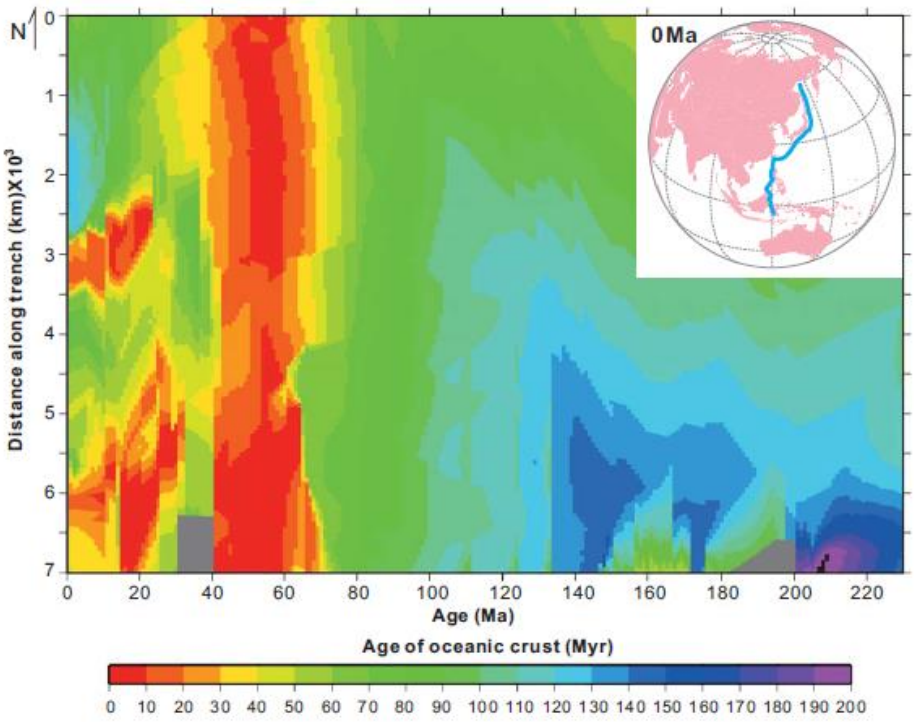

Figure 12